On the Orthogonal Subgrid Scale Pressure Stabilization of Small and Finite Deformation J2 Plasticity

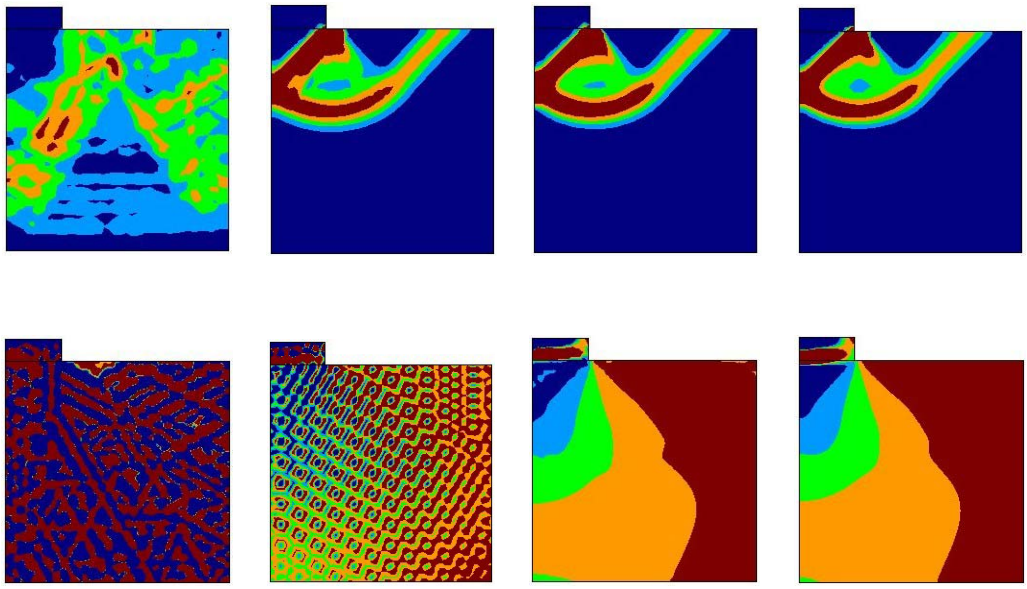

C. Agelet de Saracibar, M. Chiumenti
M. Cervera, Q. Valverde

On the Orthogonal Subgrid Scale Pressure Stabilization of Small and Finite Deformation J2 Plasticity

C. Agelet de Saracibar*, M. Chiumenti*, M. Cervera*
and Q. Valverde+

*International Center for Numerical Methods in Engineering (CIMNE)
Universidad Politécnica de Cataluña (UPC)
Edificio C1, Campus Norte, Gran Capitán s/n,
E-08034 Barcelona, Spain
agelet@cimne.upc.es, chiument@cimne.upc.es, cervera@cimne.upc.es

+Departamento de Ingenieria, Sección Ingenieria Mecánica,
Pontificia Universidad Católica del Perú, Lima, Perú
qvalver@pucp.edu.pe

October 6, 2004

Abstract

The use of stabilization methods is becoming an increasingly well-accepted technique due to their success in dealing with numerous numerical pathologies that arise in a variety of applications in computational mechanics.

In this monograph a multiscale finite element method technique to deal with pressure stabilization of nearly incompressibility problems in nonlinear solid mechanics at small and finite deformations J2 plasticity is presented. A mixed formulation involving pressure and displacement fields is used as starting point. Within the finite element discretization setting, continuous linear interpolation for both fields is considered. To overcome the Babuška-Brezzi stability condition, a multiscale stabilization method based on the Orthogonal Subgrid Scale (OSGS) technique is introduced. Suitable nonlinear expression of the stabilization parameters are proposed. The main advantage of the method is the possibility of using linear triangular or tetrahedral finite elements, which are easy to generate and, therefore, very convenient for practical industrial applications.

Numerical results obtained using the OSGS stabilization technique are compared with results provided by the P1 standard Galerkin displacements linear triangular/tehrahedral element, P1/P1 standard mixed linear displacements/linear pressure triangular/tetrahedral element and Q1/P0 mixed bilinear/trilinear displacements/constant pressure quadrilateral/hexahedral element for 2D/3D nearly incompressible problems in the context of nonlinear small and finite deformation J2 plasticity models.

KEYWORDS: Multiscale methods, Subgrid scale methods, Orthogonal subgrid scale methods, Stabilized finite element methods, Stabilization, Incompressibility, Plasticity, Finite deformation

Contents

List of Figures

List of Tables

1 Introduction

The use of stabilized methods is becoming an increasingly well-accepted technique due to their success in dealing with numerous numerical pathologies that arise in a variety of applications in computational mechanics. This

monograph deals with the application of multiscale methods, in particular the Orthogonal Subgrid Scale (OSGS) method, to the pressure stabilization of the formulation of nearly incompressibility problems in nonlinear solid mechanics using low order finite elements. Both small deformation and finite deformation J2 plasticity problems are considered. The goal is to consistently derive, within the framework of the OSGS method, a modified variational mixed formulation of the original problem with enhanced stability properties.

It is well known that the standard irreductible Galerkin finite element method with low-order piecewise polynomials perform miserably in nearly incompressible problems, exhibiting spurious wild oscillations of the mean pressure and leading to a response which is almost completely locked due to the incompressibility constraint. In the computational literature these devastating numerical difficulties are referred to as *locking* phenomena. Actually, the exact incompressibility problem does not admit an irreductible formulation and, consequently, a mixed displacement/pressure framework is necessary in that case. Even though, many standard mixed finite element formulations, particularly those using low order interpolations, also perform poorly or totally fail to perform for nearly incompressibility or incompressibility problems, producing results throughly polluted by spurious oscillations of the pressure.

To overcome these difficulties, over the years different strategies were suggested to reduce or avoid volumetric locking and pressure oscillations in finite element solutions. For an engineering oriented presentation see the well known books of Zienkiewicz and Taylor [45], Hughes [19] and Simo and Hughes (1998) [39]. For a more mathematically oriented presentation see the book of Brezzi and Fortin [3]. Different mixed and enhanced finite element formulations were proposed and degrees of success were obtained. See, e.g., Simo, Taylor and Pister [42], Simo [35], [36], [40], Miehe [29], Simo and Rifai [41], Simo and Armero [37]. Unfortunately, few approaches were succesfully applied to low order finite elements, as shown for instance in Reddy and Simo [32] for the enhanced assumed strain method. This was due to the strictness of the inf-sup or Ladyzhenskaya-Babuška-Brezzi (LBB) condition when the standard Galerkin finite element projection was straightforwardly applied to mixed low order finite elements, as it imposes severe restrictions on the compatibility of the interpolations used for the displacement and pressure fields [3], [45]. One significant effort in that direction was the so called mini element [1], an attractive linear displacement/pressure triangle enhanced with a cubic displacement bubble function. The mini element satisfies the LBB condition, but it is only marginally stable and it does not perform very well in many practical situations. Despite these not very good satisfactory re-

sults, there still exists a great practical interest in the use of stable low order elements, mainly motivated by the fact that, nowadays, tetrahedral finite element meshes are relatively easy to generate for real life complex geometries. Therefore, stabilization techniques for low order finite elements is a very active research area in solid mechanics. Some recent formulations have been proposed by Zienkiewicz et al. [46], Klaas, Maniatty and Shephard [24], Oñate et al. [30], [31] and Maniatty et al. [27], [28].

On the other hand, research on stabilization methods for incompressibility, as well as other phenomena, in Computational Fluid Dynamics (CFD) has been always in the front line of research because of the innumerable practical applications of the field [2], [4], [15], [21], [22]. In Hughes [20] and Hughes et al. [23] the variational multiscale method was introduced as a new computational mechanics paradigma to address stabilization problems in CFD. Within the multiscale method it is assumed that there is a component of the continuous (exact) solution which can not be captured by the finite element solution. This component which is not captured by the finite element solution is called the subgrid scale or the subscale. The consideration of this subgrid scale leads to a modified variational formulation with enhanced stability properties and allows the use of a convenient mixed velocity/pressure equal linear interpolation. Since their inception, multiscale methods have been extensively and successfully used in CFD. In Codina [13], [14] the Orthogonal Subgrid Scales (OSGS) method was introduced, leading to better sustained and better performing stabilization procedures.

In Computational Solid Mechanics (CSM), variational multiscale techniques have been used by Garikipati and Hughes [16], [17] in strain localization problems. Recently, a variational multiscale stabilization method based on the OSGS has been applied to both incompressibility and nearly incompressibility problems in small deformations elasticity by Valverde et al. [44], Chiumenti et al. [11] and Christ et al. [10], J2 plasticity by Valverde et al. [44], Chiumenti et al. [12], Cervera et al. [6] and Christ et al. [10], softening and localization in J2 plasticity by Cervera, Chiumenti and Agelet de Saracibar [7] and shear band localization using a J2 continuum damage model by Cervera, Chiumenti and Agelet de Saracibar [9], [8].

The goal of this monograph is to consistently address the formulation of multiscale methods, in particular the OSGS method, to incompressibility or nearly incompressibility problems within the framework of small and finite deformation J2 plasticity models and using low order finite elements.

The outline of the remaining of the monograph is as follows. Section 2 deals with the strong form, variational form and discrete variational form of the mixed formulation of the nearly incompressibility problem in solid mecanics, within a small deformation J2 plasticity framework. Section 3

deals with the multiscale formulation of J2 plasticity models at small deformations. Within the multiscale technique framework, the variational multiscale forms are derived, a nonlinear expression for the stabilization parameter is proposed and the subsgrid scale displacements are approximated using an OSGS stabilization method. Section 4 deals with the strong form, variational form and discrete variational form of the mixed formulation of the nearly incompressibility problem in nonlinear solid mecanics, within a finite deformation J2 plasticity framework. Section 5 deals with the multiscale formulation of J2 plasticity models at finite deformations.Within the multiscale technique framework, the variational multiscale forms are derived, a nonlinear expression for the stabilization parameter is proposed and the subsgrid scale displacements are approximated using an OSGS stabilization method. Some computational and implementation aspects are discussed in Section 6. An assessment of the behaviour of the formulation is presented in Section 7, where some representative numerical simulations are shown and compared with results obtained using P1 Galerkin displacements linear triangular (2D) or tetrahedral (3D) elements, P1/P1 mixed linear displacement/linear pressure triangular (2D) or tetrahedral (3D) elements and Q1/P0 bilinear (2D) or trilinear (3D) displacement/constant pressure quadrilateral (2D) or hexahedral (3D) elements. Some concluding remarks are addressed in Section 8. Finally, after an acknowledgement section, an Appendix including the derivation of the linearization of the variational momentum balance residual has been included.

2 Nearly Incompressibility Problem in Solid Mechanics: Infinitesimal J2 Plasticity

Let us begin introducing some standard notation. Let Ω be an open and bounded domain of $\mathbb{R}^{n_{\text{dim}}}$, where n_{dim} is the number of space dimensions, $\overline{\Omega}$ its closure and Γ its boundary which is considered split into two disjoint sets such that $\Gamma = \overline{\partial\Omega_u \cup \partial\Omega_t}$ and $\partial\Omega_u \cap \partial\Omega_t = \emptyset$. The space of square integrable functions in Ω is denoted by $L^2(\Omega)$ and the space of functions of which its derivatives up to order $m \geq 0$ (integer) belong to $L^2(\Omega)$ by $H^m(\Omega)$. The space $H_0^m(\Omega)$ consists of those functions that belong to $H^m(\Omega)$ and vanish on $\partial\Omega_u$. Bold characters are used to denote vector counterpart of all these spaces. The L^2 inner product in Ω and in $\partial\Omega$ are denoted by $(\cdot,\cdot)$ and $(\cdot,\cdot)_{\partial\Omega}$, respectively. Hereafter, orthogonality will be understood with respect to this product.

2.1 Strong form

Consider a displacemet field $\mathbf{u}$ and a mean-pressure field p. The mixed Cauchy stress tensor can be written as $\boldsymbol{\sigma}(\mathbf{u}, p) = p\,\mathbf{1} + \mathbf{s}(\mathbf{u})$. Appropriate boundary conditions will be taken as $\mathbf{u} = \overline{\mathbf{u}}$ on $\partial\Omega_u$ and $\boldsymbol{\sigma} \cdot \mathbf{n} = \overline{\mathbf{t}}$ on $\partial\Omega_t$, where $\overline{\mathbf{u}} : \partial\Omega_u \to \mathbb{R}^{n_{\text{dim}}}$ and $\overline{\mathbf{t}} : \partial\Omega_t \to \mathbb{R}^{n_{\text{dim}}}$ are the prescribed displacement and traction vectors, respectively. Consider also the infinite-dimensional spaces $\mathcal{V} = \left\{\mathbf{u} \in \mathbf{H}^1(\Omega) \mid \mathbf{u} = \overline{\mathbf{u}} \quad \text{on} \quad \partial\Omega_u\right\}$ and $\mathcal{Q} = L^2(\Omega)$ for the displacement and pressure fields, respectively. We shall be interested also in the space $\mathcal{W} = \mathcal{V} \times \mathcal{Q}$. Then the strong form of the mixed formulation for the nearly incompressibility problem in solid mechanics, within the infinitesimal deformation framework, consists in finding a displacement field $\mathbf{u} \in \mathcal{V}$ and a mean-pressure field $p \in \mathcal{Q}$ such that

$$\nabla p + \nabla \cdot \mathbf{s}(\mathbf{u}) + \mathbf{f} = \mathbf{0} \quad \text{in} \quad \Omega \tag{1}$$

$$\tfrac{1}{\kappa} p - \nabla \cdot \mathbf{u} = 0 \quad \text{in} \quad \Omega \tag{2}$$

where $\mathbf{s}(\mathbf{u}) = \text{dev}[\boldsymbol{\sigma}(\mathbf{u},p)]$ is the deviatoric part of the (mixed) Cauchy stress tensor $\boldsymbol{\sigma}(\mathbf{u},p)$, $\mathbf{f} : \Omega \to \mathbb{R}^{n_{\text{dim}}}$ is the prescribed body force per unit volume vector and κ is the bulk modulus. These equations must be supplied with an appropiate constitutive equation for the deviatoric part of the Cauchy stress tensor, which for the infinitesimal plasticity case will take the form $\mathbf{s}(\mathbf{u}) = 2\mu\,\text{dev}[\nabla^s \mathbf{u} - \boldsymbol{\varepsilon}^p]$ where $\nabla^s \mathbf{u}$ is the symmetric gradient of the displacements tensor, $\boldsymbol{\varepsilon}^p$ is the plastic strain tensor, μ is the shear modulus and $\text{dev}[\cdot]$ denotes the deviatoric operator.

Using an abstract compact notation, the problem defined by (1) and (2) can be written as: find $\mathbf{U} \in \mathcal{W}$ such that

$$\mathcal{L}(\mathbf{U}) = \mathbf{F} \quad \text{in} \quad \Omega \tag{3}$$

where $\mathbf{U}$, $\mathcal{L}(\mathbf{U})$ and $\mathbf{F}$ are defined as

$$\mathbf{U} = \begin{bmatrix} \mathbf{u} \\ p \end{bmatrix}, \quad \mathcal{L}(\mathbf{U}) = \begin{bmatrix} -\nabla p - \nabla \cdot \mathbf{s}(\mathbf{u}) \\ -\frac{1}{\kappa}\, p + \nabla \cdot \mathbf{u} \end{bmatrix}, \quad \mathbf{F} = \begin{bmatrix} \mathbf{f} \\ 0 \end{bmatrix} \tag{4}$$

2.2 Variational form

Consider the infinite-dimensional space $\mathcal{V}_0 = \mathbf{H}_0^1(\Omega)$. We shall be interested also in the space $\mathcal{W}_0 = \mathcal{V}_0 \times \mathcal{Q}$. Then the variational formulation of the nearly incompressibility problem in solid mechanics defined by (3) can be written as: find $\mathbf{U} \in \mathcal{W}$ such that, for any $\mathbf{V} \in \mathcal{W}_0$,

$$(\mathcal{L}(\mathbf{U}), \mathbf{V}) = (\mathbf{F}, \mathbf{V}) \tag{5}$$

Using the definitions given in (4) and setting $\mathbf{V} = [\mathbf{v}, q]^T$ the explicit expression for the variational form given by (5) takes the form

$$\begin{aligned} -(\nabla p, \mathbf{v}) - (\nabla \cdot \mathbf{s}(\mathbf{u}), \mathbf{v}) &= (\mathbf{f}, \mathbf{v}) \qquad \forall \mathbf{v} \in \mathcal{V}_0 \quad (6) \\ -(\tfrac{1}{\kappa} p, q) + (\nabla \cdot \mathbf{u}, q) &= 0 \qquad \forall\, q \in \mathcal{Q} \quad (7) \end{aligned}$$

Integrating by parts the left-hand side of (6), the above variational forms can be written as:

$$\begin{aligned} (p, \nabla \cdot \mathbf{v}) + (\mathbf{s}(\mathbf{u}), \nabla^s \mathbf{v}) &= l(\mathbf{v}) \qquad \forall\, \mathbf{v} \in \mathcal{V}_0 \quad (8) \\ -(\tfrac{1}{\kappa} p, q) + (\nabla \cdot \mathbf{u}, q) &= 0 \qquad \forall\, q \in \mathcal{Q} \quad (9) \end{aligned}$$

where the operator $l(\mathbf{v}) := (\mathbf{f}, \mathbf{v}) + \left(\overline{\mathbf{t}}, \mathbf{v}\right)_{\partial\Omega}$ has been introduced and the fact that $\mathbf{s}(\mathbf{u})$ is a symmetric tensor has been used.

Then, introducing an abstract compact notation, the variational formulation of the nearly incompressibility problem in solid mechanics given by (5) can be alternatively written as: find $\mathbf{U} \in \mathcal{W}$ such that, for any $\mathbf{V} \in \mathcal{W}_0$,

$$B(\mathbf{U}, \mathbf{V}) = L(\mathbf{V}) \quad (10)$$

where

$$\begin{aligned} B(\mathbf{U}, \mathbf{V}) &= (p, \nabla \cdot \mathbf{v}) + (\mathbf{s}(\mathbf{u}), \nabla^s \mathbf{v}) - (\tfrac{1}{\kappa} p, q) + (\nabla \cdot \mathbf{u}, q) \quad (11) \\ L(\mathbf{V}) &= l(\mathbf{v}) \quad (12) \end{aligned}$$

2.3 Discrete variational form

The standard Galerkin projection of this variational problem is now straightforward. Let $\mathcal{P}_h$ denote a finite element partition of the domain Ω. The diameter of an element domain $e \in \mathcal{P}_h$ is denoted by h_e and the diameter of the finite element partition by $h = \max\{h_e \mid e \in \mathcal{P}_h\}$. We can now construct conforming finite element spaces $\mathcal{V}_h \subset \mathcal{V}$, $\mathcal{Q}_h \subset \mathcal{Q}$ and $\mathcal{W}_h = \mathcal{V}_h \times \mathcal{Q}_h$ in the usual manner, as well as the corresponding subspaces $\mathcal{V}_{h,0} \subset \mathcal{V}_0$ and $\mathcal{W}_{h,0} = \mathcal{V}_{h,0} \times \mathcal{Q}_h$. In principle, functions in $\mathcal{V}_h$ are continuous, whereas functions in $\mathcal{Q}_h$ not necessarily. Likewise, the polynomial orders of these spaces may be different. Then, the discrete version of the variational problem (10) consists in finding $\mathbf{U}_h \in \mathcal{W}_h$ such that for any $\mathbf{V}_h \in \mathcal{W}_{h,0}$

$$B(\mathbf{U}_h, \mathbf{V}_h) = L(\mathbf{V}_h) \quad (13)$$

Remark 1 *As it is well known, convenient displacement-pressure interpolations, such as equal linear interpolations, turn out to violate the inf-sup or*

Babuška-Brezzi condition. To circumvent this condition, the idea now is to replace the discrete variational problem (13) by a suitable discrete stabilized variational problem, such that the variational form B is replaced by a possibly mesh dependent variational form B_{stab} with enhanced stability properties. Eventually, the linear form L may be also replaced by a possibly mesh dependent form L_{stab}. This is done in the next sections through the introduction of the subgrid scale method.

3 Multiscale Formulation of J2 Plasticity Models at Small Deformations

In this section, a stabilization of the mixed formulation of J2 plasticity models at small deformations is introduced within the framework of multiscale methods. The variational multiscale form is considered first. Then an approximate solution for the subgrid scales is sought. Within the OSGS method, we are taking the orthogonal space to the finite element solution space as the natural space of the subscales. A suitable nonlinear expression of the (scalar) stabilization parameter is proposed for small deformation plasticity models. Finally, the finite element projection of the pressure gradient is introduced as a third independent field and the resulting stabilized multiscale variational forms are derived.

3.1 Variational multiscale form

Multiscale approach. Within the paradigmatic framework of the multiscale methods introduced by Hughes [20], the subgrid scale method seeks to approximate the effect of the component of the continuous solution which can not be captured by the finite element mesh used to obtain the discrete finite element solution. The unresolved component is referred to as the *subgrid scale* or *subscale*. Let $\mathcal{W} = \mathcal{W}_h \oplus \widetilde{\mathcal{W}}$, where $\widetilde{\mathcal{W}}$ is any suitable space to complete $\mathcal{W}_h$ in $\mathcal{W}$. Obviously, $\widetilde{\mathcal{W}}$ is an infinite-dimensional space, but once the final method is formulated, it will be approximated by a finite-dimensional space, although we will keep the same symbol for it in order to simplify the notation. We will refer to $\widetilde{\mathcal{W}}$ as the *space of the subgrid scales* or the *space of the subscales*. Likewise, let $\mathcal{W}_0 = \mathcal{W}_{h,0} \oplus \widetilde{\mathcal{W}}_0$, with $\widetilde{\mathcal{W}}_0$ any space to complete $\mathcal{W}_{h,0}$ in $\mathcal{W}_0$. With the above definitions in hand, we consider that there exists a component $\widetilde{\mathbf{U}} \in \widetilde{\mathcal{W}}$ of the exact continuous solution $\mathbf{U} \in \mathcal{W}$ which can not be captured by the solution provided by the finite element method $\mathbf{U}_h \in \mathcal{W}_h$,

such that

$$\mathbf{U} = \mathbf{U}_h + \widetilde{\mathbf{U}} \tag{14}$$

where for the nearly incompressibility problem in solid mechanics $\mathbf{U}$, $\mathbf{U}_h$ and $\widetilde{\mathbf{U}}$ take the form

$$\mathbf{U} = \left[\begin{array}{c} \mathbf{u} \\ p \end{array} \right], \qquad \mathbf{U}_h = \left[\begin{array}{c} \mathbf{u}_h \\ p_h \end{array} \right], \qquad \widetilde{\mathbf{U}} = \left[\begin{array}{c} \widetilde{\mathbf{u}} \\ \widetilde{p} \end{array} \right] \tag{15}$$

where $\mathbf{U}_h$ is the resolved component of the primary variable provided by the finite element solution and may be interpreted as the projection of the exact solution $\mathbf{U}$ onto the finite-dimensional space introduced by the finite element discretization. Therefore $\widetilde{\mathbf{U}}$ is the component of the exact continuous solution which can not be captured by the discrete finite element solution. It is now necessary to introduce some additional finite-dimensional subspaces associated to the previously defined infinite-dimensional spaces.

Variational multiscale approach. Introducing the split of $\mathbf{U}$ given by (14), the variational multiscale formulation of the nearly incompressibility problem in solid mechanics given by (10) can be written as: find $\mathbf{U}_h \in \mathcal{W}_h$ and $\widetilde{\mathbf{U}} \in \widetilde{\mathcal{W}}$ such that:

$$B(\mathbf{U}_h + \widetilde{\mathbf{U}}, \mathbf{V}_h) = L(\mathbf{V}_h) \qquad \forall\, \mathbf{V}_h \in \mathcal{W}_{h,0} \tag{16}$$

$$B(\mathbf{U}_h + \widetilde{\mathbf{U}}, \widetilde{\mathbf{V}}) = L(\widetilde{\mathbf{V}}) \qquad \forall\, \widetilde{\mathbf{V}} \in \widetilde{\mathcal{W}}_0 \tag{17}$$

Proposition 2 *We will assume that the subgrid scale associated to the pressure field is zero $\widetilde{p} = 0$, i.e. we will assume that the exact pressure field may be captured by the finite element solution while the subgrid scale associated to the displacement field is considered.*

Assuming that $\widetilde{p} = 0$, i.e., that the exact pressure field may be captured by the finite element solution and, therefore, the subgrid scale associated to the pressure is zero, the variational multiscale formulation given by (16) and (17) can be written as: find $(\mathbf{u}_h, p_h) \in \mathcal{W}_h$ and $(\widetilde{\mathbf{u}}, 0) \in \widetilde{\mathcal{W}}$ such that:

$$(p_h, \nabla \cdot \mathbf{v}_h) + (\mathbf{s}(\mathbf{u}_h + \widetilde{\mathbf{u}}), \nabla^s \mathbf{v}_h) = l(\mathbf{v}_h) \qquad \forall\, \mathbf{v}_h \in \mathcal{V}_{h,0} \tag{18}$$

$$(\nabla \cdot \mathbf{u}_h - \tfrac{1}{\kappa} p_h, q_h) + (\nabla \cdot \widetilde{\mathbf{u}}, q_h) = 0 \qquad \forall\, q_h \in \mathcal{Q}_h \tag{19}$$

$$(p_h, \nabla \cdot \widetilde{\mathbf{v}}) + (\mathbf{s}(\mathbf{u}_h + \widetilde{\mathbf{u}}), \nabla^s \widetilde{\mathbf{v}}) = l(\widetilde{\mathbf{v}}) \qquad \forall\, \widetilde{\mathbf{v}} \in \widetilde{\mathcal{V}}_0 \tag{20}$$

Remark 3 *Note that due to the fact that the subscale associated to the pressure field has been assumed to be zero, the variational equation associated to the pressure subgrid scale in (17) leads to a zero identity.*

Time discrete variational multiscale form. Consider a time discretization of the time interval of interest $\mathbb{I} = [0, T]$, being $[t_n, t_{n+1}]$ a typical discrete subinterval. We will denote as $(\cdot)_n$ and $(\cdot)_{n+1}$ the time discrete values of the variable $(\cdot)$ at the times t_n and t_{n+1}, respectively. Then the time discrete variational multiscale formulation (16) and (17) can be written as: find $(\mathbf{u}_{h,n+1}, p_{h,n+1}) \in \mathcal{W}_h$ and $(\widetilde{\mathbf{u}}_{n+1}, 0) \in \widetilde{\mathcal{W}}$ such that:

$$\begin{aligned} (p_{h,n+1}, \nabla \cdot \mathbf{v}_h) + (\mathbf{s}\,(\mathbf{u}_{h,n+1}+\widetilde{\mathbf{u}}_{n+1}), \nabla^s \mathbf{v}_h) &= l_{n+1}(\mathbf{v}_h) \quad \forall\ \mathbf{v}_h \in \mathcal{V}_{h,0} \quad (21) \\ (\nabla \cdot \mathbf{u}_{h,n+1} - \tfrac{1}{\kappa} p_{h,n+1}, q_h) + (\nabla \cdot \widetilde{\mathbf{u}}_{n+1}, q_h) &= 0 \qquad\qquad \forall\ q_h \in \mathcal{Q}_h \quad (22) \end{aligned}$$

$$(p_{h,n+1}, \nabla \cdot \widetilde{\mathbf{v}}) + (\mathbf{s}\,(\mathbf{u}_{h,n+1}+\widetilde{\mathbf{u}}_{n+1}), \nabla^s \widetilde{\mathbf{v}}) = l_{n+1}(\widetilde{\mathbf{v}}) \qquad \forall\ \widetilde{\mathbf{v}} \in \widetilde{\mathcal{V}}_0 \qquad (23)$$

where $l_{n+1}(\mathbf{v}_h) := (\mathbf{f}, \mathbf{v}_h) + \left(\overline{\mathbf{t}}_{n+1}, \mathbf{v}_h\right)_{\partial\Omega}$ and $l_{n+1}(\widetilde{\mathbf{v}}) := (\mathbf{f}, \widetilde{\mathbf{v}}) + \left(\overline{\mathbf{t}}_{n+1}, \widetilde{\mathbf{v}}\right)_{\partial\Omega}$. Note that the last equation represents an infinite-dimensional variational form for the subgrid scales.

Proposition 4 Stress split. Linearization of the deviatoric stress tensor. *Consider the linearization of the deviatoric stress term* $\mathbf{s}\,(\mathbf{u}_{h,n+1}+\widetilde{\mathbf{u}}_{n+1})$. *Using a Taylor series expansion about the displacement solution provided by the finite element approximation* $\mathbf{u}_{h,n+1}$ *and keeping only the linear terms, yields*

$$\mathbf{s}\,(\mathbf{u}_{h,n+1}+\widetilde{\mathbf{u}}_{n+1}) = \mathbf{s}\,(\mathbf{u}_{h,n+1}) + D\mathbf{s}\,(\mathbf{u}_{h,n+1}) \cdot \nabla^s \widetilde{\mathbf{u}}_{n+1} \qquad (24)$$

where the directional derivative $D\mathbf{s}\,(\mathbf{u}_{h,n+1}) \cdot \nabla^s \widetilde{\mathbf{u}}_{n+1}$ *takes the form*

$$D\mathbf{s}\,(\mathbf{u}_{h,n+1}) \cdot \nabla^s \widetilde{\mathbf{u}}_{n+1} = \mathbf{c}^{dev}_{h,n+1} : \nabla^s \widetilde{\mathbf{u}}_{n+1} \qquad (25)$$

and $\mathbf{c}^{dev}_{h,n+1}$ *denotes the deviatoric part of the consistent (algorithmic) tangent moduli [39]. Substituting (25) into (24) yields*

$$\boxed{\mathbf{s}\,(\mathbf{u}_{h,n+1}+\widetilde{\mathbf{u}}_{n+1}) = \mathbf{s}\,(\mathbf{u}_{h,n+1}) + \mathbf{c}^{dev}_{h,n+1} : \nabla^s \widetilde{\mathbf{u}}_{n+1}} \qquad (26)$$

Therefore, we consider an additive split of the deviatoric stress $\mathbf{s}_{n+1} := \mathbf{s}\,(\mathbf{u}_{h,n+1}+\widetilde{\mathbf{u}}_{n+1})$ *at time step* $n+1$ *into a finite element approximation term* $\mathbf{s}_{h,n+1} := \mathbf{s}\,(\mathbf{u}_{h,n+1})$ *and a linear term of the subgrid scales* $\widetilde{\mathbf{s}}_{n+1} := \widetilde{\mathbf{s}}\,(\mathbf{u}_{h,n+1}, \widetilde{\mathbf{u}}_{n+1})$ *which can not be captured by the finite element approximation*

$$\boxed{\mathbf{s}_{n+1} := \mathbf{s}_{h,n+1} + \widetilde{\mathbf{s}}_{n+1}} \qquad (27)$$

where

$$\begin{aligned} \mathbf{s}_{n+1} &= \mathbf{s}\,(\mathbf{u}_{h,n+1}+\widetilde{\mathbf{u}}_{n+1}) \quad (28) \\ \mathbf{s}_{h,n+1} &= \mathbf{s}\,(\mathbf{u}_{h,n+1}) = 2\mu\,\mathrm{dev}\left[\nabla^s \mathbf{u}_{h,n+1} - \boldsymbol{\varepsilon}^p_{h,n+1}\right] \quad (29) \\ \widetilde{\mathbf{s}}_{n+1} &= \mathbf{c}^{dev}_{h,n+1} : \nabla^s \widetilde{\mathbf{u}}_{n+1} \quad (30) \end{aligned}$$

Remark 5 *The stress tensor associated to the subgrid scales* $\widetilde{\mathbf{s}}\left(\mathbf{u}_{h,n+1},\widetilde{\mathbf{u}}_{n+1}\right)$*, which in general will be a function of the current displacements provided by the finite element solution, should be viewed as an* incremental *perturbation relative to the current stress tensor solution provided by the finite element approximation.*

Using the additive split of the deviatoric stress tensor $\mathbf{s}_{n+1}$, substituting (27) into the time discrete variational forms (21), (22), (23), the time discrete variational multiscale formulation (16) and (17) can be written as: find $(\mathbf{u}_{h,n+1}, p_{h,n+1}) \in \mathcal{W}_h$ and $(\widetilde{\mathbf{u}}_{n+1}, 0) \in \widetilde{\mathcal{W}}$ such that:

$$\begin{aligned}(p_{h,n+1}, \nabla\cdot\mathbf{v}_h) + (\mathbf{s}_{h,n+1}, \nabla^s\mathbf{v}_h) + (\widetilde{\mathbf{s}}_{n+1}, \nabla^s\mathbf{v}_h) &= l_{n+1}\left(\mathbf{v}_h\right) \;\; \forall\, \mathbf{v}_h \in \mathcal{V}_{h,0} \quad (31)\\ (\nabla\cdot\mathbf{u}_{h,n+1} - \tfrac{1}{\kappa}p_{h,n+1}, q_h) + (\nabla\cdot\widetilde{\mathbf{u}}_{n+1}, q_h) &= 0 \qquad\qquad \forall\, q_h \in \mathcal{Q}_h \quad (32)\end{aligned}$$

$$(p_{h,n+1}, \nabla\cdot\widetilde{\mathbf{v}}) + (\mathbf{s}_{h,n+1}, \nabla^s\widetilde{\mathbf{v}}) + (\widetilde{\mathbf{s}}_{n+1}, \nabla^s\widetilde{\mathbf{v}}) = l_{n+1}\left(\widetilde{\mathbf{v}}\right) \quad \forall\, \widetilde{\mathbf{v}} \in \widetilde{\mathcal{V}}_0 \qquad (33)$$

The goals now are twofold. First, to find an approximate solution for the (displacement) subgrid scales within the infinite-dimensional variational problem (33). For this, the infinite-dimensional space of the subgrid scales will be approximated by a finite-dimensional space which, within the OSGS method, will be the orthogonal space to the finite element space. Second, to substitute the approximate solution for the subgrid scales into the finite-dimensional variational problem given by (31) and (32).

3.2 Orthogonal Subgrid Scales (OSGS)

Algorithmic variational form for the subgrid scales. Integrating by parts *within each element* the first two terms of the left-hand-side of (33) and taking into account the equilibrium of (exact) tractions at the interelement boundaries, yields

$$\sum_{e=1}^{n_{elm}} (\widetilde{\mathbf{s}}_{n+1}, \nabla^s\widetilde{\mathbf{v}})|_{\Omega_e} = \sum_{e=1}^{n_{elm}} (\nabla p_{h,n+1} + \nabla\cdot\mathbf{s}_{h,n+1} + \mathbf{f}, \widetilde{\mathbf{v}})|_{\Omega_e} \quad \forall\, \widetilde{\mathbf{v}} \in \widetilde{\mathcal{V}}_0$$

which at the *element level* yields,

$$(\widetilde{\mathbf{s}}_{n+1}, \nabla^s\widetilde{\mathbf{v}})|_{\Omega_e} = (\nabla p_{h,n+1} + \nabla\cdot\mathbf{s}_{h,n+1} + \mathbf{f}, \widetilde{\mathbf{v}})|_{\Omega_e} \quad \forall\, \widetilde{\mathbf{v}} \in \widetilde{\mathcal{V}}_0 \qquad (34)$$

where the right-hand side term represents the variational form of the residual of the momentum balance equation given by the finite element approximation.

Table 1. Hyperelastic J2-flow model at small deformations

i. Additive split of strains

$\boldsymbol{\varepsilon}(\mathbf{u}) = \boldsymbol{\varepsilon}^e(\mathbf{u}) + \boldsymbol{\varepsilon}^p(\mathbf{u})$

ii. Free energy with uncoupled volumetric and deviatoric contributions

$\psi = \frac{1}{2}\kappa\,\mathrm{tr}^2[\boldsymbol{\varepsilon}(\mathbf{u})] + \mu\,\mathrm{dev}^2[\boldsymbol{\varepsilon}^e(\mathbf{u})] + \frac{1}{2}H\xi^2 + \frac{1}{3}\overline{H}\,\|\boldsymbol{\xi}\|^2$

iii. Mixed elastic and hardening response

$\sigma(\mathbf{u},p) = p\mathbf{1} + \mathbf{s}, \quad p = \kappa\,\mathrm{tr}[\boldsymbol{\varepsilon}(\mathbf{u})], \quad \mathbf{s}(\mathbf{u}) = 2\mu\,\mathrm{dev}[\boldsymbol{\varepsilon}^e(\mathbf{u})]$

$q = -H\xi, \quad \overline{\mathbf{q}} = -\frac{2}{3}\overline{H}\boldsymbol{\xi}$

iv. Von Mises yield condition

$\phi(\mathbf{s}, q, \overline{\mathbf{q}}) := \|\mathbf{s} - \overline{\mathbf{q}}\| - \sqrt{\frac{2}{3}}(\sigma_0 - q) \leqslant 0$

v. Associative flow rule

$\dot{\boldsymbol{\varepsilon}}^p = \gamma\ \mathbf{n}, \quad \dot{\xi} = \gamma\sqrt{\frac{2}{3}}, \quad \dot{\boldsymbol{\xi}} = -\gamma\ \mathbf{n}; \quad \mathbf{n} = \frac{\mathbf{s}-\overline{\mathbf{q}}}{\|\mathbf{s}-\overline{\mathbf{q}}\|}$

vi. Kuhn-Tucker loading/unloading conditions

$\gamma \geqslant 0, \quad \phi \leqslant 0, \quad \gamma\phi = 0$

vii. Consistency condition

$\gamma\dot{\phi} = 0 \quad \text{if} \quad \phi = 0$

Table 1: Hyperelastic J2-flow model at small deformations

Algorithm approximation of the stabilization parameters matrix. Consider now a (inverse) stabilization matrix $\boldsymbol{\tau}_{e,n+1}^{-1}$ such that the following variational approximation holds for the subgrid scales *at the element level*

$$(\widetilde{\mathbf{s}}_{n+1}, \nabla^s\widetilde{\mathbf{v}})|_{\Omega_e} := \left(\boldsymbol{\tau}_{e,n+1}^{-1}\widetilde{\mathbf{u}}_{n+1}, \widetilde{\mathbf{v}}\right)\big|_{\Omega_e} \qquad \forall\ \widetilde{\mathbf{v}} \in \widetilde{\mathcal{V}}_0 \tag{35}$$

which, using the algorithmic approximation for the constitutive equation for the subgrid scales given by 30, yields

$$\left(\mathbf{c}_{h,n+1}^{dev} : \nabla^s\widetilde{\mathbf{u}}_{n+1}, \nabla^s\widetilde{\mathbf{v}}\right)\big|_{\Omega_e} := \left(\boldsymbol{\tau}_{e,n+1}^{-1}\widetilde{\mathbf{u}}_{n+1}, \widetilde{\mathbf{v}}\right)\big|_{\Omega_e} \qquad \forall\ \widetilde{\mathbf{v}} \in \widetilde{\mathcal{V}}_0 \tag{36}$$

Consider now a J2-plastic flow with linear isotropic and kinematic hardening. A summary of the J2-plastic flow model is shown in Table 1. Table 2 shows the main steps involved in the radial return mapping algorithm and consistent tangent elastoplastic moduli [39]. Assuming plastic loading, the deviatoric part of the consistent (algorithmic) tangent elastoplastic moduli $\mathbf{c}_{h,n+1}^{dev}$ takes the form (see Table 2) [39]:

$$\mathbf{c}_{h,n+1}^{dev} = 2\mu\ \theta_{n+1}(\mathbb{I} - \tfrac{1}{3}\mathbf{1}\otimes\mathbf{1}) - 2\mu\ \overline{\theta}_{n+1}\mathbf{n}_{n+1}\otimes\mathbf{n}_{n+1} \tag{37}$$

Table 2. Hyperelastic J2-flow model at small deformations
Radial return mapping algorithm. Linear isotropic/kinematic hardening
Step 1. Database and initial data
Given the database $\{\boldsymbol{\varepsilon}_n^p, \xi_n, \boldsymbol{\xi}_n\}$ at time t_n and
prescribed displacement $\{\mathbf{u}_{n+1}\}$, such that $\boldsymbol{\varepsilon}_{n+1} = \nabla^s \mathbf{u}_{n+1}$
Step 2. Trial elastic state
$\mathbf{s}_{n+1}^{trial} := 2\mu \operatorname{dev}\left[\boldsymbol{\varepsilon}_{n+1} - \boldsymbol{\varepsilon}_n^p\right], \quad q_{n+1}^{trial} := -H\xi_n, \quad \overline{\mathbf{q}}_{n+1}^{trial} := -\frac{2}{3}\overline{H}\boldsymbol{\xi}_n$
$f_{n+1}^{trial} := \left\|\mathbf{s}_{n+1}^{trial} - \overline{\mathbf{q}}_{n+1}^{trial}\right\| - \sqrt{\frac{2}{3}}\left(\sigma_0 - q_{n+1}^{trial}\right),$
$\mathbf{n}_{n+1} = \left(\mathbf{s}_{n+1}^{trial} - \overline{\mathbf{q}}_{n+1}^{trial}\right) / \left\|\mathbf{s}_{n+1}^{trial} - \overline{\mathbf{q}}_{n+1}^{trial}\right\|$
Step 3. Check for plastic loading
IF $f_{n+1}^{trial} \leqslant 0$ THEN
Set $(\cdot)_{n+1} := (\cdot)_{n+1}^{trial}$ and EXIT
END IF
Step 4. Radial return mapping
$\mathbf{s}_{n+1} := 2\mu\ \theta_{n+1}\mathbf{s}_{n+1}^{trial}, \quad \theta_{n+1} := 1 - 2\mu\frac{\gamma_{n+1}}{\left\|\mathbf{s}_{n+1}^{trial} - \overline{\mathbf{q}}_{n+1}^{trial}\right\|}, \quad \gamma_{n+1} = \frac{f_{n+1}^{trial}/(2\mu)}{1+(H+\overline{H})/(3\mu)}$
Step 5. Update database
$\boldsymbol{\varepsilon}_{n+1}^p = \boldsymbol{\varepsilon}_n^p + \gamma_{n+1}\mathbf{n}_{n+1}, \quad \xi_{n+1} = \xi_n + \gamma_{n+1}\sqrt{\frac{2}{3}}, \quad \boldsymbol{\xi}_{n+1} = \boldsymbol{\xi}_n - \gamma_{n+1}\mathbf{n}_{n+1}$
Step 6. Consistent elastoplastic tangent moduli
$\mathbb{C}_{n+1} = \kappa\ \mathbf{1}\otimes\mathbf{1} + 2\mu\ \theta_{n+1}\left[\mathbb{I} - \frac{1}{3}\mathbf{1}\otimes\mathbf{1}\right] - 2\mu\ \overline{\theta}_{n+1}\mathbf{n}_{n+1}\otimes\mathbf{n}_{n+1}$
$\theta_{n+1} := 1 - 2\mu\frac{\gamma_{n+1}}{\left\|\mathbf{s}_{n+1}^{trial} - \overline{\mathbf{q}}_{n+1}^{trial}\right\|}, \quad \overline{\theta}_{n+1} = 1/\left(1 + \left(H + \overline{H}\right)/(3\mu)\right) - (1 - \theta_{n+1})$

Table 2: Hyperelastic J2-flow model at small deformations. Radial return mapping algorithm. Linear isotropic/kinematic hardening

Proposition 6 Algorithmic approximation of the scalar stabilization parameter. *In order to introduce an approximate solution for the subgrid scales* $\widetilde{\mathbf{u}}_{n+1}$*, the following simple scalar approximation to the constitutive equation for the subgrid scales is considered [6]*

$$\widetilde{\mathbf{s}}_{n+1} := \mathbf{c}^{dev}_{h,n+1} : \nabla^s \widetilde{\mathbf{u}}_{n+1} \approx 2\widetilde{\mu}_{n+1} \operatorname{dev}\left[\nabla^s \widetilde{\mathbf{u}}_{n+1}\right] \tag{38}$$

where the consistent elastoplastic moduli has been taken as

$$\mathbf{c}^{dev}_{h,n+1} \approx 2\widetilde{\mu}_{n+1}(\mathbb{I} - \tfrac{1}{3}\mathbf{1} \otimes \mathbf{1})$$

and the (secant) subgrid scale shear modulus for plastic loading is defined as [6]

$$\widetilde{\mu}_{n+1} = \mu \, \frac{\left\|\operatorname{dev}[\boldsymbol{\varepsilon}^e_{h,n+1}]\right\|}{\|\operatorname{dev}[\boldsymbol{\varepsilon}_{h,n+1}]\|} \tag{39}$$

Substituting (38) into (36) yields the following variational approximation for the subscales at the element level

$$\left(\boldsymbol{\tau}^{-1}_{e,n+1}\widetilde{\mathbf{u}}_{n+1}, \widetilde{\mathbf{v}}\right)\big|_{\Omega_e} := \left(2\widetilde{\mu}_{n+1} \operatorname{dev}\left[\nabla^s \widetilde{\mathbf{u}}_{n+1}\right], \nabla^s \widetilde{\mathbf{v}}\right)\big|_{\Omega_e} \quad \forall\ \widetilde{\mathbf{v}} \in \widetilde{\mathcal{V}}_0 \tag{40}$$

where the inverse of the (scalar) stabilization parameter $\tau_{e,n+1}$ *is locally (at the element level) defined at time* $n+1$ *as [6]:*

$$\boxed{\tau^{-1}_{e,n+1} = \tfrac{2\widetilde{\mu}_{n+1}}{ch^2_e}} \tag{41}$$

where c *is a mesh-size independent constant to be determined.*

Remark 7 *For elastic loading/unloading the subgrid scale shear module* $\widetilde{\mu}_{n+1}$ *remains constant and takes the same value as the shear modulus* μ *[11], [44].*

Subgrid Scales. Algebraic Subgrid Scales (ASGS) and Orthogonal Subgrid Scales (OSGS). Using (38), (41), (35) and (34) the following variational approximation for the subscales *at the element level* holds

$$(\widetilde{\mathbf{u}}_{n+1}, \widetilde{\mathbf{v}})|_{\Omega_e} = (\boldsymbol{\tau}_{e,n+1}(\nabla p_{h,n+1} + \nabla \cdot \mathbf{s}_{h,n+1} + \mathbf{f}), \widetilde{\mathbf{v}})|_{\Omega_e} \quad \forall\ \widetilde{\mathbf{v}} \in \widetilde{\mathcal{V}}_0$$

and the subgrid scales can be approximated as

$$\boxed{\widetilde{\mathbf{u}}_{n+1} = \tau_{e,n+1}\left(\nabla p_{h,n+1} + \nabla \cdot \mathbf{s}_{h,n+1} + \mathbf{f}\right) + \mathbf{v}_{h,ort}}$$

where $\mathbf{v}_{h,ort} \in \widetilde{\mathcal{W}}^{\perp}$ belongs to the orthogonal space of the subscales. Here different options are available to approximate the subscales, according to

the expression chosen for $\mathbf{v}_{h,ort}$. Consider the following two options, leading to the so called Algebraic Subgrid Scales (ASGS) and Orthogonal Subgrid Scales (OSGS) methods, respectively.

Algebraic Subgrid Scales Method (ASGS). Within the ASGS method, we take $\mathbf{v}_{h,ort} = \mathbf{0}$ and the subgrid scale associated to the displacement field is approximated as

$$\boxed{\widetilde{\mathbf{u}}_{n+1} = \tau_{e,n+1} \left(\nabla p_{h,n+1} + \nabla \cdot \mathbf{s}_{h,n+1} + \mathbf{f} \right)}$$

Note that within the ASGS, the subscales can be viewed as proportional to the residual of the momentum balance equation provided by the finite element solution.

Orthogonal Subgrid Scales Method (OSGS). Within the OSGS method, we take $\mathbf{v}_{h,ort} = -\tau_{e,n+1} P_h \left(\nabla p_{h,n+1} + \nabla \cdot \mathbf{s}_{h,n+1} + \mathbf{f} \right)$, where $P_h(\cdot)$ represents the L_2 projection onto the finite element space $\mathcal{W}_h$, and the subgrid scale associated to the displacement field is approximated as

$$\boxed{\widetilde{\mathbf{u}}_{n+1} = \tau_{e,n+1} P_h^{\perp} \left(\nabla p_{h,n+1} + \nabla \cdot \mathbf{s}_{h,n+1} + \mathbf{f} \right)}$$

where $P_h^{\perp}(\cdot) = (\cdot) - P_h(\cdot)$ is the L_2 orthogonal projection onto $\mathcal{W}_h^{\perp}$. Note that within the OSGS we are implicitly considering that $\widetilde{\mathcal{W}} \approx \mathcal{W}_h^{\perp}$, i.e., we are taking the orthogonal space to the finite element solution space as space of the subgrid scales. In this work we will adopt the OSGS method as the variational multiscale stabilization method.

Remark 8 *We will assume that the body forces per unit volume belongs to the finite element solution space, i.e.,* $P_h^{\perp}(\mathbf{f}) = \mathbf{0}$. *Furthermore, for linear elements the deviatoric stress tensor is constant within the elements and therefore the orthogonal projection onto the finite element space of the divergence of the deviatoric stress tensor is zero, i.e.,* $P_h^{\perp}(\nabla \cdot \mathbf{s}_{h,n+1}) = \mathbf{0}$. *For higher order elements, we will still assume that this contribution is negligible and thus, that the following approximation* $P_h^{\perp}(\nabla \cdot \mathbf{s}_{h,n+1}) = \mathbf{0}$ *holds. Then, the approximation at the element level for the subscales using the OSGS method leads to the following simple expression*

$$\boxed{\widetilde{\mathbf{u}}_{n+1} = \tau_{e,n+1} P_h^{\perp} \left(\nabla p_{h,n+1} \right)} \tag{42}$$

3.3 Discrete stabilized variational form

The goal now is to introduce the approximation found for the subscales using the OSGS method into the finite-dimensional variational problem given by

(31) and (32). Integrating by parts the last term of the left-hand side of (32) *within each element* and *neglecting the interelement boundary terms* or *assuming that the subgrid scales vanish at the element boundaries* (such as for bubble enhancements), the variational stabilized equations (31) and (32) can be written as:

$$(p_{h,n+1}, \nabla \cdot \mathbf{v}_h) + (\mathbf{s}_{h,n+1}, \nabla^s \mathbf{v}_h) + \\ + \sum_{e=1}^{n_{elm}} (\widetilde{\mathbf{s}}_{n+1}, \nabla^s \mathbf{v}_h)|_{\Omega_e} = l_{n+1}(\mathbf{v}_h) \quad \forall\, \mathbf{v}_h \in \mathcal{V}_{h,0}$$

$$\left(\nabla \cdot \mathbf{u}_{h,n+1} - \tfrac{1}{\kappa} p_{h,n+1}, q_h\right) - \sum_{e=1}^{n_{elm}} (\widetilde{\mathbf{u}}_{n+1}, \nabla q_h)|_{\Omega_e} = 0 \quad \forall\, q_h \in \mathcal{Q}_h$$

Using the constitutive equation (38), integrating now by parts the last term of the left-hand side of (31) *within each element* and *neglecting the interelement boundary terms* or *assuming that the subgrid scales vanish at the element boundaries* (such as for bubble enhancements), the last term of the left-hand side of (31) can be written *at the element level* as

$$\begin{aligned} (\widetilde{\mathbf{s}}_{n+1}, \nabla^s \mathbf{v}_h)|_{\Omega_e} &= \left(2\widetilde{\mu}_{n+1} \operatorname{dev}\left[\nabla^s \widetilde{\mathbf{u}}_{n+1}\right], \nabla^s \mathbf{v}_h\right)\big|_{\Omega_e} = \\ &= \left(\nabla^s \widetilde{\mathbf{u}}_{n+1}, 2\widetilde{\mu}_{n+1} \operatorname{dev}\left[\nabla^s \mathbf{v}_h\right]\right)\big|_{\Omega_e} = \\ &= -\left(\widetilde{\mathbf{u}}_{n+1}, \nabla \cdot \left(2\widetilde{\mu}_{n+1} \operatorname{dev}\left[\nabla^s \mathbf{v}_h\right]\right)\right)\big|_{\Omega_e} \end{aligned}$$

and, substituting this result into the above variational forms, yields

$$(p_{h,n+1}, \nabla \cdot \mathbf{v}_h) + (\mathbf{s}_{h,n+1}, \nabla^s \mathbf{v}_h) - \\ - \sum_{e=1}^{n_{elm}} \left(\widetilde{\mathbf{u}}_{n+1}, \nabla \cdot \left(2\widetilde{\mu}_{n+1} \operatorname{dev}\left[\nabla^s \mathbf{v}_h\right]\right)\right)\big|_{\Omega_e} = l_{n+1}(\mathbf{v}_h) \qquad \forall\, \mathbf{v}_h \in \mathcal{V}_{h,0} \quad (43)$$

$$\left(\nabla \cdot \mathbf{u}_{h,n+1} - \tfrac{1}{\kappa} p_{h,n+1}, q_h\right) - \sum_{e=1}^{n_{elm}} (\widetilde{\mathbf{u}}_{n+1}, \nabla q_h)|_{\Omega_e} = 0 \qquad \forall\, q_h \in \mathcal{Q}_h \qquad (44)$$

Remark 9 *Note that for linear elements* $2\widetilde{\mu}_{n+1} \operatorname{dev}\left[\nabla^s \mathbf{v}_h\right]$ *is constant within the elements and therefore the last term of the left-hand side of (43) is zero, i.e.* $\nabla \cdot \left(2\widetilde{\mu}_{n+1} \operatorname{dev}\left[\nabla^s \mathbf{v}_h\right]\right) = 0$.

Then, using the above Remark and introducing the approximation for the subscales given by (42) the stabilized variational formulation can be written as: find $(\mathbf{u}_{h,n+1}, p_{h,n+1}) \in \mathcal{W}_h$ such that

$$(p_{h,n+1}, \nabla \cdot \mathbf{v}_h) + (\mathbf{s}_{h,n+1}, \nabla^s \mathbf{v}_h) = l_{n+1}(\mathbf{v}_h) \qquad \forall\ \mathbf{v}_h \in \mathcal{V}_{h,0} \tag{45}$$

$$\left(\nabla \cdot \mathbf{u}_{h,n+1} - \tfrac{1}{\kappa} p_{h,n+1}, q_h\right) - \boxed{-\sum_{e=1}^{n_{elm}} \left(\tau_{e,n+1} P_h^{\perp}(\nabla p_{h,n+1}), \nabla q_h\right)\big|_{\Omega_e}} = 0 \qquad \forall\ q_h \in \mathcal{Q}_h \tag{46}$$

Remark 10 *Note that (45), (46) correspond to the time discrete counterpart of the discrete stabilized variational problem defined as: find* $\mathbf{U}_h \in \mathcal{W}_h$ *such that for any* $\mathbf{V}_h \in \mathcal{W}_{h,0}$

$$\boxed{B_{stab}(\mathbf{U}_h, \mathbf{V}_h) = L_{stab}(\mathbf{V}_h)}$$

where the OSGS stabilized (mesh-dependent) forms $B_{stab}(\mathbf{U}_h, \mathbf{V}_h)$ *and* $L_{stab}(\mathbf{V}_h)$ *can be written as*

$$\boxed{B_{stab}(\mathbf{U}_h, \mathbf{V}_h) := B(\mathbf{U}_h, \mathbf{V}_h) - \sum_{e=1}^{n_{elm}} \left(\tau_{e,n+1} P_h^{\perp}(\nabla p_{h,n+1}), \nabla q_h\right)\big|_{\Omega_e}}$$

$$\boxed{L_{stab}(\mathbf{V}_h) := L(\mathbf{V}_h)}$$

Set $\Pi_{h,n+1} := P_h(\nabla p_{h,n+1})$ as the projection of the pressure gradient onto the finite element space $\mathcal{W}_h$. Let $\Upsilon = \mathbf{H}^1$ and $\Upsilon_h \subset \Upsilon$ be the space of the pressure gradient projection and its finite element associated subspace, respectively. Then, taking $\Pi_{h,n+1} \in \Upsilon_h$ as an additional independent continuous variable, the orthogonal projection of the discrete pressure gradient can be written as $P_h^{\perp}(\nabla p_{h,n+1}) := \nabla p_{h,n+1} - \Pi_{h,n+1}$ and the following variational form holds

$$(\nabla p_{h,n+1}, \boldsymbol{\eta}_h)|_{\Omega_e} - (\Pi_{h,n+1}, \boldsymbol{\eta}_h)|_{\Omega_e} = 0 \qquad \forall\ \boldsymbol{\eta}_h \in \mathcal{V}_{h,0}$$

Finally, introducing the discrete pressure gradient projection as a third continuous independent variable, the stabilized variational problem can be written as: find $(\mathbf{u}_{h,n+1}, p_{h,n+1}, \Pi_{h,n+1}) \in \mathcal{V}_h \times \mathcal{Q}_h \times \Upsilon_h$ such that:

$$(p_{h,n+1}, \nabla \cdot \mathbf{v}_h) + (\mathbf{s}_{h,n+1}, \nabla^s \mathbf{v}_h) = l_{n+1}(\mathbf{v}_h) \qquad \forall\ \mathbf{v}_h \in \mathcal{V}_{h,0} \tag{47}$$

$$\left(\nabla \cdot \mathbf{u}_{h,n+1} - \tfrac{1}{\kappa} p_{h,n+1}, q_h\right) - \sum_{e=1}^{n_{elm}} \left(\tau_{e,n+1}(\nabla p_{h,n+1} - \Pi_{h,n+1}), \nabla q_h\right)|_{\Omega_e} = 0 \qquad \forall\ q_h \in \mathcal{Q}_h \tag{48}$$

$$\sum_{e=1}^{n_{elm}} (\nabla p_{h,n+1} - \Pi_{h,n+1}, \boldsymbol{\eta}_h)|_{\Omega_e} = 0 \qquad \forall\ \boldsymbol{\eta}_h \in \mathcal{V}_{h,0} \tag{49}$$

Remark 11 *Note that within the OSGS method the variational stabilization term at the element level* $-(\tau_{e,n+1}(\nabla p_{h,n+1} - \Pi_{h,n+1}), \nabla q_h)|_{\Omega_e}$ *is proportional to the difference between the continuous (projected) and the discontinuous (elemental) pressure gradients, while within the ASGS method the stabilization term is proportional to the residual itself. Therefore, in both cases, the stabilization terms decreases very rapidly upon mesh refinement, but for the OSGS method this happens at a greater rate.*

Remark 12 *Note that in the final stabilized variational problem there is only a remaining stabilization term which appears in (48), while (47) remains the same as for the original problem. On the other hand, a further variable has been introduced. However, as it is shown in the next section, this drawback can easily be overcome to get a computational robust and efficient procedure.*

Remark 13 *To gain further insight on the OSGS stabilization technique, note that the resulting stabilized variational equations could be viewed (assuming that the stabilization parameter is constant) as the variational form of the following stabilized continuous (strong form) equations*

$$\begin{aligned} \nabla p + \nabla \cdot \mathbf{s}(\mathbf{u}) + \mathbf{f} &= \mathbf{0} \quad in \quad \Omega \\ \tfrac{1}{\kappa} p - \nabla \cdot \mathbf{u} - \tau \left(\nabla^2 p - \nabla \cdot \Pi \right) &= 0 \quad in \quad \Omega \\ \nabla p - \Pi &= \mathbf{0} \quad in \quad \Omega \end{aligned}$$

with the appropriate boundary conditions.

3.4 Computational and implementation aspects

Once the finite element discretization has been performed, the matrix form of the algebraic system resulting from the variational system (47), (48), (49) takes the form

$$\mathbb{F}_{dev}(\mathbb{U}_{n+1}) + \mathbb{G}\mathbb{P}_{n+1} = \mathbb{F} \tag{50}$$

$$\mathbb{G}^T \mathbb{U}_{n+1} - (\mathbb{M}_p + \mathbb{L}_{\tau,n+1}) \mathbb{P}_{n+1} + \mathbb{G}^T_{\tau,n+1} \Pi_{n+1} = \mathbf{0} \tag{51}$$

$$\mathbb{G}_{\tau,n+1} \mathbb{P}_{n+1} - \mathbb{M}_{\tau,n+1} \Pi_{n+1} = \mathbf{0} \tag{52}$$

where capital letters $\mathbb{U}_{n+1}$, $\mathbb{P}_{n+1}$ and Π_{n+1} denote the vectors of displacement, pressure and pressure gradient projection nodal unknowns at time step $n+1$, $\mathbb{F}$ denotes the vector of nodal external forces, $\mathbb{F}_{dev}(\mathbb{U}_{n+1})$ denotes the vector

of nodal internal forces arising from the deviatoric stress tensor and $\mathbb{G}$, $\mathbb{G}^T$, $\mathbb{M}_p$, $\mathbb{L}_{\tau,n+1}$, $\mathbb{G}^T_{\tau,n+1}$, $\mathbb{G}_{\tau,n+1}$ and $\mathbb{M}_{\tau,n+1}$ denote the matrices arising from the gradient operator, divergence operator, pressure mass-like, stabilized laplacian operator, stabilized divergence operator, stabilized gradient operator and stabilized displacement mass-like terms, respectively. Note that the stabilization matrices become time-dependent, because the stabilization factor may depend on the displacement unknown $\mathbb{U}_{n+1}$.

Remark 14 *From (52), dropping the $n+1$ subindices to simplify the notation, it should be noted that* formally *expressing the nodal pressure gradient projection vector Π in terms of the nodal pressure unknowns $\mathbb{P}$ and substituting the result $\Pi = \mathbb{M}_\tau^{-1}\mathbb{G}_\tau\mathbb{P}$ into (51) yields*

$$\mathbb{G}^T\mathbb{U} - \left(\mathbb{M}_p + \mathbb{L}_\tau - \mathbb{G}^T_\tau\mathbb{M}_\tau^{-1}\mathbb{G}_\tau\right)\mathbb{P} = \mathbf{0}$$

where $\mathbb{L}_\tau - \mathbb{G}^T_\tau\mathbb{M}_\tau^{-1}\mathbb{G}_\tau$ can be identified as the sought stabilization matrix to be added to the pressure mass-like matrix $\mathbb{M}_p$ to obtain a discrete stabilized constitutive equation for the pressure field. For the exact incompressibility case, the matrix term $\mathbb{M}_p$ drops out and (51) yields

$$\mathbb{G}^T\mathbb{U} - \left(\mathbb{L}_\tau - \mathbb{G}^T_\tau\mathbb{M}_\tau^{-1}\mathbb{G}_\tau\right)\mathbb{P} = \mathbf{0}$$

where $-\left(\mathbb{L}_\tau - \mathbb{G}^T_\tau\mathbb{M}_\tau^{-1}\mathbb{G}_\tau\right)\mathbb{P}$ represents the stabilization term to be added to the discrete incompressibility condition $\mathbb{G}^T\mathbb{U} = \mathbf{0}$.

Remark 15 *It should be noted that condensation of the nodal pressure gradient projection unknowns Π at the element level is not feasible in practice because it is a continuous variable. To perform the condensation at the global level it is not computational efficient because it would yield to a reduced system of equations but with a totally spoiled banded structure.*

A computational efficient and robust solution algorithm can be built up solving for $\mathbb{U}_{n+1}$ and $\mathbb{P}_{n+1}$, within an incremental iterative Newton-Raphson procedure, keeping fixed Π_n from the previous computed time step, using $\mathbb{L}_{\tau,n}$ and $\mathbb{G}^T_{\tau,n}$ (evaluated at time t_n instead of t_{n+1}) and considering the exact linearization of the modified algebraic system

$$\begin{aligned}
\mathbb{F}_{dev}\left(\mathbb{U}_{n+1}\right) + \mathbb{G}\mathbb{P}_{n+1} &= \mathbb{F} \\
\mathbb{G}^T\mathbb{U}_{n+1} - \left(\mathbb{M}_p + \mathbb{L}_{\tau,n}\right)\mathbb{P}_{n+1} &= -\mathbb{G}^T_{\tau,n}\Pi_n
\end{aligned}$$

leading to the following algebraic linear system of equations

$$\begin{aligned}
\mathbb{K}_T^{dev}\left(\mathbb{U}^{(i)}_{n+1}\right)\Delta\mathbb{U}^{(i)}_{n+1} + \mathbb{G}\Delta\mathbb{P}^{(i)}_{n+1} &= -\mathbb{R}_u\left(\mathbb{U}^{(i)}_{n+1}, \mathbb{P}^{(i)}_{n+1}\right) \\
\mathbb{G}^T\Delta\mathbb{U}^{(i)}_{n+1} - \left(\mathbb{M}_p + \mathbb{L}_{\tau,n}\right)\Delta\mathbb{P}^{(i)}_{n+1} &= -\mathbb{R}_p\left(\mathbb{U}^{(i)}_{n+1}, \mathbb{P}^{(i)}_{n+1}\right)
\end{aligned}$$

where the discrete residual vectors $\mathbb{R}_u\left(\mathbb{U}_{n+1}^{(i)}, \mathbb{P}_{n+1}^{(i)}\right)$ and $\mathbb{R}_p\left(\mathbb{U}_{n+1}^{(i)}, \mathbb{P}_{n+1}^{(i)}\right)$ take the form

$$\begin{aligned}
\mathbb{R}_u\left(\mathbb{U}_{n+1}^{(i)}, \mathbb{P}_{n+1}^{(i)}\right) &= \mathbb{F}_{dev}\left(\mathbb{U}_{n+1}^{(i)}\right) + \mathbb{G}\mathbb{P}_{n+1}^{(i)} - \mathbb{F} \\
\mathbb{R}_p\left(\mathbb{U}_{n+1}^{(i)}, \mathbb{P}_{n+1}^{(i)}\right) &= \mathbb{G}^T\mathbb{U}_{n+1}^{(i)} - \left(\mathbb{M}_p + \mathbb{L}_{\tau,n}\right)\mathbb{P}_{n+1}^{(i)} + \mathbb{G}_{\tau,n}^T\Pi_n
\end{aligned}$$

$\mathbb{K}_{T_{n+1}}^{dev}\left(\mathbb{U}_{n+1}^{(i)}\right)$ denote the deviatoric part of the consistent tangent operator, and $\Delta\mathbb{U}_{n+1}^{(i)} := \mathbb{U}_{n+1}^{(i+1)} - \mathbb{U}_{n+1}^{(i)}$ and $\Delta\mathbb{P}_{n+1}^{(i)} := \mathbb{P}_{n+1}^{(i+1)} - \mathbb{P}_{n+1}^{(i)}$ denote the increments of nodal displacement and Kirchhoff pressure unknowns, respectively.

The discrete nodal pressure gradient projection vector at time t_{n+1} is computed as

$$\Pi_{n+1} = \mathbb{M}_{\tau,n+1}^{-1}\mathbb{G}_{\tau,n+1}\mathbb{P}_{n+1}$$

when the converged values for the discrete nodal displacement and pressure vectors $\mathbb{U}_{n+1}$ and $\mathbb{P}_{n+1}$, respectively, have been obtained.

Remark 16 *Computation of the discrete nodal pressure gradient projection vector* Π_{n+1} *can be performed in a straightforward manner by considering a lumped structure of the pressure mass-like matrix* $\mathbb{M}_{\tau,n+1}^{-1}$.

Typical element entries $(\cdot)^{AB}$ corresponding to nodes A and B for the above matrices take the form

$$\begin{aligned}
\mathbb{K}_T^{dev}\big|_{\Omega_e}^{AB} &= \int_{\Omega_e} \mathbf{B}_u^A \mathbf{C}_T^{dev} \mathbf{B}_u^B \, dV_0 \\
\mathbb{G}\big|_{\Omega_e}^{AB} &= \int_{\Omega_e} \nabla N_u^A N_p^B \, dV_0 \\
\mathbb{M}_p\big|_{\Omega_e}^{AB} &= \int_{\Omega_e} \tfrac{1}{\kappa} N_p^A N_p^B \, dV_0 \\
\mathbb{L}_\tau\big|_{\Omega_e}^{AB} &= \int_{\Omega_e} \tau_e (\nabla N_p^A)^T \nabla N_p^B \, dV_0 \\
\mathbb{G}_\tau\big|_{\Omega_e}^{AB} &= \int_{\Omega_e} \tau_e \nabla N_p^A N_p^B \, dV_0 \\
\mathbb{M}_\tau\big|_{\Omega_e}^{AB} &= \int_{\Omega_e} \tau_e N_\Pi^A N_\Pi^B \, dV_0 \, \mathbf{1}
\end{aligned}$$

where N_u^A, N_p^A and N_Π^A denote the interpolation shape functions at node A for the displacement, pressure and pressure gradient projection fields, respectively, ∇N_u^A and ∇N_p^A denote the gradient of the interpolation shape functions at node A for the displacement and pressure fields, respectively, and $\mathbf{B}_u^A$ denotes the interpolation matrix at node A for the infinitesimal strain field.

4 Nearly Incompressibility Problem in Solid Mechanics: Finite Deformation J2 Plasticity

Let us begin introducing some standard notation. Let Ω be an open and bounded domain of $\mathbb{R}^{n_{\text{dim}}}$, where n_{dim} is the number of space dimensions, $\overline{\Omega}$ its closure and Γ its boundary which is considered split into two disjoint sets such that $\Gamma = \overline{\partial\Omega_u \cup \partial\Omega_t}$ and $\partial\Omega_u \cap \partial\Omega_t = \emptyset$. The space of square integrable functions in Ω is denoted by $L^2(\Omega)$ and the space of functions of which its derivatives up to order $m \geq 0$ (integer) belong to $L^2(\Omega)$ by $H^m(\Omega)$. The space $H_0^m(\Omega)$ consists of those functions that belong to $H^m(\Omega)$ and vanish on $\partial\Omega_u$. Bold characters are used to denote vector counterpart of all these spaces. The L^2 inner product in Ω and in $\partial\Omega$ are denoted by $(\cdot,\cdot)$ and $(\cdot,\cdot)_{\partial\Omega}$, respectively. Hereafter, orthogonality will be understood with respect to this product.

4.1 Strong form

Let us consider an elastoplastic (isotropic) material model at finite deformations within the framework of phenomenological models derived from a micromechanical description of single-crystal metal plasticity. An essential feature of this micromechanical description is the introduction of an intermediate local stress-free configuration, relative to which the elastic response of the material is characterized. From a phenomenological standpoint this notion leads to a local multiplicative decomposition of the deformation gradient of the form $\mathbf{F} = \mathbf{F}^e\mathbf{F}^p$, where $\mathbf{F}^e$ and $\mathbf{F}^p$ denote the elastic and plastic deformation gradients, respectively. In addition, in accordance with a standard assumption in metal plasticity, we assume that the plastic flow is isochoric and therefore the following relations hold: $\det[\mathbf{F}^p] = 1$, $J := \det[\mathbf{F}] = \det[\mathbf{F}^e]$. Consistent with the assumptions of isotropy, isochoric plastic flow and the notion of an intermediate stress-free configuration, we characterize the stress response by an uncoupled volumetric/isochoric stored-energy function of the form [39],

$$W\left(J, \overline{\mathbf{b}}^e\right) = U(J) + \overline{W}\left(\overline{\mathbf{b}}^e\right) \tag{53}$$

where the volumetric part $U(J)$ of the stored energy function $W\left(J, \overline{\mathbf{b}}^e\right)$ is a convex function of the determinant of the (elastic) deformation gradient $J := \det[\mathbf{F}]$ and the isochoric part $\overline{W}\left(\overline{\mathbf{b}}^e\right)$ of the stored energy function

$W\left(J,\overline{\mathbf{b}}^{e}\right)$ is a function of the isochoric elastic left Cauchy-Green tensor $\overline{\mathbf{b}}^{e}$ defined as $\overline{\mathbf{b}}^{e}:=J^{-\frac{2}{3}}\mathbf{b}^{e}$, where $\mathbf{b}^{e}=\mathbf{F}^{e}\mathbf{F}^{eT}$ is the elastic left Cauchy-Green tensor. Here we consider the following explicit forms for the volumetric and isochoric parts of the stored-energy function

$$U\left(J\right) = \tfrac{1}{2}\kappa\log^{2}\left(J\right) \tag{54}$$

$$\overline{W}\left(\overline{\mathbf{b}}^{e}\right) = \tfrac{1}{2}\mu\left(\operatorname{tr}\left[\overline{\mathbf{b}}^{e}\right]-3\right) \tag{55}$$

where $\mu>0$ and $\kappa>0$ are interpreted as the shear modulus and the bulk modulus, and $\operatorname{tr}\left[\cdot\right]=\mathbf{1}:\left[\cdot\right]$ denotes the spatial trace operator, where $\mathbf{1}$ is the second order unit tensor.

Following a standard derivation [39], [42] the (mixed) Kirchhoff stress tensor can be written as

$$\boldsymbol{\tau}\left(\mathbf{u},\pi\right) = \pi\mathbf{1}+\mathbf{s}\left(\mathbf{u}\right)$$

where the Kirchhoff pressure $\pi:=\frac{1}{3}\operatorname{tr}\left[\boldsymbol{\tau}(\mathbf{u},\pi)\right]$, to be viewed as an independent variable, and the deviatoric component of the (mixed) Kirchhoff stress tensor $\mathbf{s}\left(\mathbf{u}\right):=\operatorname{dev}\left[\boldsymbol{\tau}(\mathbf{u},\pi)\right]$ take the form

$$\begin{aligned}\pi &= JU'\left(J\right)\\ \mathbf{s}\left(\mathbf{u}\right) &= \mu\operatorname{dev}\left[\overline{\mathbf{b}}^{e}\right]\end{aligned}$$

Note that the uncoupled volumetric/isochoric stored-energy function results in uncoupled volumetric/deviatoric stress response, where $\operatorname{dev}\left[\cdot\right]:=\left(\mathbf{I}-\frac{1}{3}\mathbf{1}\otimes\mathbf{1}\right):\left[\cdot\right]$ is the spatial deviatoric operator and $\mathbf{I}$ is the fourth-order identity tensor. $U'\left(J\right)$ denotes the derivative of $U\left(J\right)$ with respect to J. In what follows, it will be implicitly assumed that $J=J\left(\mathbf{u}\right)$ is a function of the displacement field $\mathbf{u}$.

Appropriate boundary conditions will be taken as $\mathbf{u}=\overline{\mathbf{u}}$ on $\partial\Omega_{u}$ and $\boldsymbol{\tau}\ \mathbf{F}^{-T}\ \mathbf{N}=\overline{\mathbf{t}}^{N}$ on $\partial\Omega_{t}$, where $\overline{\mathbf{u}}:\ \partial\Omega_{u}\rightarrow\mathbb{R}^{n_{\dim}}$ and $\overline{\mathbf{t}}^{N}:\ \partial\Omega_{t}\rightarrow\mathbb{R}^{n_{\dim}}$ are the prescribed displacement and nominal traction vectors, respectively, and $\mathbf{N}$ is the unit outer normal field to $\partial\Omega$. Consider the infinite-dimensional spaces $\mathcal{V}=\left\{\mathbf{u}\in\mathbf{H}^{1}\left(\Omega\right)\mid\mathbf{u}=\overline{\mathbf{u}}\quad\text{on}\quad\partial\Omega_{u}\right\}$ and $\mathcal{Q}=L^{2}\left(\Omega\right)$ for the displacement and Kirchhoff pressure fields, respectively. We shall be interested also in the space $\mathcal{W}=\mathcal{V}\times\mathcal{Q}$. Then the strong form of the mixed formulation for the nearly incompressibility problem in finite deformation solid mechanics consists in finding a displacement field $\mathbf{u}\in\mathcal{V}$ and a Kirchhoff pressure field $\pi\in\mathcal{Q}$ such that

$$J\ \nabla\left(J^{-1}\pi\right)\ +\ J\ \nabla\cdot\left(J^{-1}\mathbf{s}\left(\mathbf{u}\right)\right)+\ \mathbf{f} = \mathbf{0}\quad\text{in}\quad\Omega \tag{56}$$

$$\pi-JU'\left(J\right) = 0\quad\text{in}\quad\Omega \tag{57}$$

where $\mathbf{f}: \Omega \to \mathbb{R}^{n_{\dim}}$ is the prescribed body force per unit reference volume vector, $\nabla(\cdot)$ denotes the spatial gradient operator and $\nabla \cdot (\cdot)$ denotes the spatial divergence operator.

Using an abstract compact notation, the problem defined by (56) and (57) can be written as: find $\mathbf{U} \in \mathcal{W}$ such that

$$\mathcal{L}(\mathbf{U}) = \mathbf{F} \quad \text{in} \quad \Omega \tag{58}$$

where $\mathbf{U}$, $\mathcal{L}(\mathbf{U})$ and $\mathbf{F}$ are defined as

$$\mathbf{U} = \begin{bmatrix} \mathbf{u} \\ \pi \end{bmatrix}, \quad \mathcal{L}(\mathbf{U}) = \begin{bmatrix} -J\,\nabla(J^{-1}\pi) \; - \; J\,\nabla\cdot(J^{-1}\mathbf{s}(\mathbf{u})) \\ -\pi + JU'(J) \end{bmatrix}, \quad \mathbf{F} = \begin{bmatrix} \mathbf{f} \\ 0 \end{bmatrix} \tag{59}$$

4.2 Variational form

Consider the infinite-dimensional space $\mathcal{V}_0 = \mathbf{H}_0^1(\Omega)$. We shall be interested also in the space $\mathcal{W}_0 = \mathcal{V}_0 \times \mathcal{Q}$. Then the variational formulation of the nearly incompressibility problem in solid mechanics defined by (58) can be written as: find $\mathbf{U} \in \mathcal{W}$ such that for any $\mathbf{V} \in \mathcal{W}_0$

$$(\mathcal{L}(\mathbf{U}), \mathbf{V}) = (\mathbf{F}, \mathbf{V}) \tag{60}$$

Using the definitions given in (59) and setting $\mathbf{V} = [\mathbf{v}, q]^T$ the explicit expression for the variational form given by (60) is

$$-(J\,\nabla\left(J^{-1}\pi\right), \mathbf{v}) - (J\,\nabla\cdot\left(J^{-1}\mathbf{s}(\mathbf{u})\right), \mathbf{v}) = (\mathbf{f}, \mathbf{v}) \quad \forall\, \mathbf{v} \in \mathcal{V}_0 \tag{61}$$

$$-(\pi, q) + (JU'(J), q) = 0 \quad \forall\, q \in \mathcal{Q} \tag{62}$$

Integrating by parts the left-hand side of (61), the above variational forms can be written as:

$$\begin{aligned} (\pi, \nabla\cdot\mathbf{v}) + (\mathbf{s}(\mathbf{u}), \nabla^s\mathbf{v}) &= l(\mathbf{v}) \quad \forall\, \mathbf{v} \in \mathcal{V}_0 \\ -(\pi, q) + (JU'(J), q) &= 0 \quad \forall\, q \in \mathcal{Q} \end{aligned}$$

where the operator $l(\mathbf{v}) := (\mathbf{f}, \mathbf{v}) + \left(\overline{\mathbf{t}}^N, \mathbf{v}\right)_{\partial\Omega}$ has been introduced and the fact that $\mathbf{s}(\mathbf{u})$ is a symmetric tensor has been used.

Introducing an abstract compact notation, the variational formulation of the nearly incompressibility problem in solid mechanics given by (60) can be alternatively written as: find $\mathbf{U} \in \mathcal{W}$ such that for any $\mathbf{V} \in \mathcal{W}_0$

$$B(\mathbf{U}, \mathbf{V}) = L(\mathbf{V}) \tag{63}$$

where

$$B(\mathbf{U}, \mathbf{V}) = (\pi, \nabla\cdot\mathbf{v}) + (\mathbf{s}(\mathbf{u}), \nabla^s\mathbf{v}) - (\pi, q) + (JU'(J), q) \tag{64}$$

$$L(\mathbf{V}) = l(\mathbf{v}) \tag{65}$$

4.3 Discrete variational form

The standard Galerkin projection of this variational problem is now straightforward. Let $\mathcal{P}_h$ denote a finite element partition of the domain Ω. The diameter of an element domain $e \in \mathcal{P}_h$ is denoted by h_e and the diameter of the finite element partition by $h = \max\{h_e \mid e \in \mathcal{P}_h\}$. We can now construct conforming finite element spaces $\mathcal{V}_h \subset \mathcal{V}$, $\mathcal{Q}_h \subset \mathcal{Q}$ and $\mathcal{W}_h = \mathcal{V}_h \times \mathcal{Q}_h$ in the usual manner, as well as the corresponding subspaces $\mathcal{V}_{h,0} \subset \mathcal{V}_0$ and $\mathcal{W}_{h,0} = \mathcal{V}_{h,0} \times \mathcal{Q}_h$. In principle, functions in $\mathcal{V}_h$ are continuous, whereas functions in $\mathcal{Q}_h$ not necessarily. Likewise, the polynomial orders of these spaces may be different. Then, the discrete version of the variational problem (63) consists in finding $\mathbf{U}_h \in \mathcal{W}_h$ such that for any $\mathbf{V}_h \in \mathcal{W}_{h,0}$

$$B(\mathbf{U}_h, \mathbf{V}_h) = L(\mathbf{V}_h) \tag{66}$$

Remark 17 *As it is well known, convenient displacement-pressure interpolations, such as equal linear interpolations, turn out to violate the inf-sup or Babuška-Brezzi condition. To circumvent this condition, the idea now is to replace the discrete variational problem (66) by a suitable discrete stabilized variational problem, such that the variational form B is replaced by a possibly mesh dependent variational form B_{stab} with enhanced stability properties. Eventually, the linear form L may be also replaced by a possibly mesh dependent form L_{stab}. This is done in the next sections through the introduction of the subgrid scale method.*

5 Multiscale Formulation of J2 Plasticity Models at Finite Deformations

In this section, a stabilization of the mixed formulation of J2 plasticity models at finite deformations is introduced within the framework of multiscale methods. The variational multiscale form is considered first. Then an approximate solution for the subgrid scales is sought. Within the OSGS method, we are taking the orthogonal space to the finite element solution space as the natural space of the subscales. A suitable nonlinear expression of the (scalar) stabilization parameter is proposed for finite deformation plasticity models. Finally, the finite element projection of the Kirchhoff pressure gradient is introduced as a third independent field and the resulting stabilized multiscale variational forms are derived.

5.1 Variational multiscale form

Multiscale approach. Within the paradigmatic framework of the multiscale methods introduced by Hughes [20], the subgrid scale method seeks to approximate the effect of the component of the continuous solution which can not be captured by the finite element mesh on the discrete finite element solution. The unresolved component is referred to as the *subgrid scale* or *subscale*. Let $\mathcal{W} = \mathcal{W}_h \oplus \widetilde{\mathcal{W}}$, where $\widetilde{\mathcal{W}}$ is any suitable space to complete $\mathcal{W}_h$ in $\mathcal{W}$. Obviously, $\widetilde{\mathcal{W}}$ is an infinite-dimensional space, but once the final method will be formulated, it is approximated by a finite-dimensional space, although we will keep the same symbol for it in order to simplify the notation. We will refer to $\widetilde{\mathcal{W}}$ as the *space of the subgrid scales* or the *space of the subscales*. Likewise, let $\mathcal{W}_0 = \mathcal{W}_{h,0} \oplus \widetilde{\mathcal{W}}_0$, with $\widetilde{\mathcal{W}}_0$ any space to complete $\mathcal{W}_{h,0}$ in $\mathcal{W}_0$. With the above definitions in hand, we consider that there is a component $\widetilde{\mathbf{U}} \in \widetilde{\mathcal{W}}$ of the exact continuous solution $\mathbf{U} \in \mathcal{W}$ which can not be captured by the solution provided by the finite element method $\mathbf{U}_h \in \mathcal{W}_h$, such that

$$\mathbf{U} = \mathbf{U}_h + \widetilde{\mathbf{U}} \tag{67}$$

where for the nearly incompressibility problem in solid mechanics $\mathbf{U}$, $\mathbf{U}_h$ and $\widetilde{\mathbf{U}}$ take the form

$$\mathbf{U} = \begin{bmatrix} \mathbf{u} \\ \pi \end{bmatrix}, \qquad \mathbf{U}_h = \begin{bmatrix} \mathbf{u}_h \\ \pi_h \end{bmatrix}, \qquad \widetilde{\mathbf{U}} = \begin{bmatrix} \widetilde{\mathbf{u}} \\ \widetilde{\pi} \end{bmatrix} \tag{68}$$

where $\mathbf{U}_h$ is the resolved component of the primary variable provided by the finite element solution and may be interpreted as the projection of the exact solution $\mathbf{U}$ onto the finite-dimensional space introduced by the finite element discretization, Therefore $\widetilde{\mathbf{U}}$ is the component of the exact continuous solution which can not be captured by the discrete finite element solution. It is now necessary to introduce some additional finite-dimensional subspaces associated to the previously defined infinite-dimensional spaces.

Variational multiscale approach. Introducing the split of $\mathbf{U}$ given by (67), the variational multiscale formulation of the nearly incompressibility problem in solid mechanics given by (63) can be written as: find $\mathbf{U}_h \in \mathcal{W}_h$ and $\widetilde{\mathbf{U}} \in \widetilde{\mathcal{W}}$ such that:

$$B(\mathbf{U}_h + \widetilde{\mathbf{U}}, \mathbf{V}_h) = L(\mathbf{V}_h) \qquad \forall\ \mathbf{V}_h \in \mathcal{W}_{h,0} \tag{69}$$

$$B(\mathbf{U}_h + \widetilde{\mathbf{U}}, \widetilde{\mathbf{V}}) = L(\widetilde{\mathbf{V}}) \qquad \forall\ \widetilde{\mathbf{V}} \in \widetilde{\mathcal{W}}_0 \tag{70}$$

Assuming that $\widetilde{\pi} = 0$, i.e. that the exact Kirchhoff pressure field may be captured by the finite element solution and therefore the subgrid scale associated to the Kirchhoff pressure is zero, the variational multiscale formulation

given by (69) and (70) can be written as: find $(\mathbf{u}_h, \pi_h) \in \mathcal{W}_h$ and $(\widetilde{\mathbf{u}}, 0) \in \widetilde{\mathcal{W}}$ such that:

$$\begin{aligned} (\pi_h, \nabla \cdot \mathbf{v}_h) + (\mathbf{s}(\mathbf{u}_h + \widetilde{\mathbf{u}}), \nabla^s \mathbf{v}_h) &= l(\mathbf{v}_h) \qquad \forall\, \mathbf{v}_h \in \mathcal{V}_{h,0} \qquad (71) \\ (J(\mathbf{u}_h + \widetilde{\mathbf{u}}) U'(J(\mathbf{u}_h + \widetilde{\mathbf{u}})) - \pi_h, q_h) &= 0 \qquad \forall\, q_h \in \mathcal{Q}_h \qquad (72) \end{aligned}$$

$$(\pi_h, \nabla \cdot \widetilde{\mathbf{v}}) + (\mathbf{s}(\mathbf{u}_h + \widetilde{\mathbf{u}}), \nabla^s \widetilde{\mathbf{v}}) = l(\widetilde{\mathbf{v}}) \qquad \forall\, \widetilde{\mathbf{v}} \in \widetilde{\mathcal{V}}_0 \qquad (73)$$

Note that due to the fact that the subscale associated to the Kirchhoff pressure field has been assumed to be zero, the second equation in (70) leads to a zero identity.

Time discrete variational multiscale form. Consider a time discretization of the time interval of interest $I = [0, T]$, being $[t_n, t_{n+1}]$ a typical discrete subinterval. We will denote as $(\cdot)_n$ and $(\cdot)_{n+1}$ the time discrete values of the variable $(\cdot)$ at the times t_n and t_{n+1}, respectively. Then the time discrete variational multiscale formulation (69) and (70) can be written as: find $(\mathbf{u}_{h,n+1}, \pi_{h,n+1}) \in \mathcal{W}_h$ and $(\widetilde{\mathbf{u}}_{n+1}, 0) \in \widetilde{\mathcal{W}}$ such that:

$$(\pi_{h,n+1}, \nabla \cdot \mathbf{v}_h) + (\mathbf{s}(\mathbf{u}_{h,n+1} + \widetilde{\mathbf{u}}_{n+1}), \nabla^s \mathbf{v}_h) = l_{n+1}(\mathbf{v}_h) \;\; \forall\, \mathbf{v}_h \in \mathcal{V}_{h,0} \qquad (74)$$

$$(J(\mathbf{u}_{h,n+1} + \widetilde{\mathbf{u}}_{n+1}) U'(J(\mathbf{u}_{h,n+1} + \widetilde{\mathbf{u}}_{n+1})) - \pi_{h,n+1}, q_h) = 0 \qquad \forall\, q_h \in \mathcal{Q}_h \qquad (75)$$

$$(\pi_{h,n+1}, \nabla \cdot \widetilde{\mathbf{v}}) + (\mathbf{s}(\mathbf{u}_{h,n+1} + \widetilde{\mathbf{u}}_{n+1}), \nabla^s \widetilde{\mathbf{v}}) = l_{n+1}(\widetilde{\mathbf{v}}) \qquad \forall\, \widetilde{\mathbf{v}} \in \widetilde{\mathcal{V}} \qquad (76)$$

where $l_{n+1}(\mathbf{v}_h) := (\mathbf{f}, \mathbf{v}_h) + \left(\overline{\mathbf{t}}^N_{n+1}, \mathbf{v}_h\right)_{\partial\Omega}$ and $l_{n+1}(\widetilde{\mathbf{v}}) := (\mathbf{f}, \widetilde{\mathbf{v}}) + \left(\overline{\mathbf{t}}^N_{n+1}, \widetilde{\mathbf{v}}\right)_{\partial\Omega}$. Note that the last equation represents an infinite-dimensional variational form for the subgrid scales.

Proposition 18 Deviatoric stress and Kirchhoff pressure split. *Consider the linearization of* $J(\mathbf{u}_{h,n+1} + \widetilde{\mathbf{u}}_{n+1}) U'(J(\mathbf{u}_{h,n+1} + \widetilde{\mathbf{u}}_{n+1}))$ *and* $\mathbf{s}(\mathbf{u}_{h,n+1} + \widetilde{\mathbf{u}}_{n+1})$. *To deal with this linearizations we will perform a Taylor series expansion about the current displacement solution provided by the finite element aproximation and keep only the linear terms in the subgrid scales.*

Linearization of $[JU'(J)]|_{\mathbf{u}_{h,n+1} + \widetilde{\mathbf{u}}_{n+1}}$. *The linearization of the Kirchhoff pressure* $[JU'(J)]|_{\mathbf{u}_{h,n+1} + \widetilde{\mathbf{u}}_{n+1}}$ *yields*

$$[JU'(J)]|_{\mathbf{u}_{h,n+1} + \widetilde{\mathbf{u}}_{n+1}} = [JU'(J)]|_{\mathbf{u}_{h,n+1}} + D[JU'(J)]|_{\mathbf{u}_{h,n+1}} \cdot \widetilde{\mathbf{u}}_{n+1}$$

where the directional derivative $D\left[JU'\left(J\right)\right]\big|_{\mathbf{u}_{h,n+1}} \cdot \widetilde{\mathbf{u}}_{n+1}$ *along the direction* $\widetilde{\mathbf{u}}_{n+1}$ *evaluated at* $\mathbf{u}_{h,n+1}$ *takes the form*

$$D\left[JU'\left(J\right)\right]\big|_{\mathbf{u}_{h,n+1}} \cdot \widetilde{\mathbf{u}}_{n+1} = \left[JU'\left(J\right)\right]'\big|_{\mathbf{u}_{h,n+1}} DJ\big|_{\mathbf{u}_{h,n+1}} \cdot \widetilde{\mathbf{u}}_{n+1}$$

and, taking into account that the directional derivative $DJ\big|_{\mathbf{u}_{h,n+1}} \cdot \widetilde{\mathbf{u}}_{n+1}$ *takes the form*

$$DJ\big|_{\mathbf{u}_{h,n+1}} \cdot \widetilde{\mathbf{u}}_{n+1} = J\left(\mathbf{u}_{h,n+1}\right) \nabla \cdot \widetilde{\mathbf{u}}_{n+1}$$

where $\nabla \cdot (\cdot)$ *denotes the spatial divergence operator, the linearization of the (exact) volumetric term* $\left[JU'\left(J\right)\right]\big|_{\mathbf{u}_{h,n+1}+\widetilde{\mathbf{u}}_{n+1}}$ *yields*

$$\boxed{\left[JU'\left(J\right)\right]\big|_{\mathbf{u}_{h,n+1}+\widetilde{\mathbf{u}}_{n+1}} = \left[JU'\left(J\right)\right]\big|_{\mathbf{u}_{h,n+1}} + \left[JU'\left(J\right)\right]'\big|_{\mathbf{u}_{h,n+1}} J\big|_{\mathbf{u}_{h,n+1}} \nabla \cdot \widetilde{\mathbf{u}}_{n+1}}$$

For the explicit form of the volumetric part of the stored-energy function given by (54), the following relations hold $JU'\left(J\right) = \kappa \log\left(J\right)$, $\left[JU'\left(J\right)\right]' = \kappa\, J^{-1}$ *and, introducing the short notation* $J_{n+1} := J\big|_{\mathbf{u}_{h,n+1}+\widetilde{\mathbf{u}}_{n+1}}$ *and* $J_{h,n+1} := J\big|_{\mathbf{u}_{h,n+1}}$*, the linearization yields*

$$\boxed{\log J_{n+1} = \log J_{h,n+1} + \nabla \cdot \widetilde{\mathbf{u}}_{n+1}}$$

and, therefore, the following relation holds $J_{n+1} = J_{h,n+1} \exp\left(\nabla \cdot \widetilde{\mathbf{u}}_{n+1}\right)$.

Linearization of $\mathbf{s}\left(\mathbf{u}_{h,n+1}+\widetilde{\mathbf{u}}_{n+1}\right)$. *The linearization of the deviatoric stress* $\mathbf{s}\left(\mathbf{u}_{h,n+1}+\widetilde{\mathbf{u}}_{n+1}\right)$ *yields*

$$\mathbf{s}\left(\mathbf{u}_{h,n+1}+\widetilde{\mathbf{u}}_{n+1}\right) = \mathbf{s}\left(\mathbf{u}_{h,n+1}\right) + D\mathbf{s}\left(\mathbf{u}_{h,n+1}\right) \cdot \nabla^s \widetilde{\mathbf{u}}_{n+1} \tag{77}$$

where

$$D\mathbf{s}\left(\mathbf{u}_{h,n+1}\right) \cdot \nabla^s \widetilde{\mathbf{u}}_{n+1} = \mathbf{c}^{dev}_{h,n+1} : \nabla^s \widetilde{\mathbf{u}}_{n+1} \tag{78}$$

where, assuming plastic loading, $\mathbf{c}^{dev}_{h,n+1}$ *denotes the deviatoric part of the consistent (algorithmic) tangent moduli, e.g., for plastic loading the deviatoric part of the consistent elastoplastic moduli arising from the linearization of the radial return mapping for a J2 plasticiy model [39]. Substituting (78) into (77) yields*

$$\boxed{\mathbf{s}\left(\mathbf{u}_{h,n+1} + \widetilde{\mathbf{u}}_{n+1}\right) = \mathbf{s}\left(\mathbf{u}_{h,n+1}\right) + \mathbf{c}^{dev}_{h,n+1} : \nabla^s \widetilde{\mathbf{u}}_{n+1}}$$

Therefore the deviatoric stress $\mathbf{s}_{n+1} := \mathbf{s}\left(\mathbf{u}_{h,n+1} + \widetilde{\mathbf{u}}_{n+1}\right)$ *at time step* $n+1$*, can be additively splitted into a finite element approximation term* $\mathbf{s}_{h,n+1} := \mathbf{s}\left(\mathbf{u}_{h,n+1}\right)$ *and a linear term of the subgrid scales* $\widetilde{\mathbf{s}}_{n+1} := \widetilde{\mathbf{s}}\left(\mathbf{u}_{h,n+1}, \widetilde{\mathbf{u}}_{n+1}\right)$ *which can not be captured by the finite element approximation*

$$\boxed{\mathbf{s}_{n+1} = \mathbf{s}_{h,n+1} + \widetilde{\mathbf{s}}_{n+1}} \tag{79}$$

where

$$\mathbf{s}_{n+1} = \mathbf{s}\left(\mathbf{u}_{h,n+1} + \widetilde{\mathbf{u}}_{n+1}\right) \tag{80}$$

$$\mathbf{s}_{h,n+1} = \mathbf{s}\left(\mathbf{u}_{h,n+1}\right) = \mu \operatorname{dev}\left[\overline{\mathbf{b}}^{e}_{h,n+1}\right] \tag{81}$$

$$\widetilde{\mathbf{s}}_{n+1} = \mathbf{c}^{dev}_{h,n+1} : \nabla^{s} \widetilde{\mathbf{u}}_{n+1} \tag{82}$$

Remark 19 *The deviatoric stress tensor associated to the subgrid scales* $\widetilde{\mathbf{s}}_{n+1} := \widetilde{\mathbf{s}}\left(\mathbf{u}_{h,n+1}, \widetilde{\mathbf{u}}_{n+1}\right)$*, which in general will be a function of the current displacements provided by the finite element solution, should be viewed as an* incremental *perturbation relative to the current stress tensor solution provided by the finite element approximation.*

Using the additive split of the deviatoric stress tensor $\mathbf{s}_{n+1}$, substituting (79) into the time discrete variational forms (74), (75) (divided by the bulk modulus) and (76), the time discrete variational multiscale formulation (69) and (70) can be written as: find $(\mathbf{u}_{h,n+1}, \pi_{h,n+1}) \in \mathcal{W}_h$ and $(\widetilde{\mathbf{u}}_{n+1}, 0) \in \widetilde{\mathcal{W}}$ such that:

$$\left(\pi_{h,n+1}, \nabla \cdot \mathbf{v}_h\right) + \left(\mathbf{s}_{h,n+1}, \nabla^{s} \mathbf{v}_h\right) + \left(\widetilde{\mathbf{s}}_{n+1}, \nabla^{s} \mathbf{v}_h\right) = l_{n+1}\left(\mathbf{v}_h\right) \quad \forall\ \mathbf{v}_h \in \mathcal{V}_{h,0} \tag{83}$$

$$\left(\log J_{h,n+1} - \tfrac{1}{\kappa}\pi_{h,n+1}, q_h\right) + \left(\nabla \cdot \widetilde{\mathbf{u}}_{n+1}, q_h\right) = 0 \qquad \forall\ q_h \in \mathcal{Q}_h \tag{84}$$

$$\left(\pi_{h,n+1}, \nabla \cdot \widetilde{\mathbf{v}}\right) + \left(\mathbf{s}_{h,n+1}, \nabla^{s} \widetilde{\mathbf{v}}\right) + \left(\widetilde{\mathbf{s}}_{n+1}, \nabla^{s} \widetilde{\mathbf{v}}\right) = l_{n+1}\left(\widetilde{\mathbf{v}}\right) \quad \forall\ \widetilde{\mathbf{v}} \in \widetilde{\mathcal{V}}_0 \tag{85}$$

The goals now are twofold. First, to find an approximate solution for the (displacement) subgrid scales within the infinite-dimensional variational problem (85). For this, the infinite-dimensional space of the subgrid scales will be approximated by a finite-dimensional space which, within the OSGS method, will be the orthogonal space to the finite element space. Second, to substitute the approximate solution for the subgrid scales into the finite-dimensional variational problem given by (83) and (84).

5.2 Orthogonal Subgrid Scales (OSGS)

Algorithmic variational form for the subgrid scales. Integrating by parts *within each element* the first two terms of the left-hand-side of (85) and taking into account the equilibrium of (exact) tractions at the interelement boundaries yields

$$\sum_{e=1}^{n_{elm}} (\widetilde{\mathbf{s}}_{n+1}, \nabla^s \widetilde{\mathbf{v}})|_{\Omega_e} =$$
$$\sum_{e=1}^{n_{elm}} \left(J_{h,n+1} \nabla (J_{h,n+1}^{-1} \pi_{h,n+1}) + J_{h,n+1} \nabla \cdot (J_{h,n+1}^{-1} \mathbf{s}_{h,n+1}) + \mathbf{f}, \widetilde{\mathbf{v}} \right)\big|_{\Omega_e} \qquad \forall \widetilde{\mathbf{v}} \in \widetilde{\mathcal{V}}_0$$

which at the *element level* yields $\forall\ \widetilde{\mathbf{v}} \in \widetilde{\mathcal{V}}_0$,

$$(\widetilde{\mathbf{s}}_{n+1}, \nabla^s \widetilde{\mathbf{v}})|_{\Omega_e} = \left(J_{h,n+1} \nabla (J_{h,n+1}^{-1} \pi_{h,n+1}) + J_{h,n+1} \nabla \cdot (J_{h,n+1}^{-1} \mathbf{s}_{h,n+1}) + \mathbf{f}, \widetilde{\mathbf{v}} \right)\big|_{\Omega_e} \tag{86}$$

where the right-hand side term represents the variational form of the residual of the momentum balance equation given by the finite element approximation.

Algorithm approximation of the stabilization parameters matrix. Consider now a (inverse) stabilization matrix $\boldsymbol{\tau}_{e,n+1}^{-1}$ such that the following variational approximation holds for the subgrid scales *at the element level*

$$(\widetilde{\mathbf{s}}_{n+1}, \nabla^s \widetilde{\mathbf{v}})|_{\Omega_e} := \left(\boldsymbol{\tau}_{e,n+1}^{-1} \widetilde{\mathbf{u}}_{n+1}, \widetilde{\mathbf{v}} \right)\big|_{\Omega_e} \qquad \forall\ \widetilde{\mathbf{v}} \in \widetilde{\mathcal{V}}_0 \tag{87}$$

which, using the algorithmic approximation for the constitutive equation for the subgrid scales given by (82), yields

$$\left(\mathbf{c}_{h,n+1}^{dev} : \nabla^s \widetilde{\mathbf{u}}_{n+1}, \nabla^s \widetilde{\mathbf{v}} \right)\big|_{\Omega_e} := \left(\boldsymbol{\tau}_{e,n+1}^{-1} \widetilde{\mathbf{u}}_{n+1}, \widetilde{\mathbf{v}} \right)\big|_{\Omega_e} \qquad \forall\ \widetilde{\mathbf{v}} \in \widetilde{\mathcal{V}}_0 \tag{88}$$

Consider now a J2-plastic flow model with isotropic hardening. A summary of the J2-plastic flow model with isotropic hardening is shown in Table 3. Table 4 shows the main steps involved in the radial return mapping algorithm and Table 5 shows the expression of the consistent tangent elastoplastic moduli considering a linear isotropic hardening law [35], [36], [37], [39], [40], [42].

Table 3. Hyperelastic J2-flow model at finite deformations

i. Multiplicative decomposition of the deformation gradient
$\mathbf{F} = \mathbf{F}^e\mathbf{F}^p$
ii. Free energy with linear isotropic hardening
$\psi\left(J, \overline{\mathbf{b}}^e, \xi\right) := U(J) + \overline{W}\left(\overline{\mathbf{b}}^e\right) + \mathcal{H}(\xi)$
$U(J) = \frac{1}{2}\kappa \log^2(J), \quad J = \det[\mathbf{F}] = \det[\mathbf{F}^e]$
$\overline{W}\left(\overline{\mathbf{b}}^e\right) = \frac{1}{2}\mu\left(\operatorname{tr}\left[\overline{\mathbf{b}}^e\right] - 3\right), \ \overline{\mathbf{b}}^e = J^{-\frac{2}{3}}\mathbf{b}^e, \ \mathbf{b}^e = \mathbf{F}^e\mathbf{F}^{eT}$
$\mathcal{H}(\xi) = \frac{1}{2}H\xi^2 - (\sigma_0 - \sigma_\infty)(\xi - (1 - \exp(-\delta\xi))/\delta)$
iii. Mixed hyperelastic and hardening reponse
$\boldsymbol{\tau}(\mathbf{u},\pi) = \ \pi\mathbf{1} + \mathbf{s}(\mathbf{u}), \ \ \pi = JU'(J), \ \ \mathbf{s}(\mathbf{u}) = \mu \operatorname{dev}\left[\overline{\mathbf{b}}^e\right]$
$q = -H\xi + (\sigma_0 - \sigma_\infty)(1 - \exp(-\delta\xi))$
iv. Von-Mises yield condition
$\phi(\mathbf{s}, q) := \|\mathbf{s}\| - \sqrt{\frac{2}{3}}(\sigma_0 - q) \leqslant 0$
v. Associative flow rule
$\mathcal{L}_v\overline{\mathbf{b}}^e = \gamma\frac{2}{3}\operatorname{tr}\left[\overline{\mathbf{b}}^e\right]\mathbf{n}, \quad \dot{\xi} = \gamma\sqrt{\frac{2}{3}}, \quad \mathbf{n} = \mathbf{s}/\|\mathbf{s}\|$
vi. Kuhn-Tucker loading/unloading conditions
$\gamma \geqslant 0, \quad \phi \leqslant 0, \quad \gamma\phi = 0$
vii. Consistency condition
$\gamma\dot{\phi} = 0 \quad \text{if} \quad \phi = 0$

Table 3: Hyperelastic J2-flow model at finite deformations

Table 4. Hyperelastic J2-flow model at finite deformations

Radial return mapping algorithm

Step 1. Database and initial data

Given the database $\left\{\overline{\mathbf{b}}^{e}_{n}, \xi_{n}\right\}$ at time step n and

prescribed motion $\boldsymbol{\varphi}_{n+1}$ and pressure π_{n+1} at time step $n+1$

Step 2. Compute elastic predictor

$\overline{\mathbf{b}}^{e,trial}_{n+1} = \overline{\mathbf{f}}_{n+1}\overline{\mathbf{b}}^{e}_{n}\overline{\mathbf{f}}^{T}_{n+1}$, $\overline{\mathbf{f}}_{n+1} = \det\left[\mathbf{f}_{n+1}\right]^{-1/3}\mathbf{f}_{n+1}$, $\quad \mathbf{f}_{n+1} = \mathbf{F}_{n+1}\mathbf{F}^{-1}_{n}$

$\xi^{trial}_{n+1} = \xi_{n}$

$\mathbf{s}^{trial}_{n+1} = \mu\,\mathrm{dev}\left[\overline{\mathbf{b}}^{e,trial}_{n+1}\right]$, $\quad q^{trial}_{n+1} = -H\xi^{trial}_{n+1} + (\sigma_0 - \sigma_\infty)(1 - \exp(-\delta\xi^{trial}_{n+1}))$

$f^{trial}_{n+1} = \left\|\mathbf{s}^{trial}_{n+1}\right\| - \sqrt{\frac{2}{3}}\left(\sigma_0 - q^{trial}_{n+1}\right)$

Step 3. Check for plastic loading

IF $f^{trial}_{n+1} \leqslant 0$ THEN

Set $(\cdot)_{n+1} := (\cdot)^{trial}_{n+1}$ and EXIT

END IF

Step 4. Radial return mapping

Set: $\overline{\mu}_{n+1} = \mu\overline{I}^{e}_{n+1}$, $\quad \overline{I}^{e}_{n+1} := \frac{1}{3}\,\mathrm{tr}\left[\overline{\mathbf{b}}^{e,trial}_{n+1}\right]$

Compute: $\gamma_{n+1} = \frac{f^{trial}_{n+1}/\left(2\overline{\mu}_{n+1}\right)}{1+H/\left(3\overline{\mu}_{n+1}\right)}$, $\quad \mathbf{n}_{n+1} := \mathbf{s}^{trial}_{n+1}/\left\|\mathbf{s}^{trial}_{n+1}\right\|$

$\mathbf{s}_{n+1} = \mathbf{s}^{trial}_{n+1} - 2\overline{\mu}_{n+1}\gamma_{n+1}\mathbf{n}_{n+1}$, $\quad \xi_{n+1} = \xi^{trial}_{n+1} + \sqrt{\frac{2}{3}}\gamma_{n+1}$

Step 5. Addition of elastic pressure

$\boldsymbol{\tau}_{n+1} = \pi_{n+1}\mathbf{1} + \mathbf{s}_{n+1}$

Step 6. Update of intermediate configuration and database

$\overline{\mathbf{b}}^{e}_{n+1} = \mathbf{s}_{n+1}/\mu + \overline{I}^{e}_{n+1}\mathbf{1}$

Table 4: Hyperelastic J2-flow model at finite deformations. Radial return mapping algorithm

Table 5. Hyperelastic J2-flow model at finite deformations

Deviatoric consistent elastoplastic moduli

$$\mathbf{c}_{n+1}^{dev} = (1-\beta_1)\ \mathbf{c}_{n+1}^{dev,trial} - \\ -2\overline{\mu}\left(\beta_3 \mathbf{n}_{n+1}\otimes\mathbf{n}_{n+1} + \beta_4\,\mathrm{sym}\left[\mathbf{n}_{n+1}\otimes\mathrm{dev}\left[\mathbf{n}_{n+1}^2\right]\right]\right)$$

$$\mathbf{c}_{n+1}^{dev,trial} = 2\overline{\mu}\left(\mathbb{I} - \tfrac{1}{3}\mathbf{1}\otimes\mathbf{1}\right) - \tfrac{2}{3}\left\|\mathbf{s}_{n+1}^{trial}\right\|\left(\mathbf{n}_{n+1}\otimes\mathbf{1} + \mathbf{1}\otimes\mathbf{n}_{n+1}\right)$$

$$\beta_0 = 1 + H/\left(3\overline{\mu}\right),\ \beta_1 := 2\overline{\mu}\tfrac{\gamma_{n+1}}{\left\|\mathbf{s}_{n+1}^{trial}\right\|},\ \beta_2 := (1-1/\beta_0)\tfrac{2}{3}\tfrac{\left\|\mathbf{s}_{n+1}^{trial}\right\|}{\overline{\mu}}\gamma_{n+1}$$

$$\beta_3 = 1/\beta_0 - \beta_1 + \beta_2,\ \ \beta_4 = (1/\beta_0 - \beta_1)\tfrac{\left\|\mathbf{s}_{n+1}^{trial}\right\|}{\overline{\mu}}$$

Table 5: Hyperelastic J2-flow model at finite deformations. Deviatoric consistent elastoplastic moduli

Proposition 20 Algorithmic approximation of the scalar stabilization parameter. *In order to introduce an approximate solution for the subgrid scales* $\widetilde{\mathbf{u}}_{n+1}$*, the following simple secant approximation to the constitutive equation for the subgrid scales is considered*

$$\widetilde{\mathbf{s}}_{n+1} := \mathbf{c}_{h,n+1}^{dev} : \nabla^s \widetilde{\mathbf{u}}_{n+1} \approx 2\widetilde{\mu}_{n+1}\,\mathrm{dev}\left[\nabla^s \widetilde{\mathbf{u}}_{n+1}\right] \tag{89}$$

where, assuming plastic loading, the deviatoric part of the consistent elastoplastic moduli has been replaced by $\mathbf{c}_{h,n+1}^{dev} \approx 2\widetilde{\mu}_{n+1}\left(\mathbb{I} - \frac{1}{3}\mathbf{1}\otimes\mathbf{1}\right)$ *and the (secant) subgrid scale shear modulus for plastic loading is defined as*

$$\widetilde{\mu}_{n+1} := \mu\ J_{h,n+1}^{-2/3}\frac{\left\|\mathrm{dev}[\overline{\mathbf{b}}_{h,n+1}^{e}]\right\|}{\left\|\mathrm{dev}[\overline{\mathbf{b}}_{h,n+1}]\right\|}$$

Substituting (89) into (88) yields the following variational approximation for the subscales at the element level

$$\begin{aligned}\left(\widetilde{\mathbf{s}}_{n+1}, \nabla^s\widetilde{\mathbf{v}}\right)|_{\Omega_e} &:= \left(2\widetilde{\mu}_{n+1}\,\mathrm{dev}\left[\nabla^s\widetilde{\mathbf{u}}_{n+1}\right], \nabla^s\widetilde{\mathbf{v}}\right)\big|_{\Omega_e} \\ &:= \left(\boldsymbol{\tau}_{e,n+1}^{-1}\widetilde{\mathbf{u}}_{n+1}, \widetilde{\mathbf{v}}\right)\big|_{\Omega_e} \qquad \forall\ \widetilde{\mathbf{v}} \in \widetilde{\mathcal{V}}_0\end{aligned}$$

where the inverse of the (scalar) stabilization parameter $\tau_{e,n+1}$ *is locally (at the element level) defined at time* $n+1$ *as*

$$\tau_{e,n+1}^{-1} = \frac{2\widetilde{\mu}_{n+1}}{ch_e^2} \tag{90}$$

where c *is a mesh-size independent constant to be determined numerically.*

Remark 21 *For elastic loading/unloading the subgrid scale shear modulus* $\widetilde{\mu}_{n+1}$ *is defined as* $\widetilde{\mu}_{n+1} = \mu\ J_{h,n+1}^{-2/3}$.

Subgrid Scales. Algebraic Subgrid Scales (ASGS) and Orthogonal Subgrid Scales (OSGS). Using (89), (90), (87) and (86) the following variational approximation for the subscales *at the element level* holds

$$(\widetilde{\mathbf{u}}_{n+1}, \widetilde{\mathbf{v}})|_{\Omega_e} =$$
$$\left(\boldsymbol{\tau}_{e,n+1}\left(J_{h,n+1}\nabla(J_{h,n+1}^{-1}\pi_{h,n+1}) + J_{h,n+1}\nabla\cdot(J_{h,n+1}^{-1}\mathbf{s}_{h,n+1}) + \mathbf{f}\right), \widetilde{\mathbf{v}}\right)\Big|_{\Omega_e} \qquad \forall\ \widetilde{\mathbf{v}} \in \widetilde{\mathcal{V}}_0$$

and the subgrid scales, at the element level, can be approximated as

$$\boxed{\widetilde{\mathbf{u}}_{n+1} = \tau_{e,n+1}\left(J_{h,n+1}\nabla(J_{h,n+1}^{-1}\pi_{h,n+1}) + J_{h,n+1}\nabla\cdot(J_{h,n+1}^{-1}\mathbf{s}_{h,n+1}) + \mathbf{f}\right) + \mathbf{v}_{h,ort}}$$

where $\mathbf{v}_{h,ort} \in \widetilde{\mathcal{W}}^{\perp}$ belongs to the orthogonal space of the subscales. Here different options are available to approximate the subscales, according to the expression chosen for $\mathbf{v}_{h,ort}$. Consider the following two options, leading to the so called Algebraic Subgrid Scales (ASGS) and Orthogonal Subgrid Scales (OSGS) methods, respectively.

Algebraic Subgrid Scales Method (ASGS). Within the ASGS method, we take $\mathbf{v}_{h,ort} = \mathbf{0}$ and the subgrid scale displacements, at the element level, are approximated as

$$\boxed{\widetilde{\mathbf{u}}_{n+1} = \tau_{e,n+1}\left(J_{h,n+1}\nabla(J_{h,n+1}^{-1}\pi_{h,n+1}) + J_{h,n+1}\nabla\cdot(J_{h,n+1}^{-1}\mathbf{s}_{h,n+1}) + \mathbf{f}\right)}$$

Remark 22 *Note that within the ASGS, the subscales can be viewed as proportional to the residual of the momentum balance equation provided by the finite element solution.*

Orthogonal Subgrid Scales Method (OSGS). Within the OSGS method, we take $\mathbf{v}_{h,ort} = -\tau_{e,n+1}P_h\left(J_{h,n+1}\nabla(J_{h,n+1}^{-1}\pi_{h,n+1}) + J_{h,n+1}\nabla\cdot(J_{h,n+1}^{-1}\mathbf{s}_{h,n+1}) + \mathbf{f}\right)$, where $P_h(\cdot)$ represents the L_2 projection onto the finite element space $\mathcal{W}_h$, and the subgrid scale displacements, at the element level, are approximated as

$$\boxed{\widetilde{\mathbf{u}}_{n+1} = \tau_{e,n+1}P_h^{\perp}\left(J_{h,n+1}\nabla(J_{h,n+1}^{-1}\pi_{h,n+1}) + J_{h,n+1}\nabla\cdot(J_{h,n+1}^{-1}\mathbf{s}_{h,n+1}) + \mathbf{f}\right)}$$

where $P_h^{\perp}(\cdot) = (\cdot) - P_h(\cdot)$ is the L_2 orthogonal projection onto $\mathcal{W}_h^{\perp}$.

In this work we will adopt the OSGS method as the variational multiscale stabilization method.

Remark 23 *Note that within the OSGS we are implicitly considering that* $\widetilde{\mathcal{W}} \approx \mathcal{W}_h^{\perp}$*, i.e., we are taking the orthogonal space to the finite element solution space as space of the subscales. Then, the subscales can be viewed as proportional to the orthogonal projection to the finite element space of the residual of the momentum balance equation provided by the finite element solution.*

Remark 24 *We will assume that the body forces per unit reference volume belongs to the finite element solution space, i.e.,* $P_h^{\perp}(\mathbf{f}) = \mathbf{0}$*. Furthermore, we will neglect the contribution arising from the spatial divergence of the deviatoric stress component, e.g., we will assume that* $P_h^{\perp}\left(J_{h,n+1}\nabla\cdot(J_{h,n+1}^{-1}\mathbf{s}_{h,n+1})\right) = \mathbf{0}$ *holds. On the other hand, for linear elements the finite element approximation of the Jacobian* $J_{h,n+1}$ *is constant within an element. Then, the approximation at the element level for the subscales using the OSGS method leads to the following simple expression*

$$\boxed{\widetilde{\mathbf{u}}_{n+1} = \tau_{e,n+1} P_h^{\perp}\left(\nabla\pi_{h,n+1}\right)} \tag{91}$$

In this work we will mainly adopt the OSGS method as the variational multiscale stabilization method.

5.3 Discrete stabilized variational form

The goal now is to introduce the approximation found for the subscales using the OSGS method into the finite-dimensional variational problem (83), (84). Using the stress split (79), integrating by parts the last term of the left-hand side of (84) *within each element* and *neglecting the interelement boundary terms* or *assuming that the subgrid scales vanish at the element boundaries* (such as for bubble enhancements), the variational stabilized equations (83) and (84) can be written as:

$$\begin{aligned}(\pi_{h,n+1},\nabla\cdot\mathbf{v}_h) + (\mathbf{s}_{h,n+1},\nabla^s\mathbf{v}_h) + \\ + \sum_{e=1}^{n_{elm}} \left(\widetilde{\mathbf{s}}_{n+1},\nabla^s\mathbf{v}_h\right)\big|_{\Omega_e} = l_{n+1}\left(\mathbf{v}_h\right) \qquad \forall\ \mathbf{v}_h \in \mathcal{V}_{h,0}\end{aligned}$$

$$\left(\log J_{h,n+1} - \tfrac{1}{\kappa}\pi_{h,n+1}, q_h\right) - \sum_{e=1}^{n_{elm}} \left(\widetilde{\mathbf{u}}_{n+1}, J_{h,n+1}\nabla(J_{h,n+1}^{-1}q_h)\right)\big|_{\Omega_e} = 0 \qquad \forall\ q_h \in \mathcal{Q}_h$$

Using the constitutive equation (89), integrating by parts the last term of the left-hand side of (83) *within each element* and *neglecting the interelement*

boundary terms or *assuming that the subgrid scales vanish at the element boundaries* (such as for bubble enhancements), the last term of the left-hand side of (83) may be written *at the element level* as

$$\begin{aligned}(\widetilde{\mathbf{s}}_{n+1}, \nabla^s \mathbf{v}_h) &= \left(2\widetilde{\mu}_{n+1} \operatorname{dev}\left[\nabla^s \widetilde{\mathbf{u}}_{n+1}\right], \nabla^s \mathbf{v}_h\right) = \\ &= \left(\nabla^s \widetilde{\mathbf{u}}_{n+1}, 2\widetilde{\mu}_{n+1} \operatorname{dev}\left[\nabla^s \mathbf{v}_h\right]\right) = \\ &= -\left(\widetilde{\mathbf{u}}_{n+1}, J_{h,n+1} \nabla \cdot \left(J_{h,n+1}^{-1} 2\widetilde{\mu}_{n+1} \operatorname{dev}\left[\nabla^s \mathbf{v}_h\right]\right)\right)\end{aligned}$$

and, substituting this result into the above variational forms, we obtain

$$\begin{aligned}&(\pi_{h,n+1}, \nabla \cdot \mathbf{v}_h) + (\mathbf{s}_{h,n+1}, \nabla^s \mathbf{v}_h) - \\ &-\sum_{e=1}^{n_{elm}} \left(\widetilde{\mathbf{u}}_{n+1}, J_{h,n+1} \nabla \cdot \left(J_{h,n+1}^{-1} 2\widetilde{\mu}_{n+1} \operatorname{dev}\left[\nabla^s \mathbf{v}_h\right]\right)\right)\Big|_{\Omega_e} = l_{n+1}(\mathbf{v}_h) \quad \forall\ \mathbf{v}_h \in \mathcal{V}_{h,0}\end{aligned} \tag{92}$$

$$\left(\log J_{h,n+1} - \tfrac{1}{\kappa}\pi_{h,n+1}, q_h\right) - \sum_{e=1}^{n_{elm}} \left(\widetilde{\mathbf{u}}_{n+1}, J_{h,n+1} \nabla (J_{h,n+1}^{-1} q_h)\right)\Big|_{\Omega_e} = 0 \qquad \forall\ q_h \in \mathcal{Q}_h \tag{93}$$

Remark 25 *Note that for linear elements* $J_{h,n+1}$ *and* $\operatorname{dev}\left[\nabla^s \mathbf{v}_h\right]$ *are constant within the elements and then* $\nabla \cdot \left(J_{h,n+1}^{-1} \operatorname{dev}\left[\nabla^s \mathbf{v}_h\right]\right) = 0$ *and* $J_{h,n+1} \nabla (J_{h,n+1}^{-1} q_h) = \nabla q_h$*. Furthermore, the last term of the left-hand side of (92) will be neglected, i.e.* $\nabla \cdot \left(J_{h,n+1}^{-1} 2\widetilde{\mu}_{n+1} \operatorname{dev}\left[\nabla^s \mathbf{v}_h\right]\right) = 0$.

Then, using the above Remark and introducing the approximation for the subscales given by (91), the stabilized variational formulation can be written as: find $(\mathbf{u}_{h,n+1}, \pi_{h,n+1}) \in \mathcal{W}_h$ such that

$$(\pi_{h,n+1}, \nabla \cdot \mathbf{v}_h) + (\mathbf{s}_{h,n+1}, \nabla^s \mathbf{v}_h) = l_{n+1}(\mathbf{v}_h) \qquad \forall\ \mathbf{v}_h \in \mathcal{V}_{h,0} \tag{94}$$

$$\begin{aligned}&\left(\log J_{h,n+1} - \tfrac{1}{\kappa}\pi_{h,n+1}, q_h\right) - \\ &\boxed{-\textstyle\sum_{e=1}^{n_{elm}} \left(\tau_{e,n+1} P_h^{\perp}(\nabla \pi_{h,n+1}), \nabla q_h\right)\Big|_{\Omega_e}} = 0 \qquad \forall\ q_h \in \mathcal{Q}_h\end{aligned} \tag{95}$$

Remark 26 *Note that (94), (95) correspond to the time discrete counterpart of the discrete stabilized variational problem defined as: find* $\mathbf{U}_h \in \mathcal{W}_h$ *such that for any* $\mathbf{V}_h \in \mathcal{W}_{h,0}$

$$\boxed{B_{stab}(\mathbf{U}_h, \mathbf{V}_h) = L_{stab}(\mathbf{V}_h)}$$

where the OSGS stabilized (mesh-dependent) forms $B_{stab}\left(\mathbf{U}_h, \mathbf{V}_h\right)$ *and* $L_{stab}\left(\mathbf{V}_h\right)$ *can be written as*

$$\boxed{B_{stab}\left(\mathbf{U}_h, \mathbf{V}_h\right) := B\left(\mathbf{U}_h, \mathbf{V}_h\right) - \sum_{e=1}^{n_{elm}} \left(\tau_{e,n+1} P_h^{\perp}\left(\nabla \pi_{h,n+1}\right), \nabla q_h\right)\big|_{\Omega_e}}$$

$$\boxed{L_{stab}\left(\mathbf{V}_h\right) := L\left(\mathbf{V}_h\right)}$$

Set $\Pi_{h,n+1} := P_h\left(\nabla \pi_{h,n+1}\right)$ as the projection of the Kirchhoff pressure gradient onto the finite element space $\mathcal{W}_h$. Let $\Upsilon = \mathbf{H}^1$ and $\Upsilon_h \subset \Upsilon$ be the space of the Kirchhoff pressure gradient projection and its finite element associated subspace, respectively. Then, taking $\Pi_{h,n+1} \in \Upsilon_h$ as an additional independent continuous variable, the orthogonal projection of the discrete Kirchhoff pressure gradient can be written as $P_h^{\perp}\left(\nabla \pi_{h,n+1}\right) := \nabla \pi_{h,n+1} - \Pi_{h,n+1}$ and the following variational form holds

$$\left(\nabla \pi_{h,n+1}, \boldsymbol{\eta}_h\right)|_{\Omega_e} - \left(\Pi_{h,n+1}, \boldsymbol{\eta}_h\right)|_{\Omega_e} = 0 \qquad \forall\ \boldsymbol{\eta}_h \in \mathcal{V}_{h,0}$$

Finally, introducing the discrete Kirchhoff pressure gradient projection as a third variable, the stabilized variational problem can be written as: find $\left(\mathbf{u}_{h,n+1}, \pi_{h,n+1}, \Pi_{h,n+1}\right) \in \mathcal{V}_h \times \mathcal{Q}_h \times \Upsilon_h$ such that:

$$\left(\pi_{h,n+1}, \nabla \cdot \mathbf{v}_h\right) + \left(\mathbf{s}_{h,n+1}, \nabla^s \mathbf{v}_h\right) = l_{n+1}\left(\mathbf{v}_h\right) \qquad \forall\ \mathbf{v}_h \in \mathcal{V}_{h,0} \tag{96}$$

$$\begin{aligned}\left(\log J_{h,n+1} - \tfrac{1}{\kappa}\pi_{h,n+1}, q_h\right) - \\ - \sum_{e=1}^{n_{elm}} \left(\tau_{e,n+1}\left(\nabla \pi_{h,n+1} - \Pi_{h,n+1}\right), \nabla q_h\right)|_{\Omega_e} = 0 \qquad \forall\ q_h \in \mathcal{Q}_h\end{aligned} \tag{97}$$

$$\sum_{e=1}^{n_{elm}} \left(\nabla \pi_{h,n+1} - \Pi_{h,n+1}, \boldsymbol{\eta}_h\right)|_{\Omega_e} = 0 \qquad \forall\ \boldsymbol{\eta}_h \in \mathcal{V}_{h,0} \tag{98}$$

Remark 27 *Note that within the OSGS method the variational stabilization term at the element level* $-\left(\tau_{e,n+1}\left(\nabla \pi_{h,n+1} - \Pi_{h,n+1}\right), \nabla q_h\right)|_{\Omega_e}$ *is proportional to the difference between the continuous (projected) and the discontinuous (elemental) Kirchhoff pressure gradients, while within the ASGS method the stabilization term is proportional to the residual itself. Therefore, in both cases, the stabilization terms decreases very rapidly upon mesh refinement, but for the OSGS method this happens at a greater rate.*

Remark 28 *Note that in the final stabilized variational problem there is only a remaining stabilization term which appears in (97), while the (96) remains the same as for the original problem. On the other hand, a further variable has been introduced. However, as it is shown in the next section, this drawback can easily be overcome to get a computational robust and efficient procedure.*

Remark 29 *To gain further insight on the OSGS stabilization technique, note that the resulting stabilized variational equations could be viewed (assuming that the stabilization parameter is constant) as the variational form of the following stabilized continuous (strong form) equations*

$$\begin{aligned} J\,\nabla\left(J^{-1}\pi\right) + J\,\nabla\cdot\left(J^{-1}\mathbf{s}\left(\mathbf{u}\right)\right) + \mathbf{f} &= \mathbf{0} \quad in \quad \Omega \\ \tfrac{1}{\kappa}\pi - \log J - \tau\left(\nabla^2\pi - \nabla\cdot\Pi\right) &= 0 \quad in \quad \Omega \\ \nabla\pi - \Pi &= \mathbf{0} \quad in \quad \Omega \end{aligned}$$

with the appropriate boundary conditions.

6 Computational and Implementation Aspects

From the computational efficiency point of view, the drawback related to the introduction of a new variable field inherent to the OSGS can be easily overcome to end up with a computational robust and efficient solution algorithm. A convenient staggered solution method can be obtained by a slight modification of the problem defined by the stabilized variational system of equations (96), (97) and (98), in which we keep fixed the Kirchhoff pressure gradient projection field $\Pi_{h,n}$ at the last converged time step t_n while solving for the displacement and Kirchhoff pressure fields $\mathbf{u}_{h,n+1}$ and $\pi_{h,n+1}$, respectively, at time t_{n+1}. The update of the Kirchhoff pressure gradient projection field is performed in a second step. Therefore the modified algorithmic stabilized variational problem can be written as a two-step problem defined as follows.

Problem 1. Given $\Pi_{h,n} \in \Upsilon_h$ find $(\mathbf{u}_{h,n+1}, \pi_{h,n+1}) \in \mathcal{V}_h \times \mathcal{Q}_h$ such that:

$$\left(\pi_{h,n+1}, \nabla\cdot\mathbf{v}_h\right) + \left(\mathbf{s}_{h,n+1}, \nabla^s\mathbf{v}_h\right) = l_{n+1}\left(\mathbf{v}_h\right) \qquad \forall\ \mathbf{v}_h \in \mathcal{V}_{h,0}$$

$$\begin{aligned} &\left(\log J_{h,n+1} - \tfrac{1}{\kappa}\pi_{h,n+1}, q_h\right) - \\ &\qquad - \sum_{e=1}^{n_{elm}} \left(\tau_{e,n}\left(\nabla_n\pi_{h,n+1} - \Pi_{h,n}\right), \nabla_n q_h\right)\big|_{\Omega_e} = 0 \qquad \forall\ q_h \in \mathcal{Q}_h \end{aligned}$$

where ∇_n denotes the spatial gradient with respect to the previous converged configuration at time step t_n. Note also that the stabilization parameter $\tau_{e,n}$ is evaluated at time step t_n.

The solution of *Problem 1* is obtained using a Newton-Raphson incremental iterative algorithm. The resulting linearized variational system of equations at time step $n+1$, iteration $i+1$, can be written as: given $\Pi_{h,n} \in \Upsilon_h$, find $\left(\Delta \mathbf{u}^{(i)}_{h,n+1}, \Delta \pi^{(i)}_{h,n+1}\right) \in \mathcal{V}_h \times \mathcal{Q}_h$ such that:

$$\begin{aligned}\left(\Delta \pi^{(i)}_{h,n+1}, \nabla \cdot \mathbf{v}_h\right) + \left(\left(\mathbf{c}^{dev\ (i)}_{h,n+1} - 2\pi^{(i)}_{h,n+1}\mathbf{I}\right) : \nabla^s \Delta \mathbf{u}^{(i)}_{h,n+1}, \nabla^s \mathbf{v}_h\right) + \\ + \left(\nabla \Delta \mathbf{u}^{(i)}_{h,n+1}\left(\pi^{(i)}_{h,n+1}\mathbf{1} + \mathbf{s}^{(i)}_{h,n+1}\right), \nabla \mathbf{v}_h\right) = \\ = -R_u\left(\mathbf{u}^{(i)}_{h,n+1}, \pi^{(i)}_{h,n+1}; \mathbf{v}_h\right) \quad \forall\ \mathbf{v}_h \in \mathcal{V}_{h,0} \quad (99)\end{aligned}$$

$$\begin{aligned}\left(\nabla \cdot \Delta \mathbf{u}^{(i)}_{h,n+1} - \tfrac{1}{\kappa}\Delta \pi^{(i)}_{h,n+1}, q_h\right) - \sum_{e=1}^{n_{elm}} \left(\tau_{e,n} \nabla_n \Delta \pi^{(i)}_{h,n+1}, \nabla_n q_h\right)\Big|_{\Omega_e} = \\ = -R_\pi\left(\mathbf{u}^{(i)}_{h,n+1}, \pi^{(i)}_{h,n+1}; q_h\right) \quad \forall\ q_h \in \mathcal{Q}_h \quad (100)\end{aligned}$$

where $R_u\left(\mathbf{u}^{(i)}_{h,n+1}, \pi^{(i)}_{h,n+1}; \mathbf{v}_h\right)$ and $R_\pi\left(\mathbf{u}^{(i)}_{h,n+1}, \pi^{(i)}_{h,n+1}; q_h\right)$ denote the variational residual equations at time step $n+1$, iteration i, and are defined as

$$\begin{aligned}R_u\left(\mathbf{u}^{(i)}_{h,n+1}, \pi^{(i)}_{h,n+1}; \mathbf{v}_h\right) := \\ = \left(\pi^{(i)}_{h,n+1}, \nabla \cdot \mathbf{v}_h\right) + \left(\mathbf{s}^{(i)}_{h,n+1}, \nabla^s \mathbf{v}_h\right) - l_{n+1}(\mathbf{v}_h) \quad \forall\ \mathbf{v}_h \in \mathcal{V}_{h,0}\end{aligned}$$

$$\begin{aligned}R_\pi\left(\mathbf{u}^{(i)}_{h,n+1}, \pi^{(i)}_{h,n+1}; q_h\right) := \left(\log J^{(i)}_{h,n+1} - \tfrac{1}{\kappa}\pi^{(i)}_{h,n+1}, q_h\right) - \\ - \sum_{e=1}^{n_{elm}} \left(\tau_{e,n}\left(\nabla_n \pi^{(i)}_{h,n+1} - \Pi_{h,n}\right), \nabla_n q_h\right)\Big|_{\Omega_e} \quad \forall\ q_h \in \mathcal{Q}_h\end{aligned}$$

Problem 2. Given $(\mathbf{u}_{h,n+1}, \pi_{h,n+1}) \in \mathcal{V}_h \times \mathcal{Q}_h$, find $\Pi_{h,n+1} \in \Upsilon_h$ such that:

$$\sum_{e=1}^{n_{elm}} \left(\nabla \pi_{h,n+1} - \Pi_{h,n+1}, \boldsymbol{\eta}_h\right)\big|_{\Omega_e} = 0 \quad \forall\ \boldsymbol{\eta}_h \in \mathcal{V}_{h,0}$$

Finite element projection. Once the finite element discretization has been introduced, the matrix form of the algebraic system resulting from the variational *Problem 1* takes the form

$$\begin{aligned}\mathbb{K}^{(i)}_{T_{n+1}} \Delta \mathbb{U}^{(i)}_{n+1} + \mathbb{G}^{(i)}_{n+1} \Delta \mathbb{P}^{(i)}_{n+1} &= -\mathbb{R}^{(i)}_{u,n+1} \\ \mathbb{G}^{(i)T}_{n+1} \Delta \mathbb{U}^{(i)}_{n+1} - \left(\mathbb{M}_p + \mathbb{L}_{\tau,n}\right) \Delta \mathbb{P}^{(i)}_{n+1} &= -\mathbb{R}^{(i)}_{\pi,n+1}\end{aligned}$$

where $\mathbb{K}^{(i)}_{T_{n+1}}$, $\mathbb{G}^{(i)}_{n+1}$, $\mathbb{M}_p$ and $\mathbb{L}_{\tau,n}$ denote the matrices arising from the finite element projection of the last three terms of the left-hand side of (99), the first term of the left-hand side of (99), the first term of the left-hand side of (100) and the third term of the left-hand side of (100), respectively, $\mathbb{R}^{(i)}_{u,n+1}$ and $\mathbb{R}^{(i)}_{\pi,n+1}$ denote the vectors arising from the finite element projection of the variational residuals $R_u\left(\mathbf{u}^{(i)}_{h,n+1}, \pi^{(i)}_{h,n+1}; \mathbf{v}_h\right)$ and $R_\pi\left(\mathbf{u}^{(i)}_{h,n+1}, \pi^{(i)}_{h,n+1}; q_h\right)$, respectively, and $\Delta\mathbb{U}^{(i)}_{n+1} := \mathbb{U}^{(i+1)}_{n+1} - \mathbb{U}^{(i)}_{n+1}$ and $\Delta\mathbb{P}^{(i)}_{n+1} := \mathbb{P}^{(i+1)}_{n+1} - \mathbb{P}^{(i)}_{n+1}$ denote the increments of nodal displacement and Kirchhoff pressure unknowns, respectively.

Remark 30 *It should be noted that the resulting system of equations is symmetric. Block-symmetry arises as a result of the specific volumetric part of the stored energy function considered, due to the fact that* $\left(JU'(J)\right)' = \kappa J^{-1}$ *and* $DJ \cdot \Delta\mathbf{u} = J\ \nabla \cdot \Delta\mathbf{u}$.

Once the finite element discretization has been introduced, the matrix form of the algebraic system resulting from the variational *Problem 2* takes the form

$$\Pi_{n+1} = \mathbb{M}^{-1}_{\tau,n+1}\mathbb{G}_{\tau,n+1}\mathbb{P}_{n+1}$$

where $\mathbb{M}_{\tau,n+1}$ and $\mathbb{G}_{\tau,n+1}$denote the matrices arising from the stabilized displacement mass-like term and spatial gradient operator, respectively, and $\mathbb{P}_{n+1}$ and Π_{n+1} denote the vectors of Kirchhoff pressure and Kirchhoff pressure gradient projection nodal unknowns at time step $n+1$, respectively. A lumped approximation to the stabilized mass-like matrix $\mathbb{M}_{\tau,n+1}$ would lead to a simple direct computation of the nodal Kirchhoff pressure gradient projection unknowns.

Finite element matrices at elemen level. Typical element entries $(\cdot)^{AB}$ corresponding to nodes A and B for the above matrices and $(\cdot)^{A}$ correspond-

ing to node A for the above residual vectors take the form

$$
\begin{aligned}
\mathbb{K}_T|_{\Omega_e}^{AB} &= \int_{\Omega_e} \left(\mathbf{B}_u^A\right)^T \left(\mathbf{C}_T^{dev} - 2\pi\mathbf{I}\right) \mathbf{B}_u^B \; dV_0 + \int_{\Omega_e} \left(\nabla N_u^A\right)^T \boldsymbol{\tau} \nabla N_u^B \; dV_0 \, \mathbf{1} \\
\mathbb{G}|_{\Omega_e}^{AB} &= \int_{\Omega_e} \nabla N_u^A N_\pi^B \; dV_0 \\
\mathbb{M}_p|_{\Omega_e}^{AB} &= \int_{\Omega_e} \tfrac{1}{\kappa} N_\pi^A N_\pi^B \; dV_0 \\
\mathbb{L}_\tau|_{\Omega_e}^{AB} &= \int_{\Omega_e} \tau_e \left(\nabla N_\pi^A\right)^T \nabla N_\pi^B \; dV_0 \\
\mathbb{G}_\tau|_{\Omega_e}^{AB} &= \int_{\Omega_e} \tau_e \nabla N_\pi^A N_\pi^B \; dV_0 \\
\mathbb{M}_\tau|_{\Omega_e}^{AB} &= \int_{\Omega_e} \tau_e N_\Pi^A N_\Pi^B \; dV_0 \mathbf{1} \\
\mathbb{R}_u|_{\Omega_e}^{A} &= \int_{\Omega_e} \left(\mathbf{B}_u^A\right)^T \boldsymbol{\tau} \; dV_0 - \int_{\Omega_e} N_u^A \, \mathbf{f} \; dV_0 - \int_{\partial\Omega_e \cap \partial\Omega_t} N_u^A \, \overline{\mathbf{t}}^N \; dS_0 \\
\mathbb{R}_\pi|_{\Omega_e}^{A} &= \int_{\Omega_e} N_\pi^A \; \left(\log J - \tfrac{1}{\kappa}\pi\right) dV_0 - \\
&\quad - \int_{\Omega_e} \tau_{e,n} \left(\nabla_n N_\pi^A\right)^T \; \left(\nabla_n \pi - \Pi_{h,n}\right) dV_0
\end{aligned}
$$

where N_u^A, N_π^A and N_Π^A denote the interpolation shape functions at node A for the displacement, Kirchhoff pressure and Kirchhoff pressure gradient projection fields, respectively, ∇N_u^A and ∇N_π^A denote the gradient of the interpolation shape functions at node A for the displacement and Kirchhoff pressure fields, respectively, and $\mathbf{B}_u^A$ denote the interpolation matrix at node A for the symmetric spatial gradient field.

7 Computational Simulations

The formulation presented in the preceeding sections is illustrated below in a number of computational simulations. Performance of the OSGS stabilized formulation is shown using triangular finite elements discretizations for 2D plane strain problems and tetrahedral finite elements discretizations for 3D problems. Numerical examples involving both infinitesimal and finite strains are considered. The Newton-Raphson method, combined with a line search procedure, is used to solve the non-linear system of equations arising from the spatial and temporal discretization of the stabilized variational problem. Simulations have been performed with an enhanced version

of the finite element program COMET [5] developed by the authors at the International Center for Numerical Methods in Engineering (CIMNE). Pre and post-processing has been performed using GiD [18], also developed at CIMNE.

7.1 Plane strain Cook's membrane

The Cook's membrane problem is a bending dominated example which has been used by many authors as a reference test in the assessment of different element formulations [41]. The problem consists of a tapered panel, clamped on one side and subjected to a shearing load $F = 1.8$ at the free end. Geometry of the problem is shown in Figure 1. The material model is assumed to be elastoplastic at small deformations. Elastic behaviour is assumed to be incompressible. A J2-flow theory plasticity model with linear isotropic hardening is used. Material constitutive parameters are: Young modulus $E = 70$, Poisson coefficient $\nu = 0.4999$, initial yield stress $\sigma_Y = 0.243$ and linear isotropic hardening parameter $H = 0.135$.

In order to test the convergence behaviour of the different formulations, the problem has been discretized into 2x2, 5x5, 10x10, 20x20 and 50x50 triangular and quadrilateral finite element meshes. The mixed mean dilatation/pressure quadrilateral Q1/P0 quadrilateral element has been considered as a reference solution. Figure 2 shows the deformed geometry using Q1/P0 quadrilateral and P1/P1 OSGS triangular 10x10 finite element meshes.

Figure 3 shows the convergence behaviour for the vertical displacement of the top corner for the different finite element meshes considered. Figure 3 shows the very poor behaviour of the standard P1 linear triangular element due to the locking effect of the Galerkin formulation in incompressibility conditions, leading to a value of the vertical displacement of the top corner much lower than the right solution, even for finer meshes. It can also be seen than the proposed stabilized mixed P1/P1OSGS triangular element converges faster than the Q1/P0 quadrilateral element to the right solution

7.2 Punching of a rectangular block

This example deals with the punching of a rectangular box under plane strain conditions. A rectangular block of $0.60\ m \times 0.20\ m$ is subjected to compression on a central area of $0.20\ m$ on the top surface, through a prescribed vertical displacement of $0.012\ m$. Geometry and loading conditions are shown on Figure 4. Boundary conditions are such that horizontal displacements

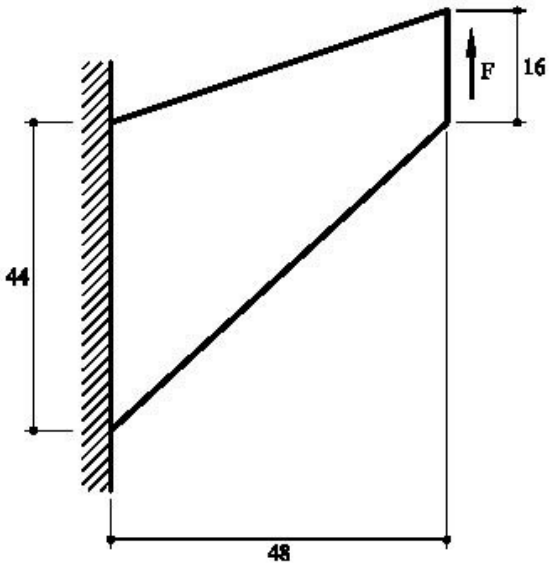

Figure 1: Plane strain Cook's membrane. Initial geometry

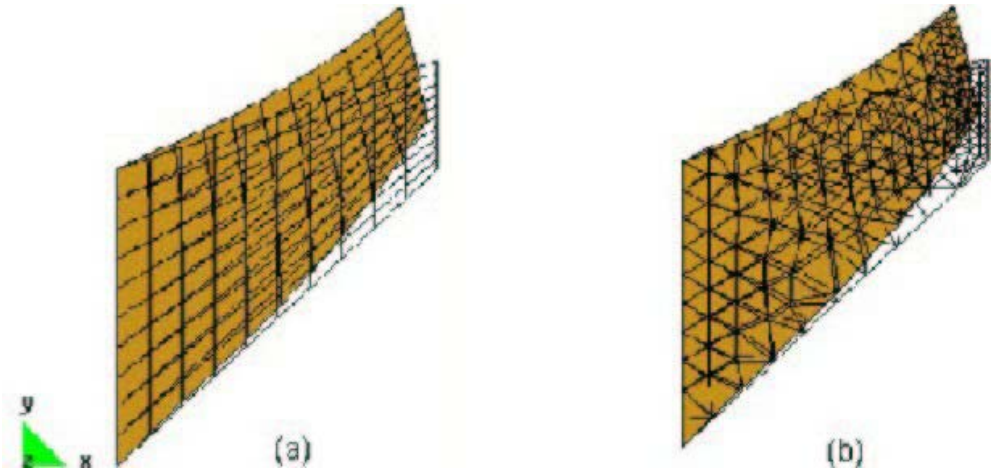

Figure 2: Plane strain Cook's membrane. Deformed geometry using 10x10 finite element meshes of: (a) Q1/P0 quadrilateral elements; and (b) P1/P1 OSGS triangular elements

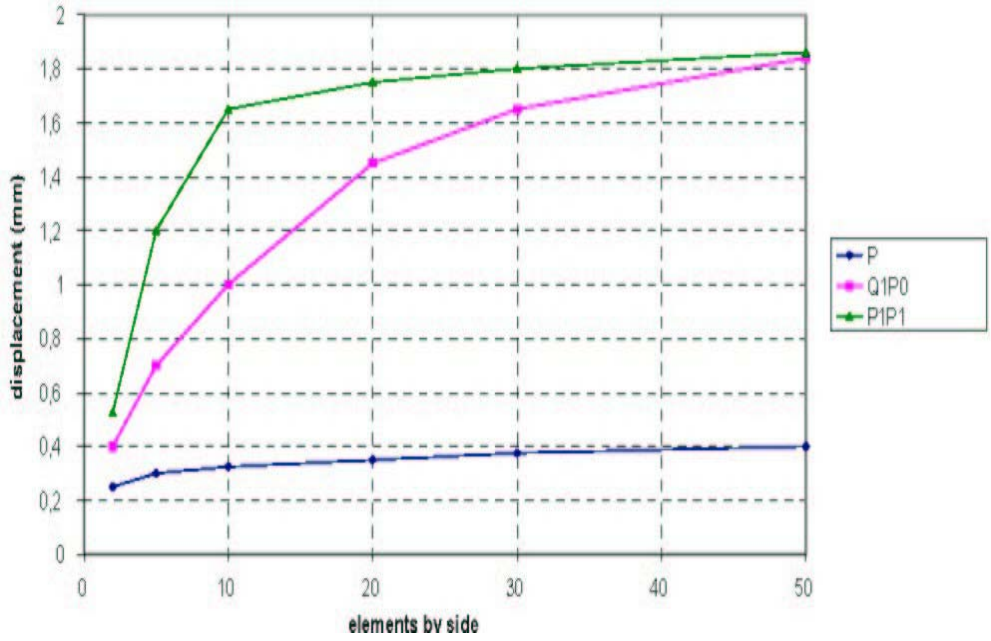

Figure 3: Plane strain Cook's membrane. Mesh convergence of vertical displacement of the top corner

are allowed and vertical displacements are prescribed to zero on the bottom surface. Horizontal displacements are prescibed to zero on the top surface and there are no prescribed displacements on the lateral surfaces. Geometry of the problem is shown in Figure 4. The material model is assumed to be elastoplastic at small deformations. Elastic behaviour is assumed to be compressible. A J2-flow theory perfect plasticity model is used. Material constitutive parameters are: Young modulus $E = 1.96 \times 10^5\ MPa$, Poisson coefficient $\nu = 0.3$ and yield stress $\sigma_Y = 150\ MPa$.

The block has been discretized using non-structured triangular meshes of P1 (standard linear displacement finite elements), P1/P1 (standard mixed linear displacement/pressure finite elements) and P1/P1 OSGS (OSGS stabilized mixed linear displacement/pressure finite elements) consisting of 357 nodes and 632 elements. A reference structured quadrilateral mesh of Q1P0 [42], consisting of 341 nodes and 632 elements, has been also considered. The prescribed displacement is applied in 30 equal loading steps.

Figures 5 and 6 show the equivalent plastic strain and pressure distribution obtained using P1 standard linear displacement triagular elements, P1/P1 standard mixed linear displacement/pressure triangular elements, P1/P1

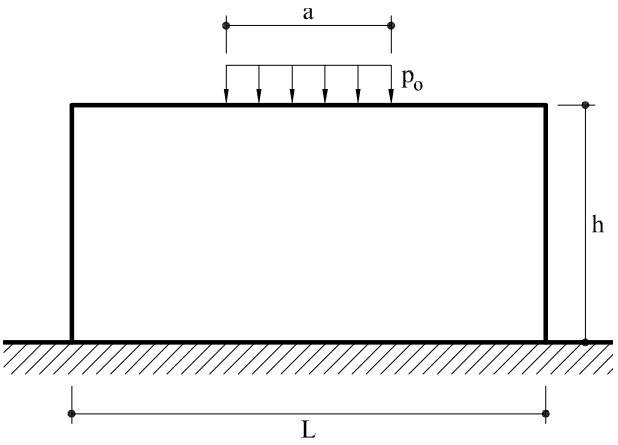

Figure 4: Punching of a rectangular block. Geometry data: $L = 0.60\ m$, $h = 0.20\ m$, $a = 0.20\ m$ and prescribed vertical displacement $\delta = 0.012\ m$.

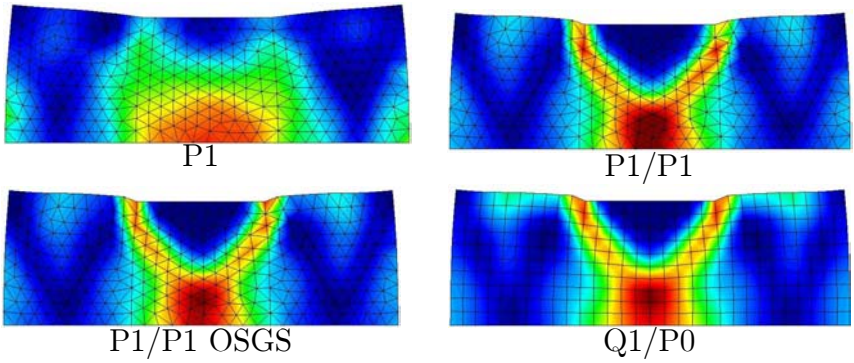

Figure 5: Punching of a rectangular block. Equivalent plastic strain distribution. (a) P1 standard linear displacement triangular element; (b) P1/P1 mixed linear/linear displacement/pressure triangular element; (c) P1/P1 OSGS stabilized mixed linear/linear triangular element; (d) Q1/P0 mixed bilinear/constant displacement/pressure quadrilateral element

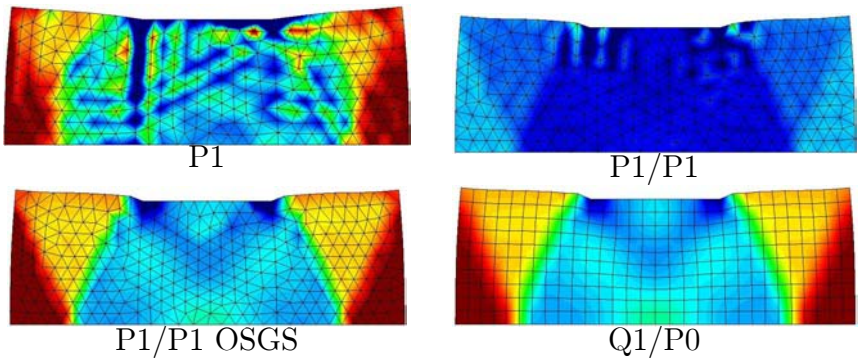

Figure 6: Punching of a rectangular block. Pressure distribution. (a) P1 standard linear displacement triangular element; (b) P1/P1 mixed linear/linear displacement/pressure triangular element; (c) P1/P1 OSGS stabilized mixed linear/linear triangular element; (d) Q1/P0 mixed bilinear/constant displacement/pressure quadrilateral element

OSGS stabilized mixed linear displacement/pressure triangular elements and Q1/P0 mixed linear displacement/constant pressure quadrilateral elements. All elements considered, except the standard P1 triangular element, are able to capture well the equivalent plastic strain distribution. Results change drastically where the pressure distribution is concerned. In this case, both standard P1 triangular element and standard mixed P1/P1 triangular element fail to capture the correct pressure distribution, while the P1/P1 OSGS triangular element and Q1/P0 quadrilateral element are both able to capture it. It is worth to note that the standard mixed P1/P1 triangular element exhibits oscillations in the pressure distribution under elastoplastic J2-flow theory, despite the fact that the elastic behaviour is compressible.

7.3 2D vertical cut

This example deals with a plane strain 2D vertical cut loaded throught a rigid footing which sustains a central point load. Figure 7a depicts the geometry of the problem; dimensions are related to a length $a = 5\ m$. Figure 7 also shows the meshes used in the analysis; (b) an unstructured mesh of 843 linear triangles (463 nodes) and (c) a structured 20 x 20 + 20 mesh of Q1/P0 quadrilaterals (462 nodes). In the unstructured mesh the automatic mesh generator uded tends to introduce patches of equilateral triangles with predominant directions at -30^o, $+30^o$ and $+90^o$. Material model is assumed to be elastoplastic at small deformations, involving incompressible elasticity and perfect J2 plasticity. As the Q1/P0 element cannot deal with the purely

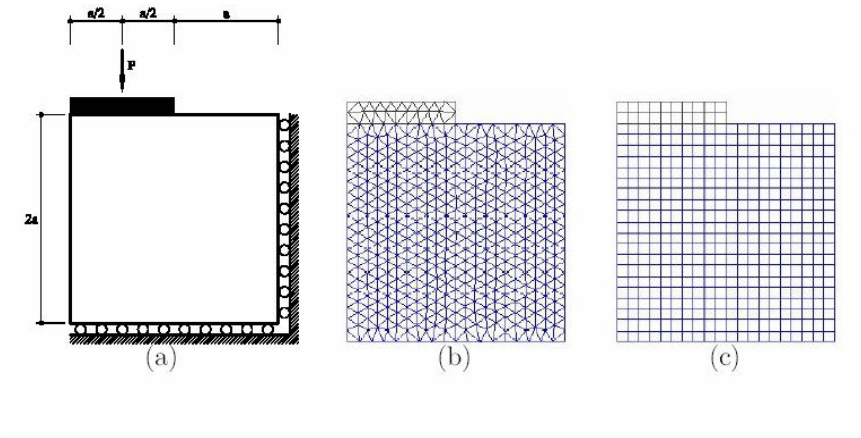

Figure 7: 2D vertical cut. (a) Geometry; (b) Unstructured triangular mesh; (c) Structured quadrilateral mesh

incompressible case the following material properties are assumed: Young's modulus $E = 10\ MPa$, Poisson's ratio $\nu = 0.499$ and yield stress $\sigma_Y = 150\ MPa$. Perfect plasticity is considered because it should allow collapse mechanics to develop neatly and limit loads clearly defined.

Figure 8 shows load versus (point of application)-displacement curves for the (a) standard irreductible P1, (b) standard mixed P1/P1, (c) stable mixed P1/P1 OSGS, and (d) Q1/P0 cases. It is remarkable that the last two achieve a well defined limit load, with practically overlapping curves; the standard mixed formulation obtains a slightly higher limit load, while the irreductible formulation clearly exhibits volumetric locking, both in the elastic and plastic regimes.

Figure 9 depicts contours of the equivalent plastic strain once the plastic flow is fully developed and the collapse mechanism can be appreciated (vertical displacement of the load of 0.05 m). Very good and similar results are obtained with the proposed formulation and with the mixed quadrilateral. On the other hand, the standard irreductible linear triangles completely fail to capture the correct plastic pattern and are badly affected by the mesh direction bias. The standard mixed linear triangles show a plastic pattern very similar to the one developed by the stable elements.

Figure 10 presents pressure contours at the same (final) time of the deformation process. Lack of stability and severe oscillations of the pressure field can be identified in both standard formulations. This is enough to completely destabilize the irreductible formulation, although for this example it seems to

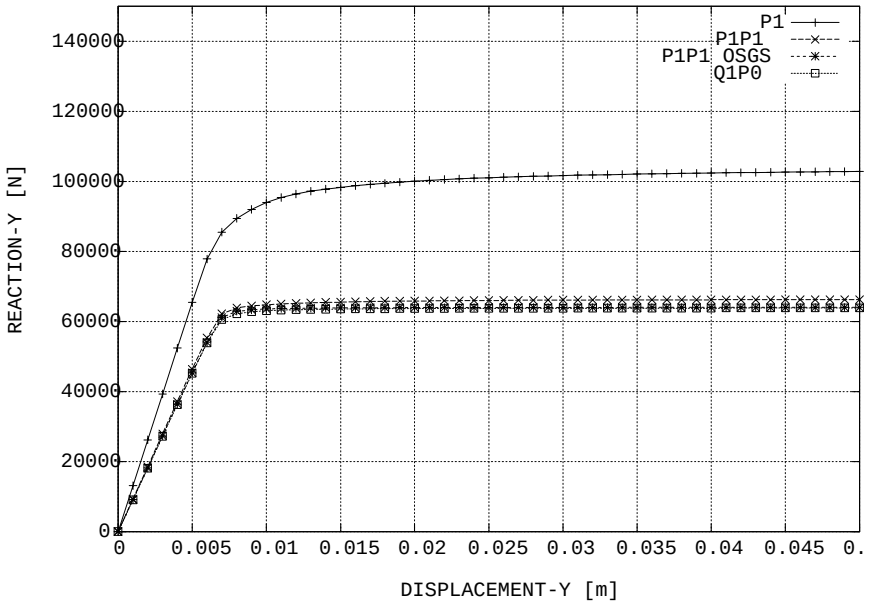

Figure 8: 2D vertical cut. Load-displacement curve

have little influence in the deformation pattern, as the plastic deformations does not depend on the pressure. Obviously, this is not always necessarily the case, and especially in nonlinear analyses. The improved performance of the proposed formulation is easily perceptible.

Concerning the CPU time required for the solution, the ratios between the four cases are 1.28/1.50/1.58/1.00, taking the quadrilateral element as reference. The proposed formulation is 58% more costly than the quadrilateral (because of the 2/1 ratio for the number of elements and the 3/2 ratio for the number of degrees of freedom), but the difference in cost with the standard mixed triangles (same number of elements and degress of freedom) is very small.

7.4 3D vertical cut

This example is a 3D version of the 2D vertical cut described above. Figure 11a depicts the geometry of the problem; dimensions are related to a length $a = 5\ m$. Figure 11b shows the unstructured mesh of linear P1/P1 OSGS tetrahedral elements used in the computations ($9,533$ nodes and $50,080$ elements). A structured 20 x 20 x 20 + 200 Q1/P0 hexahedral elements mesh ($9,503$ nodes), not shown, is used for comparison purposes.

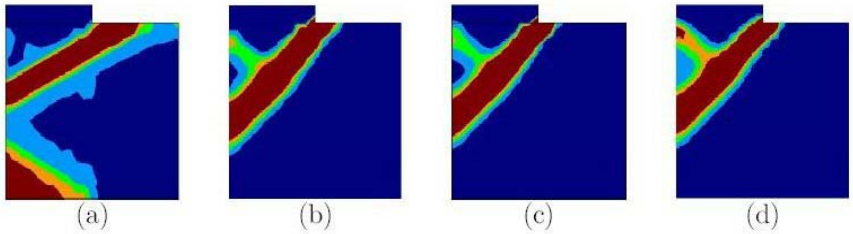

Figure 9: 2D vertical cut. Equivalent plastic strain (a) P1 element; (b) P1/P1 element; (c) P1/P1 OSGS element; (d) Q1/P0 element

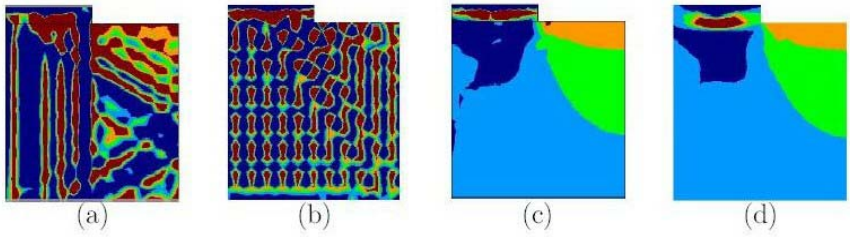

Figure 10: 2D vertical cut. Pressure (a) P1 element; (b) P1/P1 element; (c) P1/P1 OSGS element; (d) Q1/P0 element

Figure 12 shows load versus (point of application)-displacement curves for both cases considered. Again, it is remarkable that both formulations achieve a well-defined limit load.

Figure 13 displays contours of the equivalent plastic strain once the plastic flow is fully developed (vertical displacement of the load of 0.05 m). Again, it is remarkable that satisfactory results are obtained with the proposed formulation in an unstructured mesh of P1/P1 OSGS tetrahedra, and very similar to those obtained in a structured and regular mesh of Q1/P0 hexahedra.

The proposed formulation is 53% more costly than the hexahedron (because of the 6/1 ratio for the number of elements and the 4/3 ratio for the number of degrees of freedom).

7.5 2D Prandtl's punch test

This example is the well known 2D plane strain Prandtl's punch test, often used in the literature to test the ability of J2 plastic formulations to capture collapse loads and mechanisms. Figure 14 depicts the geometry of the problem, again a rigid footing with a central point load; dimensions are related to length $b = 1\ m$. Because of the symmetry only half of the domain needs to be

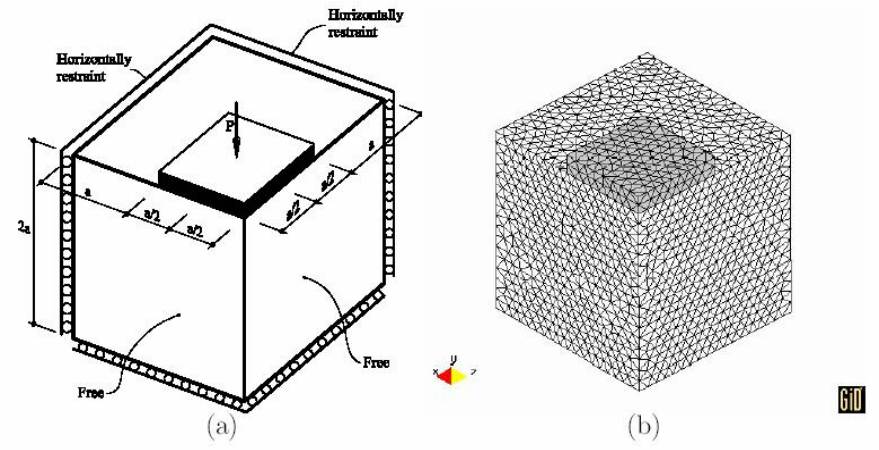

Figure 11: 3D vertical cut. (a) Geometry (b) Unstructured tetraedra mesh

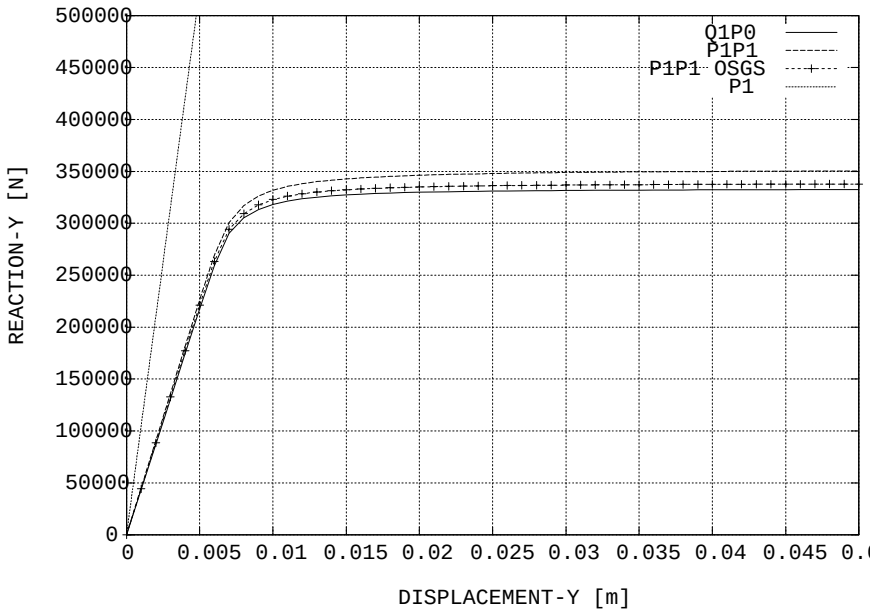

Figure 12: 3D vertical cut. Load-displacement curves

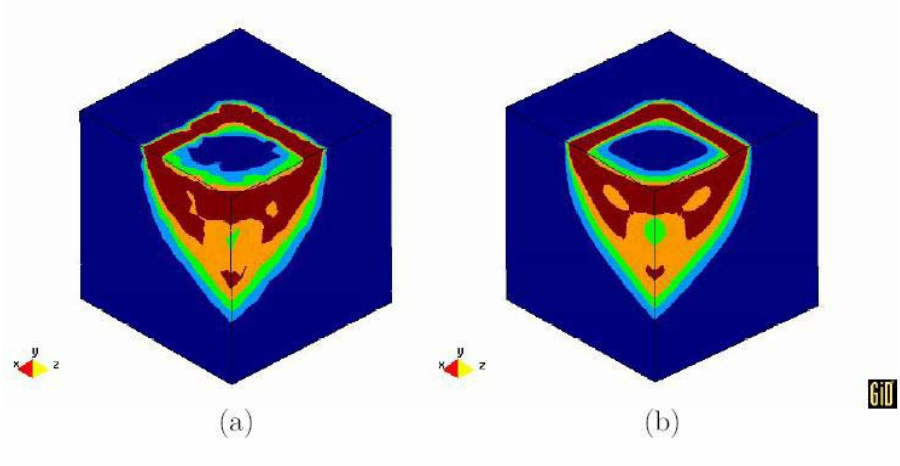

Figure 13: 3D vertical cut. Equivalent plastic strain. (a) P1/P1 OSGS tetrahedral element; (b) Q1/P0 hexahedral element

discretized. Two meshes were used in the computations, an unstructured one with linear triangles and a structured one with quadrilaterals (40 x 40 + 40 elements), both with about 1,700 nodes.

Figure 15 shows (half)-load versus (point of application)-displacement curves for P1, P1/P1, P1/P1 OSGS and Q1/P0 cases. The results confirm the observations of the previous examples: the irreductible formulation locks almost completely, while the other three formulations yield practically overlapping curves. The CPU ratios obtained are 1.26/1.53/1.62/1.0.

Figure 16 portrays contours of the equivalent plastic strain once the plastic flow is fully developed and the collapse mechanism can be appreciated (vertical displacement of the load 0.05 m). The ability of the proposed formulation to capture the correct collapse mechanism and to match the performance of the mixed quadrilateral is again demonstrated.

Finally, Figure 17 shows pressure contours at the same time of the deformation process, where the serious deficiencies of the standard formulations and the huge improvement achieved with a proper stabilization procedure are evident.

7.6 Plane strain tensile test of a rectangular bar

This example is concerned with the plane strain tensile test of a rectangular bar and has been studied by a number of authors as a localization problem using different softening behaviours [37]. The specimen considered here has

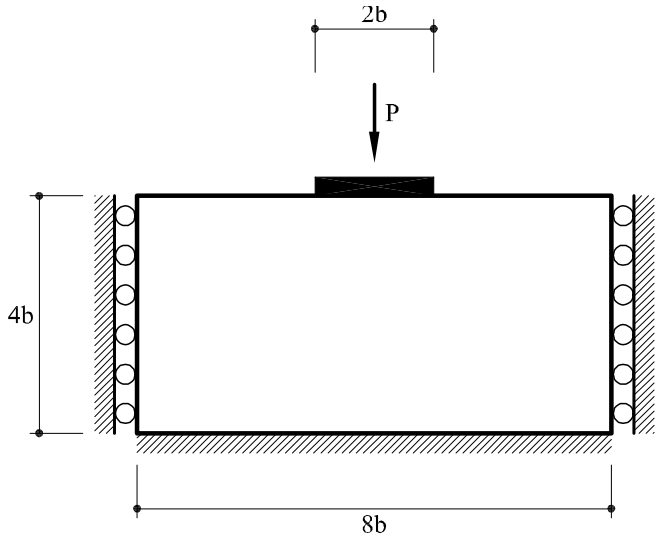

Figure 14: 2D Prandtl's punch test. Initial geometry

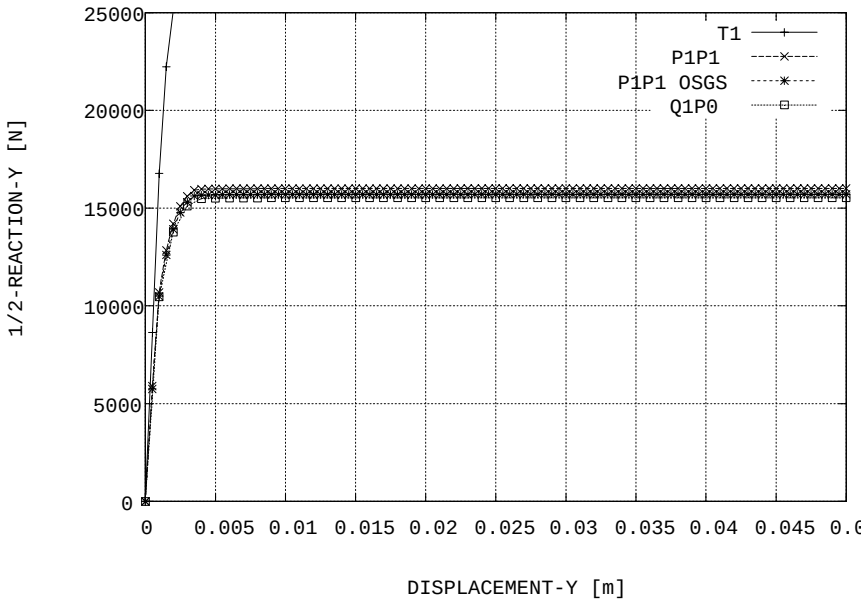

Figure 15: 2D Prandtl's punch test. (Half)-load vs displacement curves.

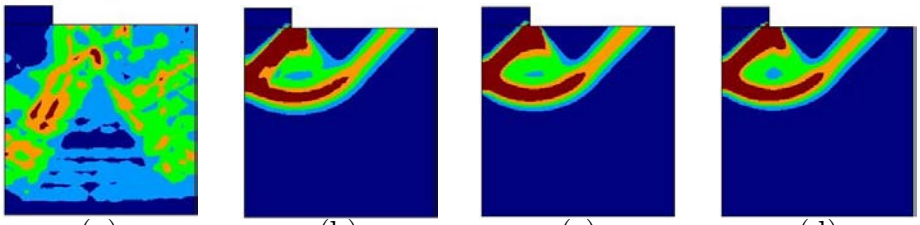

(a) (b) (c) (d)

Figure 16: 2D Prandtl's punch test. Equivalent plastic strain contours: (a) P1, (b) P1/P1, (c) P1/P1 OSGS, (d) Q1/P0

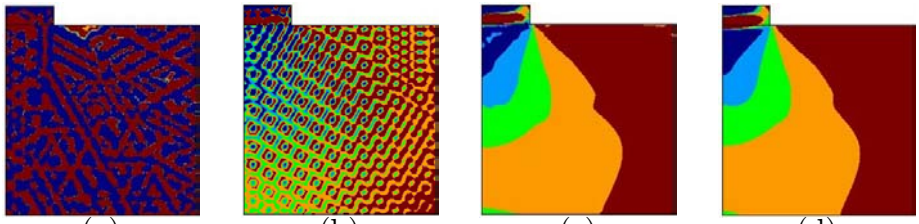

(a) (b) (c) (d)

Figure 17: 2D Prandtl's punch test. Pressure contours: (a) P1, (b) P1/P1, (c) P1/P1 OSGS, (d) Q1/P0

a width of 12.826 mm and a length of 53.334 mm and is subjected to a tensile test under ideal plane strain loading conditions. In order to trigger the necking, we consider an initial geometric imperfection in the form of a reduction of the width from its initial value at the top to 0.982% of this value at the center of the specimen. Figure 18 shows the triangular and quadrilateral mesh discretizations used in the simulations. Loading is imposed using displacement control. A maximum vertical displacement of 5 mm is applied at the top and bottom edges of the bar. The material model is assumed to be elastoplastic at finite deformations. Elastic response is given by the stored energy (53). Plastic response is modeled by a J2-flow theory with linear and saturation isotropic hardening. Material properties are summarized in Table 6. The following finite elements have been considered in the simulations: (a) Q1/P0 mixed bilinear displacements/constant pressure quadrilateral element; (b) P1 standard irreductible linear displacements triangular element; (c) P1/P1 mixed linear displacements/linear pressure triangular element; (d) P1/P1 OSGS stabilized mixed linear displacements/linear pressure triangular element.

Figure 19 shows the deformed meshes obtained at the final stage of the simulation for each one of the elements considered. Note that the P1 irreductible linear displacements triangular element does not allows to fully

Shear modulus	μ	80.1938	GPa
Bulk modulus	κ	164.206	GPa
Initial flow stress	σ_0	0.45	GPa
Residual flow stress	σ_∞	0.715	GPa
Linear hardening coefficient	H	0.12924	GPa
Saturation hardening exponent	δ	16.93	

Table 6: Plane strain tensile test of a rectangular bar. Material properties

capture the necking, while in all the other formulations necking develops properly.

Figures 20 and 21 collect the numerical results obtained at the final stage of the simulation for the equivalent plastic strain and the Kirchhoff pressure distributions for each one of the elements considered. Figure 20 clearly shows again that the P1 irreductible linear displacements triangular element can not capture properly the development of the necking, giving an incorrect distribution of the equivalent plastic strain in this area. The distributions of the equivalent plastic strain given by all the other elements formulations considered are similar. Figure 21 clearly shows once again the unability of the P1 irreductible linear displacements triangular element to deal with incompressible or quasi-incompressible problems, displaying lack of stability as high spurious oscillations of the pressure that entirely pollute the solution. This lack of stability and uncontrollable pressure oscillations are not removed using a P1/P1 mixed linear displacements/linear pressure triangular element, while stability is attained and oscillations of the pressure are fully removed using the proposed P1/P1 OSGS stabilized mixed linear displacements/linear pressure triangular element.

Figures 22 and 23 show the plots obtained for the necking displacement and force versus time, respectively, for the P1 irreductible linear displacements triangular element, P1/P1 mixed linear displacements/linear pressure triangular element, Q1/P0 mixed bilinear displacements/constant pressure quadrilateral element and P1/P1 OSGS stabilized mixed linear displacements/linear pressure triangular element. The results show again the unability of the P1 irreductible linear displacements triangular element to capture the development of the necking.

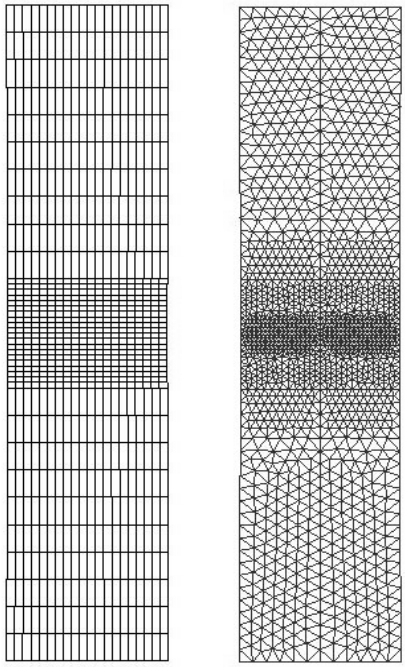

(a) (b)

Figure 18: Plane strain tensile test of a rectangular bar. Finite element discretization of the specimen. (a) Quadrilateral mesh, (b) Triangular mesh

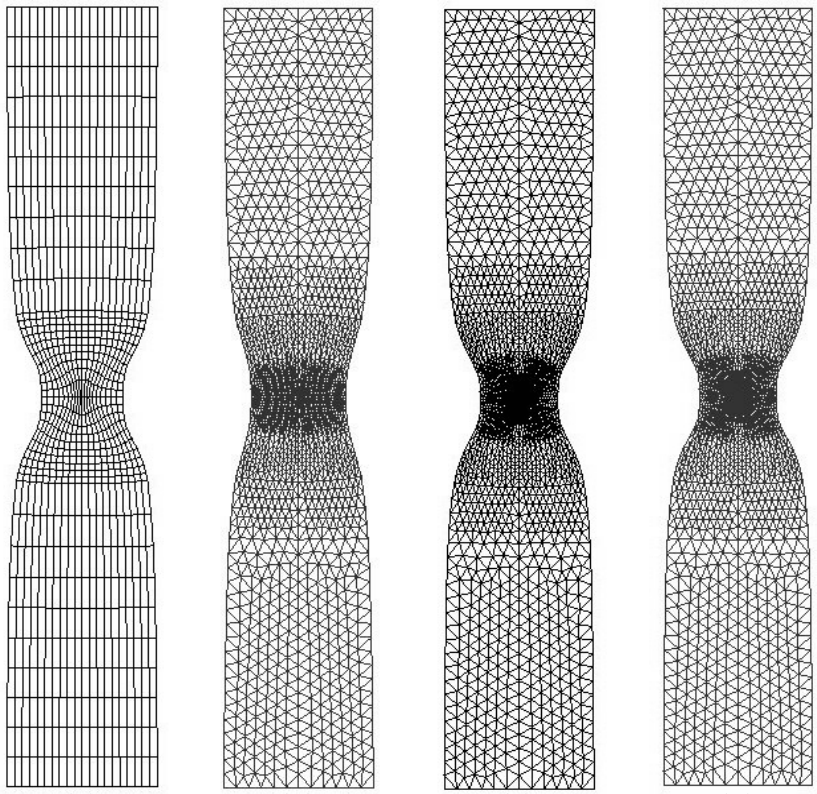

Figure 19: Plane strain tensile test of a rectangular bar. Deformed meshes. (a) Q1/P0 bilinear displacement/constant pressure quadrilateral element, (b) P1 irreductible linear displacements triangular element, (c) P1/P1 standard mixed linear displacements/linear pressure triangular element, (d) P1/P1 OSGS stabilized mixed linear displacements/linear pressure triangular element

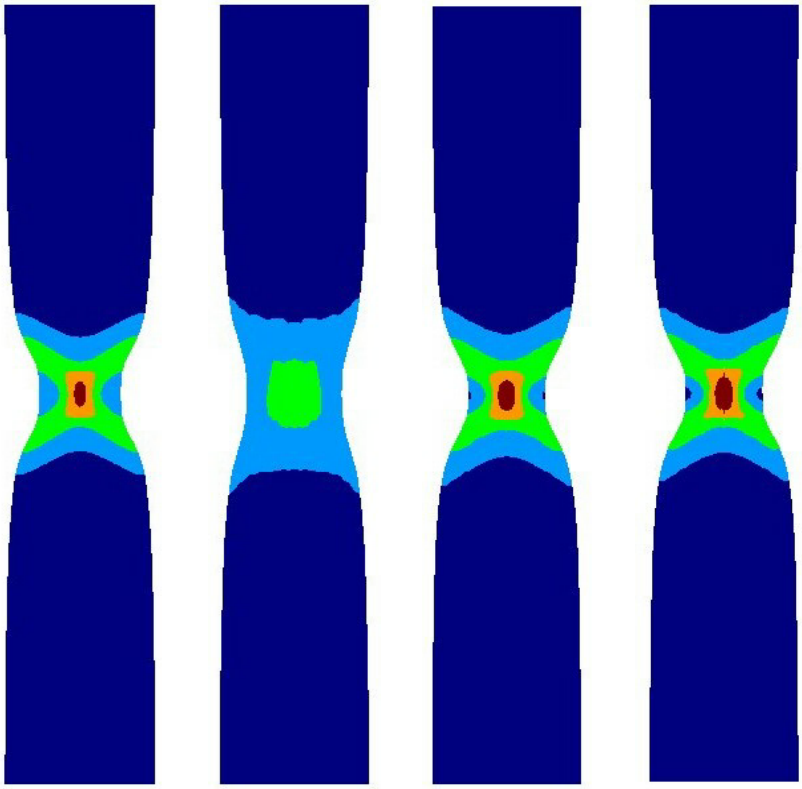

Figure 20: Plane strain tensile test of a rectangular bar. Equivalent plastic strain distribution. (a) Q1/P0 bilinear displacement/constant pressure quadrilateral element, (b) P1 irreductible linear displacements triangular element, (c) P1/P1 standard mixed linear displacements/linear pressure triangular element, (d) P1/P1 OSGS stabilized mixed linear displacements/linear pressure triangular element

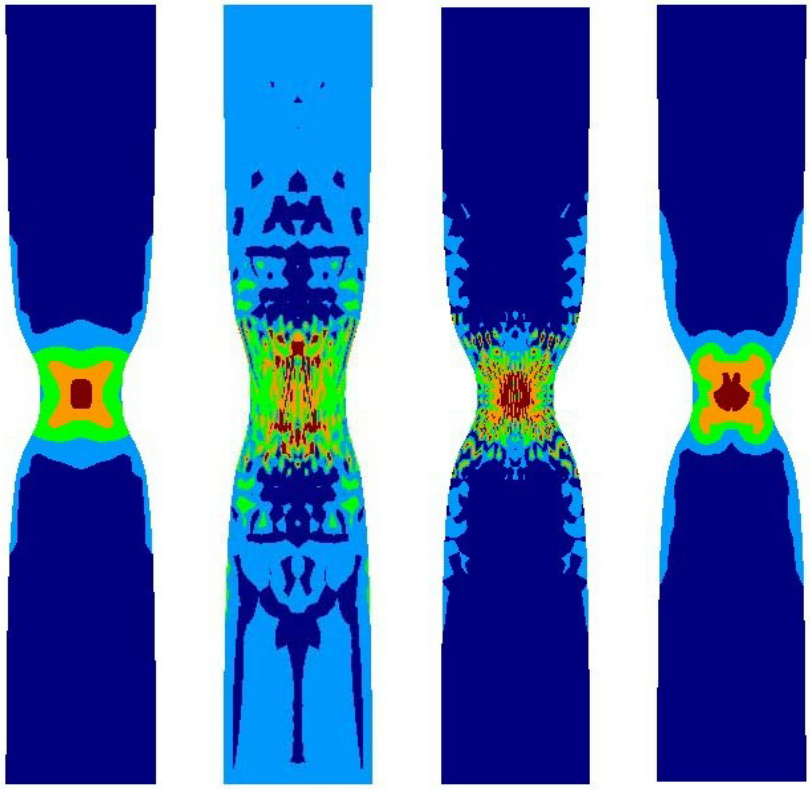

Figure 21: Plane strain tensile test of a rectangular bar. Kirchhoff pressure distribution. (a) Q1/P0 bilinear displacement/constant pressure quadrilateral element, (b) P1 irreductible linear displacements triangular element, (c) P1/P1 standard mixed linear displacements/linear pressure triangular element, (d) P1/P1 OSGS stabilized mixed linear displacements/linear pressure triangular element

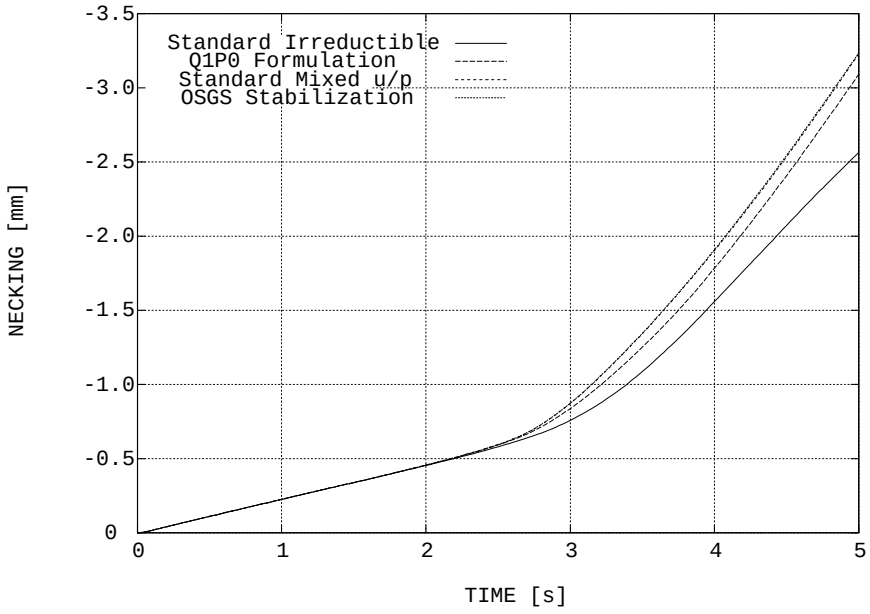

Figure 22: Plane strain tensile test of a rectangular bar. Necking displacement vs time

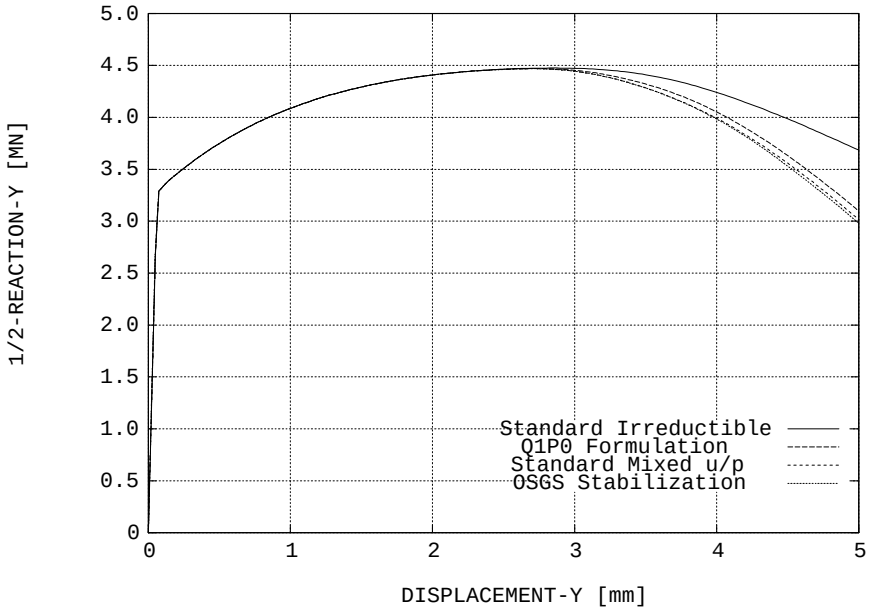

Figure 23: Plane strain tensile test of a rectangular bar. Pulling reaction vs time

Young modulus	E	$1.96E+05$	MPa
Poisson coefficient	ν	0.33	
Initial flow stress	σ_0	150	MPa
Residual flow stress	σ_∞	180	MPa
Linear hardening coefficient	H	0	MPa
Saturation hardening exponent	δ	0.7	

Table 7: Upsetting of a 3D block. Material properties

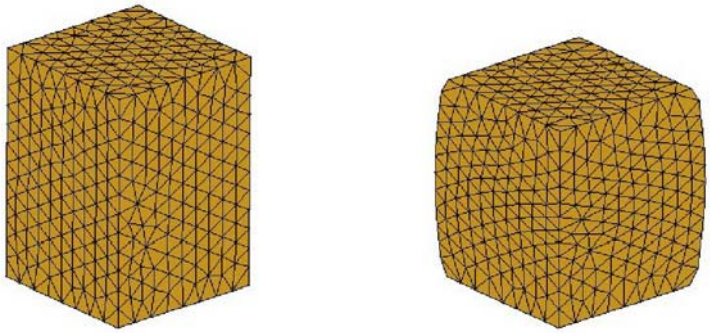

Figure 24: Upsetting of a 3D block. External view of a quarter part of the initial and deformed geometry discretized using a mesh of tetrahedra

7.7 Upsetting of a 3D block

In this example the upsetting of a 3D block is considered. A 3D steel block of $0.85 \times 0.85 \times 0.60$ m is subjected to compression by prescribing the vertical displacement of the top surface up to 15% of its initial height. Figure 24 shows an external view of a quarter part of the initial and deformed geometry discretized using a mesh of tetrahedra. Boundary conditions are such that horizontal displacements at the top surface and displacements at the bottom surface are prescribed to zero. The material model is assumed to be elasto-plastic at finite deformations. Compressible elastic response is considered. Plastic response is modeled by a J2-flow theory with exponential saturation isotropic hardening. Material properties are summarized in Table 7.

Figure 25 shows the Kirchhoff pressure distribution obtained using: (a) Q1P0 mixed trilinear displacements/constant pressure hexahedral element; (b) P1 standard linear displacements tetrahedral element; (c) P1/P1 mixed linear displacements/linear pressure tetrahedral element; and (d) P1/P1 OSGS stabilized mixed linear displacement/linear pressure tetrahedral element. As it is clearly shown, not only the standard P1 tetrahedral element, but also

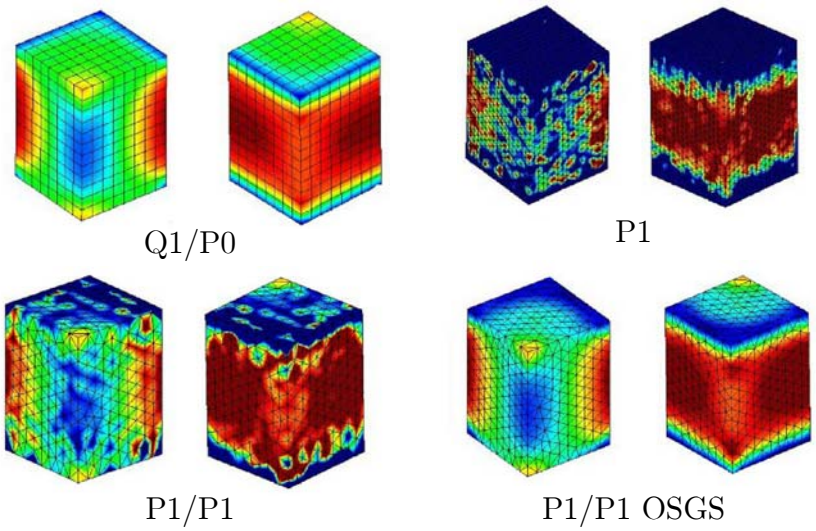

Figure 25: Upsetting of a 3D block. Kirchhoff pressure distribution. Inner and outer views of a quarter part. (a) Q1/P0 mixed bilinear displacements/constant pressure hexahedral element; (b) P1 standard linear displacements tetrahedral element; (c) P1/P1 mixed linear displacements/linear pressure tetrahedral element; (d) P1/P1 OSGS stabilized mixed linear displacements/linear pressure tetrahedral element

the standard mixed P1/P1 tetrahedral element, give an unstable response with uncontrolled oscillations of the Kirchhoff pressure distribution, while the P1/P1 OSGS stabilized tetrahedral element proposed, as well as the Q1P0 hexahedral element, provide stable pressure distributions.

7.8 Necking of a circular bar

This experimentally well-documented example is concerned with the necking of a circular bar, with a radius of 6.413 mm and length 53.334 mm, subjected to uniaxial tension [36], [37], [38], [39]. Loading is imposed using displacement control. A maximum vertical displacement of 7 mm is applied at the top and bottom edges of the bar. A small geometric imperfection (0.982% of the radius) is introduced at the center of the bar and linearly extended to the top in order to trigger the necking. The material model is assumed to be elastoplastic at finite deformations. Elastic response is given by the stored energy (53). Plastic response is modeled by a J2-flow theory with linear and saturation isotropic hardening. Material properties are summarized in Table 8 [39].

Figure 26 shows a detail of the necking on the deformed meshes at the final

Shear modulus	μ	80.1938	GPa
Bulk modulus	κ	164.206	GPa
Initial flow stress	σ_0	0.45	GPa
Residual flow stress	σ_∞	0.715	GPa
Linear hardening coefficient	H	0.12924	GPa
Saturation hardening exponent	δ	16.93	

Table 8: Necking of a circular bar. Material properties

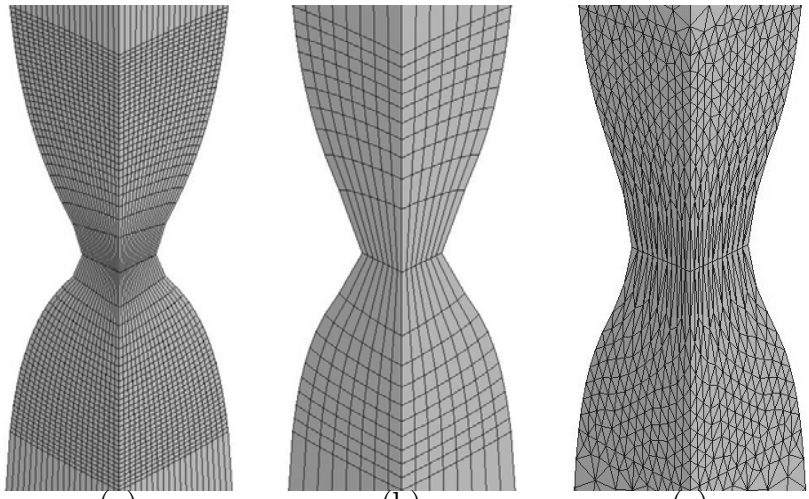

Figure 26: Necking of a circular bar. Details of deformed meshes. (a) Q1/P0 hexahedral element, finer mesh; (a) Q1/P0 hexahedral element, coarse mesh; (c) P1/P1 OSGS tetrahedra element

stage of the deformation, using Q1/P0 fine and coarse hexahedral meshes and a P1/P1 OSGS tetrahedral mesh. To properly capture the necking a high density of elements is needed in this area. Too coarse meshes at the necking area result in too highly deformed elements and a non-smooth necking.

Figure 27 shows the contours of the equivalent plastic strain at the final stage of the deformation, using Q1/P0 finer and coarse hexahedral meshes, P1 tetrahedral elements and P1/P1 OSGS tetrahedral elements. The results provided by the P1/P1 OSGS tetrahedral element compare very well with the results given by the Q1/P0 hexahedral element. On the other hand, it is clearly shown that the simulation done using P1 elements is useless.

Figure 28 shows the contours of the Kirchhoff pressure at the final stage of the deformation, using Q1/P0 fine and coarse hexahedral meshes, P1 tetra-

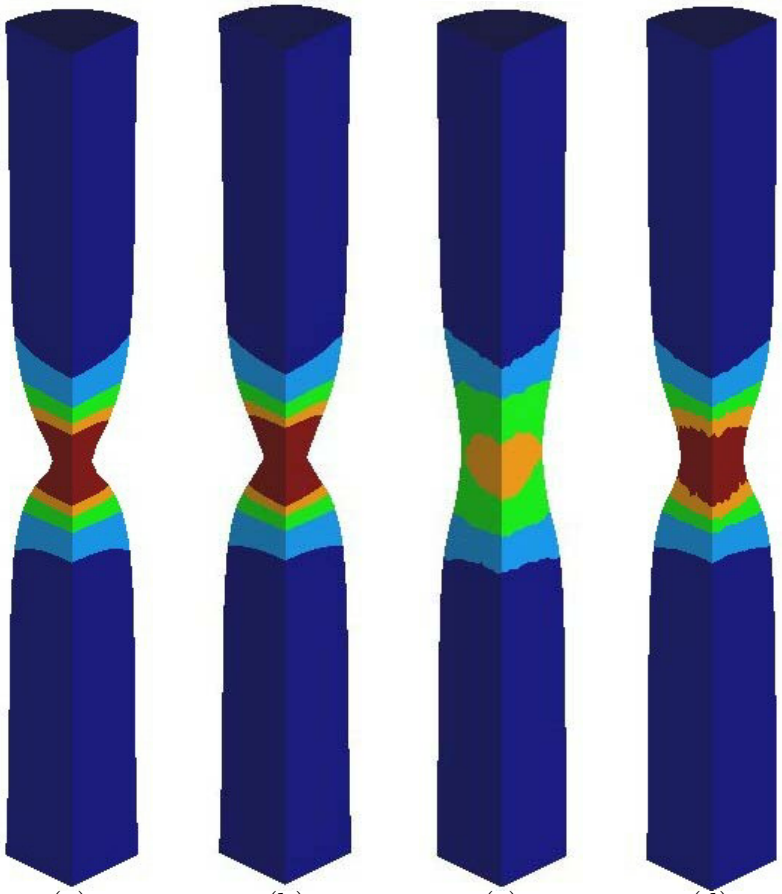

Figure 27: Necking of a circular bar. Equivalent plastic strain distribution. (a) Q1/P0 hexahedral element, finer mesh; (b) Q1/P0 hexahedral element, coarser mesh; (c) P1 linear displacemets tetrahedral element; (d) P1/P1 OSGS tetrahedral element

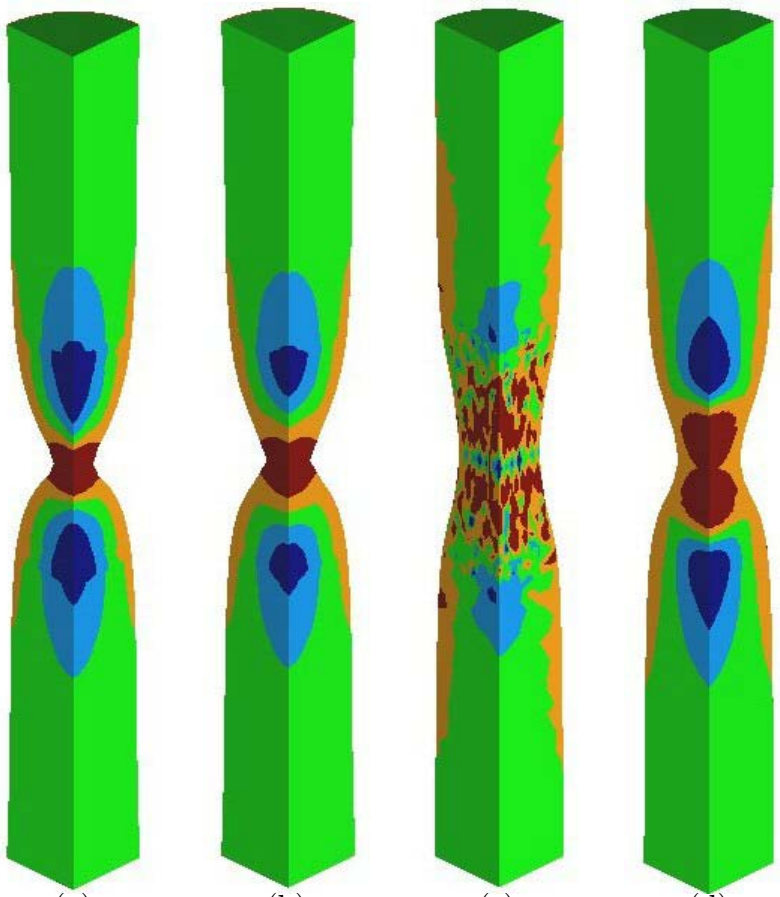

Figure 28: Necking of a circular bar. Kirchhoff pressure distribution. (a) Q1/P0 hexahedral element, finer mesh; (b) Q1/P0 hexahedral element, coarser mesh; (c) P1 linear displacemets tetrahedral element; (d) P1/P1 OSGS tetrahedral element

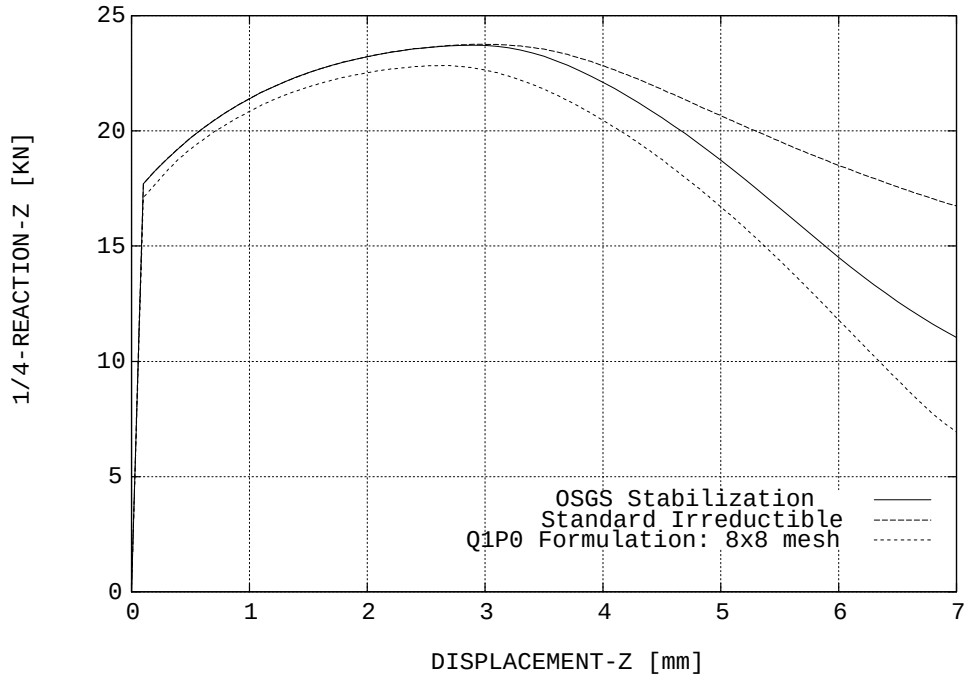

Figure 29: Necking of a circular bar. Force vs displacement curves

hedral elements and P1/P1 OSGS tetrahedral elements. Results provided by the P1/P1 OSGS tetrahedral elements compare well with the results given by the Q1/P0 hexahedral element. Results provided by P1 tetrahedral element show lack of stability in the form of uncontrollable oscillations of the Kirchhoff pressure that pollute the solution. Stability is recovered and pressure oscillations are removed using the proposed P1/P1 OSGS mixed stabilized tetrahedral element. Figure 29 shows the force (1/4 reaction) vs displacement curves obtained for the different elements and meshes considered.

8 Concluding Remarks

In this monograph a stabilization technique for incompressible J2-flow theory plasticity, within the framework of small and finite deformation theory, has been presented. The stabilization technique, which falls within the variational multiscale technique, is based on the Orthogonal Subgrid Scale (OSGS) method. Within the paradigmatic framework of the multiscale techniques the Subgrid Scale (SGS) method seeks to approximate the effect of the component of the continuous solution which can not be captured by the

finite element mesh used to obtain the discrete finite element solution. The unresolved component is referred to as the *subgrid scale* or *subscale*. Within the OSGS method we take the orthogonal space to the finite element solution space as the natural space of the subgrid scales. An approximate solution for the subgrid scales is considered and a suitable simple nonlinear expression for the stabilization parameter is proposed. Computational aspects and details of implementation have been shown. Computational simulations show the serious deficiencies of the standard formulations and the huge improvement achieved with the proposed stabilization technique. P1 standard Galerkin displacements element and P1/P1 standard mixed linear displacements/linear pressure element show lack of stability and uncontrolled oscillations of the pressure. The proposed P1/P1 OSGS stabilized element allows to completely remove the pressure oscillations providing pressure stable results within the framework of an elastoplastic J2-flow theory model at small and finite deformations.

9 Acknowledgement

The authors are thankful for the financial support given by European Commission through the Growth project GRD1-2000-25243. Useful discussions with Prof. R. Codina and Prof. E. Oñate are gratefully acknowledged.

References

[1] D.N. Arnold, F. Brezzi, M. Fortin, A stable finite element for the Stokes equations, Calcolo 21 (1984) 337-344

[2] C. Baiocchi, F. Brezzi, L.P. Franca, Virtual bubbles and Galerkin/least-square type methods, Computer Methods in Applied Mechanics and Engineering 105 (1993) 125-141

[3] F. Brezzi, M. Fortin, Mixed and Hybrid Finite Element Methods, Spinger, New York, 1991

[4] F. Brezzi, M.O. Bristeau, L.P. Franca, M. Mallet, G. Rogé, A relationship between stabilized finite element methods and the Galerkin method with bubble functions, Computer Methods in Applied Mechanics and Engineering 96 (1992) 117-129

[5] M. Cervera, C. Agelet de Saracibar, M. Chiumenti, COMET – A COupled MEchanical and Thermal analysis code. Data input manual, Ver-

sion 5.0, Technical Report IT-308, CIMNE, http://www.cimne.upc.es, 2002

[6] M. Cervera, M. Chiumenti, Q. Valverde, C. Agelet de Saracibar, Mixed linear/linear simplicial elements for incompressible elasticity and plasticity, Computer Methods in Applied Mechanics and Engineering, 192 (2003), 5249-5263

[7] M. Cervera, M. Chiumenti, C. Agelet de Saracibar, Softening, localization and stabilization: capture of discontinuous solutions in J2 plasticity, International Journal for Numerical and Analytical Methods in Geomechanics 28 (2004) 373-393

[8] M. Cervera, M. Chiumenti, C. Agelet de Saracibar, Shear band localization via local J2 continuum damage mechanics, Computer Methods in Applied Mechanics and Engineering 193 (2004) 849-880

[9] M. Cervera, M. Chiumenti, C. Agelet de Saracibar, Shear band localization via local J2 continuum damage mechanics, Monograph M78, CIMNE, 2003

[10] D. Christ, M. Cervera, M. Chiumenti, C. Agelet de Saracibar, A mixed finite element formulation for incompressibility using linear displacement and pressure interpolations, Monograph 77, CIMNE, 2003

[11] M. Chiumenti, Q. Valverde, C. Agelet de Saracibar, M. Cervera, A stabilized formulation for incompressible elasticity using linear displacement and pressure interpolations, Computer Methods in Applied Mechanics and Engineering 191 (2002) 5253-5264

[12] M. Chiumenti, Q. Valverde, C. Agelet de Saracibar, M. Cervera, A stabilized formulation for incompressible plasticity using linear triangles and tetrahedra, International Journal of Plasticity 20 (2004) 1487-1504

[13] R. Codina, Stabilization of incompressibility and convection through orthogonal sub-scales in finite element methods, Computer Methods in Applied Mechanics and Engineering 190 (2000) 1579-1599

[14] R. Codina, Stabilized finite element approximation of transient incompressible flows using orthogonal subscales, Computer Methods in Applied Mechanics and Engineering 191 (2002) 4295-4321

[15] R. Codina, J. Blasco, Stabilized finite element method for transient Navier-Stokes equations based on pressure gradient projection, Computer Methods in Applied Mechanics and Engineering 182 (2000) 287-300

[16] K. Garikipati, T.J.R. Hughes, A study of strain localization in a multiple scale framework – The one dimensional problem, Computer Methods in Applied Mechanics and Engineering 159 (1998) 193-222

[17] K. Garikipati, T.J.R. Hughes, A variational multiscale approach to strain localization – Formulation for multidimensional problems, Computer Methods in Applied Mechanics and Engineering 188 (2000) 39-60

[18] GiD: The personal pre and postprocessor, http://www.cimne.upc.es, 2002

[19] T.J.R. Hughes, The Finite Element Method: Linear Static and Dynamic Finite Element Analysis, Prentice-Hall, Inc., Englewood Cliffs, New Jersey, 1987

[20] T.J.R. Hughes, Multiscale phenomena: Green's function, Dirichlet-to-Neumann formulation, subgrid scale models, bubbles and the origins of stabilized formulations, Computer Methods in Applied Mechanics and Engineering 127 (1995) 387-401

[21] T.J.R. Hughes, L.P. Franca, M. Balestra, A finite element formulation for computational fluid dynamics: V. Circumventing the Babuška-Brezzi condition: A stable Petrov-Galerkin formulation of the Stokes problem accomodating equal-order interpolations, Computer Methods in Applied Mechanics and Engineering 59 (1986) 85-99

[22] T.J.R. Hughes, L.P. Franca, G.M. Hulbert, A new finite element formulation for computational fluid dynamics: VIII. The Galerkin/least-square method for advective-diffusive equations, Computer Methods in Applied Mechanics and Engineering 73 (1989) 173-189

[23] T.J.R. Hughes, G.R. Feijóo, L. Mazzei, J-B. Quincy, The variational multiscale method – A paradigm for computational mechanics, Computer Methods in Applied Mechanics and Engineering 166 (1998) 3-24

[24] O. Klaas, A. Maniatty, M.S. Shephard, A stabilized mixed finite element method for finite elasticity. Formulation for linear displacement and pressure interpolation, Computer Methods in Applied Mechanics and Engineering 180 (1999) 65-79

[25] M. Küssner, B.D. Reddy, The equivalent parallelogram and parallelepiped, and their application to stabilized finite elements in two and three dimensions, Computer Methods in Applied Mechanics and Engineering 190 (2001) 1967-1983

[26] A. Maniatty, Y. Liu, Stabilized finite element method for viscoplastic flow: formulation with state variable evolution, International Journal for Numerical Methods in Engineering 56 (2003) 185-209

[27] A. Maniatty, Y. Liu, O. Klaas, M.S. Shephard, Stabilized finite element method for viscoplastic flow: formulation and a simple progressive solution strategy, Computer Methods in Applied Mechanics and Engineering 190 (2001) 4609-4625

[28] A. Maniatty, Y. Liu, O. Klaas, M.S. Shephard, Higher order stabilized finite element method for hyperelastic finite deformation, Computer Methods in Applied Mechanics and Engineering 191 (2002) 1491-1503

[29] C. Miehe, Aspects of the formulation and finite element implementation of large strain isotropic elasticity, International Journal for Numerical Methods in Engineering 37 (1994) 1981-2004

[30] E. Oñate, J. Rojek, R.L. Taylor, O.C. Zienkiewicz, Linear triangles and tetrahedra for incompressible problem using a finite calculus formulation, Proceedings of European Conference on Computational Mechanics, ECCM 2001, 2001

[31] E. Oñate, J. Rojek, R.L. Taylor, O.C. Zienkiewicz, Finite calculus formulation for incompressible solids using linear triangles and tetrahedra, submitted to International Journal for Numerical Methods in Engineering (2002)

[32] B.D. Reddy, J.C. Simo, Stability and convergence of a class of enhanced assumed strain methods, SIAM Journal of Numerical Analysis 32 (1995) 1705-1728

[33] S. Reese, P. Wriggers, A stabilization technique to avoid hourglassing in finite elasticity, International Journal for Numerical Methods in Engineering 48 (2000) 79-109

[34] S. Reese, M. Küssner, B.D. Reddy, A new stabilization technique for finite elements in nonlinear elasticity, International Journal for Numerical Methods in Engineering 44 (1999) 1617-1652

[35] J.C. Simo, A framework for finite strain elastoplasticity based on maximum plastic dissipation and the multiplicative decomposition: Part I. Continuum formulation, Computer Methods in Applied Mechanics and Engineering 66 (1988) 199-219

[36] J.C. Simo, A framework for finite strain elastoplasticity based on maximum plastic dissipation and the multiplicative decomposition: Part II. Computational aspects, Computer Methods in Applied Mechanics and Engineering 68 (1988) 1-31

[37] J.C. Simo, F. Armero, Geometrically non-linear enhanced strain mixed methods and the method of incompatible modes, International Journal for Numerical Methods in Engineering 33 (1992) 1413-1449

[38] J.C. Simo, F. Armero, R.L. Taylor (1993), Improved versions of assumed enhanced strain tri-linear elements for 3D finite deformations, Computer Methods in Applied Mechanics and Engineering 110 (1993) 359-386

[39] J.C. Simo, T.J.R. Hughes, Computational Inelasticity, Springer, 1998

[40] J.C. Simo, C. Miehe, Associative coupled thermoplasticity at finite strains: Formulation, numerical analysis and implementation, Computer Methods in Applied Mechanics and Engineering 98 (1992) 41-104

[41] J.C. Simo, M.S. Rifai, A class of mixed assumed strain methods and the method of incompatible modes, International Journal for Numerical Methods in Engineering 29 (1990) 1595-1638

[42] J.C. Simo, R.L. Taylor, K.S. Pister, Variational and projection methods for the volume constraint in finite deformation elasto-plasticity, Computer Methods in Applied Mechanics and Engineering 51 (1985) 177-208

[43] R.L. Taylor, A mixed formulation for triangular and tetrahedral elements, Métodos Numéricos en Ingeniería Conference Proceedings, SEMNI 1999, Barcelona, Spain, 1999

[44] Q. Valverde, C. Agelet de Saracibar, M. Cervera, M. Chiumenti, Elementos estabilizados de bajo orden en mecánica de sólidos, Monografía M69, CIMNE, 2002

[45] O.C. Zienkiewicz, R.L. Taylor, The Finite Element Method, Fifth Edition, Volumes 1–3, Butterworth-Heinemann, 2000

[46] O.C. Zienkiewicz, J. Rojek, R.L. Taylor, M. Pastor, Triangles and tetrahedra in explicit dynamic codes for solids, International Journal for Numerical Methods in Engineering 43 (1998) 565-583

A Appendix I. Linearization of the Variational Momentum Balance Residual

Consider the (mixed) variational form of the momentum balance residual equation given by

$$R_u\left(\mathbf{u},\pi;\mathbf{v}\right)=\left(\pi,\nabla\cdot\mathbf{v}\right)+\left(\mathbf{s}\left(\mathbf{u}\right),\nabla^s\mathbf{v}\right)-\left(\mathbf{f},\mathbf{v}\right)-\left(\overline{\mathbf{t}}^N,\mathbf{v}\right)_{\partial\Omega}\qquad\forall\ \mathbf{v}\in\mathcal{V}_0 \tag{101}$$

Using the following key expressions

$$\boldsymbol{\tau} = \mathbf{P}\mathbf{F}^T \tag{102}$$

$$\nabla\mathbf{v} = \mathrm{GRAD}\left[\mathbf{v}\right]\mathbf{F}^{-1} \tag{103}$$

where $\mathbf{P}$ is the first Piola-Kirchhoff stress tensor and $\mathrm{GRAD}\left[\cdot\right]$ denotes the material gradient operator, and taking into account that $\left(\pi,\nabla\cdot\mathbf{v}\right)+\left(\mathbf{s}\left(\mathbf{u}\right),\nabla^s\mathbf{v}\right)=\left(\boldsymbol{\tau},\nabla^s\mathbf{v}\right)$, the following result holds

$$\left(\boldsymbol{\tau},\nabla^s\mathbf{v}\right)=\left(\mathbf{P}\mathbf{F}^T,\mathrm{GRAD}\left[\mathbf{v}\right]\mathbf{F}^{-1}\right)=\left(\mathbf{P},\mathrm{GRAD}\left[\mathbf{v}\right]\right) \tag{104}$$

Using (104), the variational form (101) can be written as

$$R_u\left(\mathbf{u},\pi;\mathbf{v}\right):=\left(\mathbf{P}\left(\mathbf{u},\pi\right),\mathrm{GRAD}\left[\mathbf{v}\right]\right)-\left(\mathbf{f},\mathbf{v}\right)-\left(\overline{\mathbf{t}}^N,\mathbf{v}\right)_{\partial\Omega}\qquad\forall\ \mathbf{v}\in\mathcal{V}_0 \tag{105}$$

Then the linearization of (101), using the equivalent expression (105), can be written as

$$DR_u\left(\mathbf{u},\pi;\mathbf{v}\right)\cdot\left(\Delta\mathbf{u},\Delta\pi\right)=\left(D\mathbf{P}\left(\mathbf{u},\pi\right)\cdot\left(\Delta\mathbf{u},\Delta\pi\right),\mathrm{GRAD}\left[\mathbf{v}\right]\right) \tag{106}$$

where $DR_u\left(\mathbf{u},\pi;\mathbf{v}\right)\cdot\left(\Delta\mathbf{u},\Delta\pi\right)$ and $D\mathbf{P}\left(\mathbf{u},\pi\right)\cdot\left(\Delta\mathbf{u},\Delta\pi\right)$ denote the directional derivatives of the residual and first Piola-Kirchhoff stress tensor, respectively, along the directions $\Delta\mathbf{u}$ and $\Delta\pi$. Let us compute now the linearization of the first Piola-Kirchhoff stress tensor.

Linearization of the first Piola-Kirchhoff stress tensor. The first Piola-Kirchhoff stress tensor $\mathbf{P}$ can be expressed in terms of the second Piola-Kirchhoff stress tensor $\mathbf{S}$ and the deformation gradient $\mathbf{F}$ as

$$\mathbf{P}=\mathbf{F}\mathbf{S}$$

Then the linearization of the first Piola-Kirchhoff stress tensor yields

$$D\mathbf{P}\cdot(\Delta\mathbf{u},\Delta\pi) = D\mathbf{F}\cdot\Delta\mathbf{u}\ \mathbf{S} + \mathbf{F}\ D\mathbf{S}\cdot(\Delta\mathbf{u},\Delta\pi) \tag{107}$$

where the variation of the deformation gradient $D\mathbf{F}\cdot\Delta\mathbf{u}$ and the variation of the second Piola-Kirchhoff stress tensor $D\mathbf{S}\cdot(\Delta\mathbf{u},\Delta\pi)$ take the form

$$\begin{aligned} D\mathbf{F}\cdot\Delta\mathbf{u} &= \nabla\Delta\mathbf{u}\ \mathbf{F} \\ D\mathbf{S}\cdot(\Delta\mathbf{u},\Delta\pi) &= \mathbf{F}^{-1}\ \mathcal{L}_{\Delta\mathbf{u}}\boldsymbol{\tau}\ \mathbf{F}^{-T} \end{aligned}$$

where $\mathcal{L}_{\Delta\mathbf{u}}\boldsymbol{\tau} := \Delta\boldsymbol{\tau} - \nabla(\Delta\mathbf{u})\,\boldsymbol{\tau} - \boldsymbol{\tau}\,(\nabla\Delta\mathbf{u})^T$ denotes the Lie derivative of the Kirchhoff stress tensor along the flow induced by $\Delta\mathbf{u}$. Introducing the split of the Kirchhoff stress tensor into its spherical (in terms of the Kirchhoff pressure π) and deviatoric parts $\boldsymbol{\tau} = \pi\mathbf{1} + \mathbf{s}$, the Lie derivative yields

$$\mathcal{L}_{\Delta\mathbf{u}}\boldsymbol{\tau} = \mathcal{L}_{\Delta\mathbf{u}}(\pi\mathbf{1}) + \mathcal{L}_{\Delta\mathbf{u}}\mathbf{s}$$

where

$$\mathcal{L}_{\Delta\mathbf{u}}(\pi\mathbf{1}) = \Delta\pi\mathbf{1} - 2\pi\nabla^s\Delta\mathbf{u} \tag{108}$$

$$\mathcal{L}_{\Delta\mathbf{u}}\mathbf{s} = \Delta\mathbf{s} - \nabla(\Delta\mathbf{u})\,\mathbf{s} - \mathbf{s}\,(\nabla\Delta\mathbf{u})^T = \mathbf{c}^{dev} : \nabla^s(\Delta\mathbf{u}) \tag{109}$$

where the incremental constitutive equation for the deviatoric part of the Kirchhoff stress tensor $\mathcal{L}_{\Delta\mathbf{u}}\mathbf{s} = \mathbf{c}^{dev} : \nabla^s(\Delta\mathbf{u})$ has been introduced.

Substituting (108) and (109) into (107) yields

$$\begin{aligned} D\mathbf{P}\cdot(\Delta\mathbf{u},\Delta\pi) &= \nabla\Delta\mathbf{u}\ \mathbf{F}\mathbf{S}\mathbf{F}^T\mathbf{F}^{-T} + \mathbf{F}\mathbf{F}^{-1}\mathcal{L}_{\Delta\mathbf{u}}\tau\mathbf{F}^{-T} = \\ &= \left[\nabla\Delta\mathbf{u}\ \boldsymbol{\tau} + \mathcal{L}_{\Delta\mathbf{u}}\boldsymbol{\tau}\right]\mathbf{F}^{-T} \end{aligned} \tag{110}$$

Linearization of the variational form of the residual. Substituting the linearization of the first Piola-Kirchhoff stress tensor given by (110) into (106) and using (103), yields

$$\begin{aligned} \left(D\mathbf{P}\cdot(\Delta\mathbf{u},\Delta\pi),\mathrm{GRAD}[\mathbf{v}]\right) &= \left(\left[\nabla\Delta\mathbf{u}\ \boldsymbol{\tau} + \mathcal{L}_{\Delta\mathbf{u}}\boldsymbol{\tau}\right]\mathbf{F}^{-T},\mathrm{GRAD}[\mathbf{v}]\right) = \\ &= (\nabla\Delta\mathbf{u}\ \boldsymbol{\tau},\boldsymbol{\nabla}\mathbf{v}) + (\mathcal{L}_{\Delta\mathbf{u}}\boldsymbol{\tau},\nabla^s\mathbf{v}) \end{aligned}$$

Introducing the split of the Kirchhoff stress tensor $\boldsymbol{\tau} = \pi\mathbf{1} + \mathbf{s}$ and using (108) and (109) yields

$$\begin{aligned} \left(D\mathbf{P}\cdot(\Delta\mathbf{u},\Delta\pi),\mathrm{GRAD}[\mathbf{v}]\right) &= (\nabla\Delta\mathbf{u}\,(\pi\mathbf{1}+\mathbf{s}),\nabla\mathbf{v}) + \\ &\quad + (\Delta\pi,\nabla\cdot\mathbf{v}) - (2\pi\nabla^s\Delta\mathbf{u},\nabla^s\mathbf{v}) \\ &\quad + \left(\mathbf{c}^{dev} : \nabla^s\Delta\mathbf{u},\nabla^s\mathbf{v}\right) \end{aligned}$$